

UNIVERSITY OF CALIFORNIA

Santa Barbara

MAPPING AND SPATIOTEMPORAL CHARACTERIZATION OF DEGRADED
FORESTS IN THE BRAZILIAN AMAZON THROUGH REMOTE SENSING

A Dissertation submitted in partial satisfaction of the
requirements for the degree Doctor of Philosophy
in Geography

by

Carlos Moreira de Souza Jr.

Committee in charge:

Professor Dar A. Roberts, Chair

Professor Oliver A. Chadwick

Professor Phaedon C. Kyriakidis

Professor Mark A. Cochrane

September 2005

The dissertation of Carlos Moreira de Souza Jr. is approved.

Oliver A. Chadwick

Phaedon C. Kyriakidis

Mark A. Cochrane

Dar A. Roberts, Committee Chair

September 2005

Mapping and Spatiotemporal Characterization of Degraded Forests in the Brazilian
Amazon through Remote Sensing

Copyright © 2005

by

Carlos Moreira de Souza Jr.

*To my parents, Carlos and Selma, for always
encouraging me to follow my dreams; and to
my wife, Karen, and my son, Caio, for their
love and support.*

*Para os meus pais, Carlos e Selma, por sempre
me encorajarem a perseguir meus sonhos; e para
minha esposa, Karen, e meu filho, Caio, pelo seu
amor e apoio.*

ACKNOWLEDGEMENTS

I am grateful to several people who helped me with the research activities that resulted in this dissertation. Forest inventories were assisted by André Monteiro, Frank Pantoja and Josieldo Pantoja; Sâmia Nunes and Cíntia Balieiro helped with some of the image pre-processing activities and Anderson Costa with videography interpretation. Márcio Sales introduced me to important features of the S/R statistical programming language that allowed me to implement the genetic decision tree algorithm. I am also thankful to my graduate student friends Izaya Numata, Mateo Clark and Becky Powell for the encouragement and support over the graduate lifetime. I am also very thankful to Connie Padilla for taking care of my academic and administrative paper works. This research could not be accomplished without the financial support of NASA through LBA-ECO I and II research grants whose principal investigators are Dr. Dar Roberts and Dr. Oliver Chadwick. Most of the research presented here in this dissertation was conducted at Imazon, the Amazon Institute for People and the Environment. Funding to Imazon's remote sensing and GIS laboratories, and Landsat image acquisition came from several sources: USAID, Ford Foundation, PPD-PPG-7, and Gordon and Betty Moore Foundation. Finally, I am thankful to my committee members Dr. Phaedon Kyriakidis, Dr. Oliver Chadwick and Dr. Mark Cochrane for their insights and advices, and especially to my advisor, Dr. Dar Roberts, for teaching me remote sensing, for the time he dedicated advising me, and for financially supporting my graduate studies.

VITA OF CARLOS MOREIRA DE SOUZA JR.

August 2005

EDUCATION

Bachelor of Science in Geology, Pará State Federal University, Brazil, 1991.
Master of Science in Soil Science, Pennsylvania State University, USA, June 1997.
Doctor of Philosophy in Geography, University of California, Santa Barbara, September 2005 (expected).

PROFESSIONAL EMPLOYMENT

1992-1995: Research Assistant, Amazon Institute for the People and Environment, Imazon.
1996-2000: Adjunct Researcher, Amazon Institute for the People and Environment, Imazon.
2000-Present: Senior Researcher, Amazon Institute for the People and Environment, Imazon.
2001-Present: Graduate Research Assistant, University of California – Santa Barbara.

SELECTED PUBLICATIONS

- Souza Jr., C., Roberts, D. and Cochrane, M. A. In press.** Combining Spectral and Spatial Information to Map Canopy Damages from Selective Logging and Forest Fires. **Remote Sensing of Environment.**
- Souza Jr., C. M., Roberts, D.A. and Monteiro, A.L. In press.** Multi-temporal analysis of degraded forests in the Southern Brazilian Amazon. **Earth Interactions.**
- Souza Jr. C. and Roberts, D. A. 2005.** Mapping forest degradation in the Amazon Region with Ikonos images. **International Journal of Remote Sensing.** (26) 425-429.
- Powell, R. L., Matzke, N., **Souza, Jr., C.,** Clark, M., Numata, I. Hess, L. L and Roberts, D. A. **2004.** Sources of error in accuracy assessment of thematic land-cover maps in the Brazilian Amazon. **Remote Sensing of Environment,** 90:221-234.
- Souza Jr., C., Firestone, L.A., Moreira, L. and Roberts, D.A. 2003.** Mapping forest degradation in the Eastern Amazon from SPOT 4 through spectral mixture models. **Remote Sensing of Environment,** (87):494-506.
- Monteiro, A. L.; **Souza Jr., C.** and Barreto, P. **2003.** Detection of logging in Amazonian transition forest using spectral mixture models. **International Journal of Remote Sensing,** 24(1): 151-159.

- Veríssimo, A., Cochrane, M. A. and **Souza Jr., C.** 2002 National Forests in the Amazon. **Science**, (297): 1478p.
- Veríssimo, A., M. A. Cochrane, C. **Souza Jr., C.**, and R. Salomão. 2002. Priority areas for establishing national forests in the Brazilian Amazon. **Conservation Ecology** 6(1): 4. [online] URL: <http://www.consecol.org/vol6/iss1/art4>.
- Souza Jr., C. M.** and Barreto, P. 2000. An Alternative Approach for Detecting and Monitoring Selectively Logged Forests in the Amazon. **International Journal of Remote Sensing**. (21): 173-179.
- Cochrane, M. A., Alencar, A., Schultze, M. D., **Souza Jr., C. M.**, Nepstad, D. C., Lefebvre, P. and Davidson, E. A. 1999. Positive Feedbacks in the Fire Dynamic of Closed Canopy Tropical Forests. **Science**, 1832-1835p.
- Verissimo, A., **Souza Jr., C. M.**, Stone, S., and Uhl, C. 1998 . Forest Zoning in the Eastern Brazilian Amazon. **Conservation Biology**. (12), n. 1 128-136p.
- Cochrane, M. A and **Souza Jr., C. M.** 1998. Linear Mixing Model Classification of Burned Forests in the Eastern Amazon. **International Journal of Remote Sensing**. (19)17: 3433-3440p.
- Uhl, C, Barreto, P., Verissimo, A., Vidal, E., Amaral, P, Barros, A. C., **Souza Jr., C. M.**, Gerwing, J. and Johns, J., 1997. An integrated Research Approach for Addressing Natural Resource Problems in the Brazilian Amazon. **Bioscience**, Vol. 47, (3), 160-168p.
- Souza Jr., C. M.** 1997. An Assessment of Mixing Models for Mapping Land Cover in the Eastern Amazon. **Master of Science Thesis**, Pennsylvania State University, Department of Agronomy, 159p.

AWARDS, SCHOLARSHIPS AND FELLOWSHIPS

- CNPq/LBA Scholarship to conduct training on advanced remote sensing techniques at UCSB, EUA, August 2000.
- Research grant: Monitoramento das áreas de exploração madeireira na Amazônia (Monitoring Areas of Selective Logging in the Amazon - Ref. 0102), sponsored by Programa Piloto para Proteção das Florestas Tropicais do Brasil PPG7, 2000-2001.
- ITTO Fellowship Program to develop GIS applications to forest management in the Amazon, 1997.
- USAID Scholarship (ADC Brazil Training Program/SUNY) to conduct M.Sc. at Pennsylvania State University, EUA, January 1996 to May 1997.
- USAID Scholarship (ADC Brazil Training Program/SUNY) to conduct training on remote sensing and GIS at Pennsylvania State University, EUA, October 1993 to May 1994.

FIELDS OF STUDY

Major Field: Remote Sensing

ABSTRACT

Mapping and Spatiotemporal Characterization of Degraded Forests in the Brazilian Amazon through Remote Sensing

by

Carlos Moreira de Souza Jr.

Large forested areas have recently been impoverished by degradation caused by selective logging, forest fires and fragmentation in the Amazon region, causing partial change of the original forest structure and composition. As opposed to deforestation that has been monitored with Landsat images since the late 70's, degraded forests have not been monitored in the Amazon region. In this dissertation, remote sensing techniques for identifying and mapping unambiguously degraded forests with Landsat images are proposed. The test area was the region of Sinop, located in the state of Mato Grosso, Brazil. This region was selected because a gradient of degraded forest environments exist and a robust time-series of Landsat images and forest transect data were available. First, statistical analyses were applied to identify the best set of spectral information extracted from Landsat images to detect several types of degraded forest environments. Fraction images derived from Spectral Mixture Analysis (SMA) were the best type of information for that purpose.

A new spectral index based on fraction images – Normalized Difference Fraction Index (NDFI) - was proposed to enhance the detection of canopy damaged areas in degraded forests. Second, a contextual classification algorithm was implemented to separate unambiguously forest degradation caused by anthropogenic activities from natural forest disturbances. These techniques were validated using forest transects and high resolution aerial videography images and proved to be highly accurate. Next, these techniques were applied to a time-series data set of Landsat images, encompassing 20 years, to evaluate the relationship between forest degradation and deforestation. The most important finding of the forest change detection analysis was that forest degradation and deforestation are independent events in the study area, making worse the current forest impacts in the Amazon region. Finally, the techniques developed and tested in the Sinop region were successfully applied to forty Landsat images covering other regions of the Brazilian Amazon. Standard fractions and NDFI images were computed for these other regions and both physically and spatially consistent results were obtained. An automated decision tree classification using genetic algorithm was implemented successfully to classify land cover types and sub-classes of degraded forests. The remote sensing techniques proposed in this dissertation are fully automated and have the potential to be used in tropical forest monitoring programs.

TABLE OF CONTENTS

ACKNOWLEDGEMENTS	v
VITA OF CARLOS MOREIRA DE SOUZA JR.	vi
ABSTRACT	viii
TABLE OF CONTENTS	x
LIST OF FIGURES.....	xv
LIST OF TABLES	xix
CHAPTER I: Introduction	1
1.1 Overview and Research Significance.....	1
1.2 Objectives.....	5
1.3 Summary of the Chapters.....	6
CHAPTER II: Multi-temporal Analysis of Degraded Forests in the Southern Brazilian Amazon.....	8
2.1 Introduction	8
2.2 Study Area and Forest Degradation Patterns	10
2.3 Data set.....	13
2.3.1 Satellite Imagery Data.....	13
2.3.2 Forest Transect Inventory	14
2.4 Methodology	14
2.4.1 Pre-Processing: image registration, atmospheric correction and inter-calibration.....	16
2.4.2 Endmember Selection	17

2.4.3 Spectral Mixture Analysis.....	18
2.4.4 Vegetation and Near Infrared Indices	19
2.4.5 Class Separability and Temporal Change Analyses.....	20
2.5 Results	22
2.5.1 First Year Forest Degradation Separability	22
a) Reflectance.....	22
b) Vegetation Indices	23
c) Fraction Images.....	29
2.5.2 Multi-year Forest Degradation Separability	30
a) Reflectance and Indices	31
b) Fraction Images.....	32
2.5.3 Optimal Temporal Resolution.....	33
2.6 Discussion	35
2.6.1 Degraded Forest Mapping Potential	35
2.6.2 Linking Field Measurements with Fraction Images.....	39
2.6.3 Monitoring Forest Degradation: practical application and challenges	41
2.7 Conclusion.....	43
CHAPTER III: Combining Spectral and Spatial Information to Map Canopy	
Damages from Selective Logging and Forest Fires	46
3.1 Introduction	46
3.2 Study Area.....	49
3.3 Data Set	50

3.3.1 Forest transect inventory	50
3.3.2 Satellite Imagery Data.....	52
3.4 Methodology	53
3.4.1 Image Processing	53
a) Image Registration and Radiometric Calibration	53
b) Atmospheric correction and Inter-calibration.....	53
3.4.2 Spectral Mixture Analysis - SMA.....	55
3.4.3 Normalized Difference Fraction Index – NDFI	57
3.4.4 Statistical Analysis	58
3.4.5 Contextual Classification Algorithm.....	59
3.4.6 Accuracy Assessment.....	62
3.5 Results	64
3.5.1 Class Separability.....	64
3.5.2 Forest Canopy Damage Detection	69
3.5.3 Canopy Damage Classification	73
3.6. Discussion	77
3.7 Conclusions	81
CHAPTER IV: Long Term Forest Degradation Mapping and Change Detection in the Southern Brazilian Amazon Forests.....	82
4.1. Introduction.....	82
4.2. Study Area.....	85
4.3 Data set.....	85
4.4. Methodology	86

4.4.1 Pre-processing	86
a) Georeferencing and Registration	86
b) Atmospheric Correction.....	87
c) Image Inter-calibration.....	87
4.4.2 Canopy Damage Classification	89
4.4.3 Forest Change Detection.....	92
4.5. Results	92
4.5.1 Image Classification.....	92
4.5.2 Forest Change Detection.....	94
4.5.3 Deforestation and Forest Degradation Rates	95
4.5.4 Canopy Damage Age and Frequency.....	98
4.6. Discussion	102
4.7. Conclusions	104
CHAPTER V: Generic Spectral Mixture Analysis and Decision Tree Classification	
for Monitoring Forest Changes in the Brazilian Amazon.....	105
5.1. Introduction.....	105
5.2 Methods.....	109
5.2.1 Spectral Mixture Analysis – SMA	109
a) Background	109
b) Generic Endmembers for the Amazon Region	111
5.2.2 Genetic Decision Tree Classification.....	116
a) Decision Trees.....	116
b) Genetic Decision Tree Classification Algorithm.....	118

5.4 Results	121
5.4.1 Standard Fraction Images.....	121
5.4.2 Generic Decision Tree Classification	128
5.4.3 Cross-Regional Comparison	131
5.5 Discussion	133
Conclusions	140
CHAPTER VI: Summary and Conclusions	141
6.1 Objective I.....	141
6.2 Objective II.....	143
6.3 Objective III	144
6.3 Objective IV	146
6.4 Future Research.....	147
References	151

LIST OF FIGURES

Figure 1. Map of the study area showing the location of the forest transects used to extract satellite pixel data.....	11
Figure 2. Means and standard deviations (vertical error bar) of intact forest and degraded forests classes as measured by Landsat bands: (a) reflectance; (b) vegetation and infrared indices; and (c) fraction images.	25
Figure 3. Delta change of (a) reflectance, (b) vegetation and infrared indices and (c) fraction images, computed by subtracting the mean value of Intact Forest from the mean value of each degraded forest class.	29
Figure 4. Change in fractions mean fraction values trough time for: (a) Non-mechanized Logging, (b) Managed Logging, (c) Conventional Logging and (d) Logged and Burned.	37
Figure 5. Examples of forest degradation processes and temporal changes as detected using fraction images derived from SMA (Red = Soil, Green = Green Vegetation, Blue = NPV).	40
Figure 6. Map of the study area showing the location of the forest transects and of the aerial videography transects.	51
Figure 7. Example of aerial videography moisaic used as reference data for the map accuracy assessment.	62
Figure 8. Delta changes of fractions and NDFI, calculated by subtracting the mean value of Intact Forest from the mean value of each degraded forest class.	68

Figure 9. Examples of forest degradation processes and temporal changes as detected the NDFI band.....	71
Figure 10. Fractions and NDFI means and standard deviation (vertical error bar) of the main environments found in degraded forests areas.....	72
Figure 11. Canopy damage classification examples obtained with the CCA classifier.	75
Figure 12. Image processing chain conducted in the forest change detection analyses.	88
Figure 13. Forest Change detected with the multi-temporal analysis.....	92
Figure 14. Areal percent of Forest, Canopy Damage and Non-forest quantified in the forest change detection analysis.....	95
Figure 15. Annualized deforestation and forest degradation rates.....	96
Figure 16. Canopy Damage age map of two sub-sets (15 km x 15 km) of the study area. In (a) selective logging damage is more common and in (b) forest fires are the major causes of canopy damages.	99
Figure 17. Average areal percentage of the Canopy Damage class converted by deforestation as a function of how many times the forest had been degraded..	100
Figure 18. Average Canopy Damage area converted by deforestation as a function of degradation age. The grey regions represent the percentage of degraded forest converted by deforestation, while the white one the cumulative percentage of degraded forest converted by deforestation.	102
Figure 19. Landsat scenes processed with the standard image endmembers to generate fraction images.	112
Figure 20. Image processing chain to generate standard fraction and NDFI images over the Amazon region.	113

Figure 21. Scatter plot matrix showing the PPI results.....	114
Figure 22. Image scatter plots used to identify standard image endmembers for the Brazilian Amazon.....	115
Figure 23. Binary decision tree classification components and structure.....	117
Figure 24. Genetic decision tree algorithm.....	120
Figure 25. Image endmembers defined based on the topology of the Landsat n- dimensional spectral space. Endmember bundles of each endmember were obtained from the PPI results. The mean of each endmember bundle is plotted in a dashed line.....	122
Figure 26. Examples of fraction (R=NPV, G=GV, B=Soil color composite) and NDFI images obtained with the standard image endmembers for areas Paragominas (a), Santarém (b) and Ji-paraná (c).....	127
Figure 27. Accuracy of the tree generations and mutated trees for the Land Cover (a) and Forest Degradation (b) classification schemes.....	130
Figure 28. Fractions means and standard deviation (vertical error bar) estimated using reference endmembers (a) and standard image endmembers (b) for the Sinop transects.	135
Figure 29. Examples of forest (green) and non-forest (magenta) maps obtained with the GDTCA. The Landsat scene is shown on the left; and on the right the sub- area indicated with the black box.....	138
Figure 30. Example of forest canopy damage sub-classification for the transects 3, 4 and 5. In: a) forest degradation classes: burned (brown), logged (yellow) and	

clear cut (black). The corresponding fraction color composite (R=NPV, G=GV and B=Soil) of the classified area is shown in (b). 139

LIST OF TABLES

Table 1. Characterization of the forest classes defined at the field scale.....	12
Table 2. Landsat TM/ETM+ data used in this study (orbit/point = 226/068).....	13
Table 3. Classification and disturbance history of the forest transects of the study area.	15
Table 4. Means and standard deviation of fractions, reflectance and indices of forest degradation classes through time. Numbers in bold face denote significant differences between Intact Forest (Time=0) and degraded forest classes (Time=1,..., 4) at $P < 0.01$ utilizing a Tukey test.	26
Table 5. Biophysical properties of the Intact Forest class and of the degraded forest classes estimated from the forest inventories.....	45
Table 6. Means and standard deviations for Intact Forest and the forest degradation classes. Different superscript letters represent significant statistical difference among classes using the Tukey test at $P < 0.01$. For example, Intact Forest and Non-mechanized Logging showed the same letter (a) meaning that their means are not significantly different using NDFI, whereas Managed Logging (b), Conventional Logging (c) and Logged and Burned showed different letters meaning that there are significant statistical differences among them.	67
Table 7. Accuracy assessment results of the CCA classifier: a) using the NDFI as the search image for CCA; b) using GV as the search image for CCA.	76
Table 8. Percentage of Forest and Canopy Damage changes quantified in the forest change detection analysis relative to the study area.	97

Table 9. Means and standard deviations of standard fraction images and NDFI for dense forest, transitional forest and open forest found in different regions in the Brazilian Amazon.....	124
Table 10. Accuracy of the random trees for land cover, forest degradation and degradation intensity.....	129

CHAPTER I: Introduction

1.1 Overview and Research Significance

The Brazilian Amazon rainforest covers about 40% of the remaining tropical forests in the world. Its role in keeping biodiversity, regulating regional climate and continental hydrological cycles, and storing carbon has been largely recognized (Fearnside 1996; Skole and Tucker, 1993). Over the past 30 years, the Brazilian Amazon rainforest, referred to as the Amazon from now on, has been rapidly converted to pastures and agricultural areas through deforestation (Fearnside 1989; Moran 1993; Alves and Skole, 1996). Until the year 2000, estimates of deforestation from Landsat images for the Amazon region showed that 587 thousand km² had already been deforested. When added to the partial estimates for 2001 through 2003, the deforested area reaches about 650 thousand km², with an average rate of forest loss of about 23,000 km² yr⁻¹ for this period (INPE, 2003).

Tropical deforestation has a direct impact on world wide levels of biodiversity, and on regional hydrological, biogeochemical and climate cycles (e.g., Bazzaz, 1998; Giambelluca, 2002; Houghton et al., 2000). Because of these environmental problems, Amazonian deforestation and its related impacts have called the attention of the scientific, environmental and policy making communities. For this reason, deforestation in the Amazon has been well documented, and monitoring programs that use satellite images to map deforestation have been conducted, at both national (e.g., PRODES – *Monitoramento da Floresta Amazônica Brasileira por Satélite* - by

the Brazilian space agency INPE) and international (e.g., TREES – Tropical Ecosystem Environment Observation by Satellites - by the Joint Research Center from the European Community) levels.

Deforestation also fragments the landscape and creates more edges between forests and non-forested areas (Laurance et al., 2000). By 1988, the forest area at risk of edge effect (< 1 km from the forest edge) in the Amazon was about 150% larger than the total area deforested (Skole and Tuchker, 1993). Forest edges are affected by solar radiation, wind and agricultural fires (Cochrane and Laurance, 2002). Forest inventory studies have shown that the biomass of forest edges decreases drastically within 100 meters of the edges (Laurance et al., 1998). The species diversity and composition also changes in the forest edges and the edge effect could contribute significantly to the emission of green house gases such as CO₂ (Laurance et al., 1998). All of these factors lead to a more degraded forest environment along the forest edges.

Unfortunately, deforestation and its associated forest fragmentation impacts are not the only threat to the integrity of the Amazon forests. Large forested areas have recently been impoverished by degradation caused by selective logging (Uhl and Vieira 1989; Uhl *et al.* 1997; Nepstad *et al.* 1999), forest fires (Uhl and Kauffman 1990, Cochrane and Shultz, 1999; Nepstad et al., 1999), and forest fragmentation (Laurance et al. 2000). Forest degradation changes partially the original structure and composition of the forests by decreasing forest biomass (Cochrane and Schulze

1999; Gerwing and Farias 2000), creating favorable environments for non-native species (Vidal *et al.* 1997), and causing local species extinction (Martini *et al.* 1994).

It has been estimated through field surveys and socio-economic interviews that up to 10,000-15,000 km² are logged, 80,000 km² are burned, and 38,000km² are fragmented each year (Nepstad *et al.*, 1999), making the area affected by forest degradation much larger than the area deforested annually in the Amazon. Estimates from Landsat images do not agree with the field estimates and with each other. For example, Santos *et al.* (2002) estimated from Landsat images that the area affected by selective logging in 1992 and 1996 were 1,000 km² and 1,571 km², respectively. Matricardi *et al.*, (2001) presented significantly different estimates for these years – 5,627 km² for 1992 and 9,449 km² for 1996. The differences in these satellite image estimates are associated with the methodology and mapping scale. The former estimates were based on visual interpretation of Landsat images at a 1:250,000 scale whereas the later one used a hybrid classification approach that combines automated classification (Souza Jr. and Barreto, 2000) and visual interpretation.

As opposed to deforestation, degraded forests have not been monitored on a regular basis in the Amazon region. There exist, however, a few site-specific studies that characterize degraded forests at the field scale (e.g., Johns *et al.* 1996; Gerwing 2002; Pereira *et al.*, 2002). Remote sensing techniques to map the area affected by selective logging (e.g., Stone and Lefebvre 1998; Souza Jr. and Barreto 2000) and burned forests (Cochrane and Souza Jr., 1998) have also been proposed. Additionally, there are some attempts to correlate field inventory data on forest

degradation with remotely sensed data (Asner et al., 2002; Souza Jr. et al., 2003).

The ecological field studies have shown that there are several levels of forest degradation due to different intensities and frequencies of selective logging, burning and fragmentation (Barros and Uhl 1995; Verissimo *et al.* 1995; Johns *et al.* 1996; Cochrane and Shultz, 1999; Gerwing 2002) which creates a continuum from intact forests to degraded forests. Thus, defining the boundaries between intact forests and the classes of degraded forests with remotely-sensed data becomes a challenge. This is one of the problems investigated in this Ph.D. research.

Degraded forests change rapidly, usually within one to two years, due to canopy closure and invasion of non-native species such as lianas (Guariguata and Dupuy 1997; Magnusson *et al.* 1999; Gerwing and Farias 2000). This rapid change in the degraded forest environment may cause degraded forests areas to be misclassified as intact forests, when using remote sensing data acquired with Landsat TM/ETM (Thematic Mapper/Enhanced Thematic Mapper) or SPOT 4 (*Satellite Pour L'observation de la Terre*). In addition, degraded forest can be converted to agricultural and pasture fields through deforestation, but the rate of conversion has not been investigated. These land cover change issues are another problem examined in this study. Finally, a generic image classification approach is proposed to map unambiguously forest degradation caused by anthropogenic and natural disturbances.

Even though forest fragmentation is not an object of study in this dissertation, the remote sensing methods proposed here have the potential to map forest fragments and detect forest degradation along forest edges, such as forest burning. The research

issues presented here are also relevant to improving carbon flux models in the Brazilian Amazon. Forest degradation has a direct impact on biomass loss which, although partially compensated by regeneration, still results in a net loss of carbon (Gerwing, 2002). Therefore, mapping and quantifying forest degradation changes reduce the large uncertainty in carbon balance existing in the Brazilian Amazon (Houghton et al. 2001).

This study was conducted in Sinop, Mato Grosso State (Figure 1), which is ideal for investigating the problems described above because it has a gradient of forest degradation classes, and because a robust time-series of Landsat imagery encompassing 20 years is available. Additionally, aerial videography and high spatial resolution satellite imagery is available for map accuracy assessment. The Landsat images were chosen because they offer enough spectral and spatial resolutions to monitor the Brazilian Amazon forests, and because historical data covering more than 30 years is available for the region. Finally, the image classification methods developed in this research were tested extensively through out the Amazon region.

1.2 Objectives

This research has five major objectives addressing one or more research questions. The objectives aim to:

- I) Characterize the spectral and temporal properties of degraded forests using Landsat TM/ETM+ images; the following questions were addressed:

- a. What is the best set of spectral information to detect forest degradation?
 - b. How long do the degraded forest ‘signatures’ persist?
 - c. What is the optimal temporal resolution for mapping degraded forests?
- II) Develop a technique that combines spectral and spatial information to enhance unambiguously the detection and mapping of canopy damage caused by forest degradation.
- III) Characterize the spatiotemporal dynamics of degraded forests; the following questions were addressed in this objective:
- a. What is the fate of the degraded forests?
 - b. What is the rate of forest degradation?
 - c. How much of the degraded forests is converted by deforestation?
- IV) Develop a generic image processing and classification approach for monitoring the Amazon forests.
- V) Compare relative importance of selective logging across regions.

1.3 Summary of the Chapters

This section describes chapters II through VI of this dissertation. Chapter II focuses on research objective I. A statistical multi-temporal analysis is described to evaluate the capability of reflectance, vegetation indices (NDVI and SAVI), normalized difference infrared indices (NDII5 and NDII7) and fraction images,

derived from spectral mixture analysis (SMA), to distinguish Intact Forest from four classes of degraded forests: Non-mechanized Logging, Managed Logging, Conventional Logging and Logged and Burned. For this purpose, a robust time-series data set of Landsat TM/ETM+ images was used in conjunction with forest inventory transects and data on forest disturbance history.

Chapter III focuses on objective II, where a new spectral index, the Normalized Difference Fraction Index (NDFI), is proposed for enhanced detection of forest canopy damage caused by selective logging activities and associated forest fires. The NDFI synthesizes information from several fraction images derived from spectral mixture models. In addition, a contextual classification algorithm (CCA) is presented for accurate mapping of logging- and fire-derived canopy damages. The combination of the new NDFI spectral index with the CCA allows separation of canopy changes due to logging and associated forest fires from those caused by other natural disturbances.

Chapter IV presents the results of the multi-temporal forest change analysis developed to address the research questions of objective III. A robust time-series Landsat imagery data set, encompassing 20 years, was used for this purpose. Chapter V focuses on objectives IV and V, and describes an automatic generic image processing and classification approach to monitor forest degradation in the Brazilian Amazon and provides a comparison of the relative importance of selective logging across regions. Finally, Chapter VI summarizes the main findings of each research objective and points out to future research directions.

CHAPTER II: Multi-temporal Analysis of Degraded Forests in the Southern Brazilian Amazon¹

2.1 Introduction

Selective logging, fragmentation and forest burning are the main factors contributing to forest degradation of Brazilian Amazon. The major impacts of these anthropogenic disturbances include: decreasing forest biomass (Cochrane and Schulze, 1999; Gerwing 2002), creating favorable environments for non-native species (Vidal et al., 1997), and causing local species extinctions (Martini et al., 1994). It has been estimated through field surveys and socio-economic interviews that up to 10,000-15,000 km² are logged, 80,000 km² are burned, and 38,000km² are fragmented each year (Nepstad et al., 1999), making the area affected by forest degradation much larger than the area deforested annually in the Amazon, which averages around 18,000 km²year⁻¹ (INPE, 2003).

Several methodologies have been developed for mapping selectively logged and burned forests in the Brazilian Amazon using multispectral satellite images. Examples include visual interpretation (Watrin and Rocha, 1992), supervised classification (Stone and Lefebvre, 1998), soil fraction images obtained through spectral mixture analysis (SMA) (Souza Jr. and Barreto, 2000; Monteiro et al., 2003), contextual clustering (Sgrenzaroli et al., 2002) and decision tree classification

¹ Accepted for publication: Souza Jr., et al. (in press a).

(Souza et al., 2003). Additionally, efforts have been made to link forest biophysical properties of selectively logged forests with remotely sensed data (Asner et al., 2002, Souza Jr. et al., 2000). Burned forests have also been successfully mapped with non-photosynthetic vegetation (NPV) (Roberts et al., 1993) fraction images in the eastern Amazon (Cochrane and Souza Jr., 1998).

To date, few studies have employed multi-temporal data to map forest degradation, which is an important attribute for monitoring tropical forests (Lambin, 1999). Single date or infrequent satellite acquisitions represent a potential source of error due to rapid canopy closure and regeneration of degraded forest, leading to misclassification of degraded forests as intact (Stone and Lefebvre, 1998).

Furthermore, while several authors have used at least two dates to characterize selectively logged forests (Stone and Lefebvre, 1998; Souza and Barreto, 2000; Monteiro et al., 2003, Asner et al., 2002; Asner et al., 2004a), the same types of temporal analysis have not been applied to characterize burned forest dynamics. Currently, no study has used high temporal frequency images (i.e., at least one per year) to characterize change dynamics of the full range of forest degradation classes existing in the Amazon region. As a result, the optimal temporal resolution for mapping degraded forests has yet to be determined. In this study, I seek an understanding of the temporal dynamics of degraded forests. Specifically, the following questions are addressed: 1) how long do the degraded forest ‘signatures’ persist on Landsat images?; and 2) what is the optimal temporal resolution for mapping degraded forests with Landsat images? To answer these questions, changes

in reflectance, vegetation and infrared indices, and fraction images derived from SMA are evaluated over a chronosequence of well-characterized degraded forest types. Image analysis utilized a robust time series data set of Landsat TM/ETM+ images, encompassing 20 years of images acquired for every year. Field data included nineteen forest transect inventories covering all types of degraded forests found in the study area.

2.2 Study Area and Forest Degradation Patterns

The study area is located in the state of Mato Grosso, in the vicinity of Sinop and Cláudia sawmill centers (Figure 1). Transitional forest, between ‘cerrado’ and dense forest, is the predominant vegetation type in the region. The topography varies from flat to undulating terrain, on latosol soils, and the average annual precipitation is 2,000 mm (RADAMBRASIL, 1981).

Selective logging in this area is characterized by the harvesting of high quality timber species. The harvesting intensity ranges from 10 to 40 m³/ha and is predominantly unplanned (Monteiro et al., 2004). Three types of selectively logged forest were identified in the field: Non-mechanized Logging, Managed Logging and Conventional Logging forests (Table 1). At the field scale, logged forests are composed of three main environments: i) forest islands that were not disturbed because of poor access due to topography and rivers, or due to the lack of commercial timber species; ii) areas where the forest had been cleared to create roads for machine movements (skidders and trucks) and log landings to store the harvested

timber; and iii) canopy damaged forests (i.e., harvested areas and areas damaged by tree falls and machine movements). This pattern is similar to the logging pattern found in dense forest areas in the eastern Amazon (Verissimo et al., 1992; Johns et al., 1996), differing only in the harvesting intensity (30-40 m³/ha).

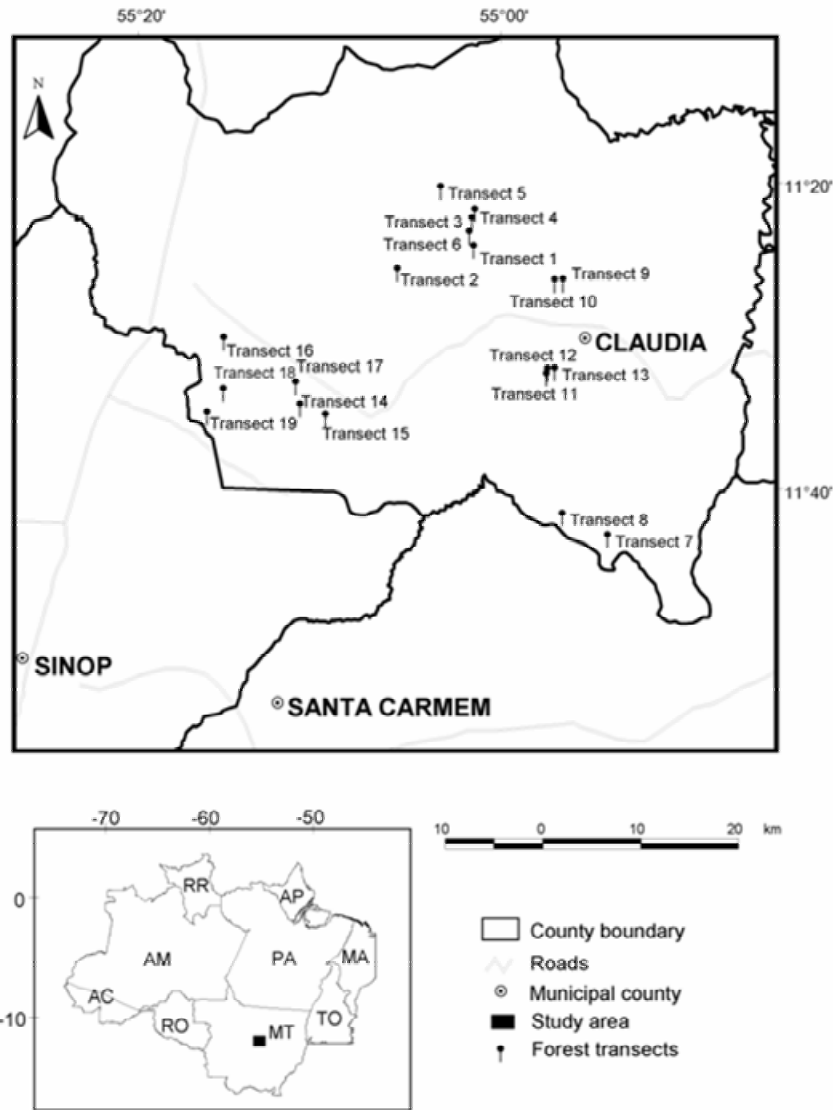


Figure 1. Map of the study area showing the location of the forest transects used to extract satellite pixel data.

Table 1. Characterization of the forest classes defined at the field scale.

Forest class	Field Description
Intact Forest	Mature and undisturbed forest
Non-mechanized logging	Logged forest without the use of vehicles such as skidders and trucks, also known as traditional logging. Log landings, roads and skid trails are not built.
Managed logging	Planned selective logging where a tree inventory is conducted, followed by planned roads, log landings, skid trails and tree fall to reduce harvesting impacts.
Conventional Logging	Conventional unplanned selective logging using skidders and trucks. Log landings, roads and skid trails are built.
Logged and burned	Either non-mechanized or conventionally logged forests that have subsequently been damaged by forest fires.

Forest burning is also frequent in this region, acting synergistically with selective logging to increase forest degradation damages (Monteiro et al., 2004). Selectively logged forests can burn when agricultural fires escape unintentionally from adjacent areas. Prolonged forest surface fires eventually reach the heat tolerance of trees and lianas, which can lead to tree mortality (Holdsworth and Uhl, 1997; Cochrane and Shultz, 1999). As a result, the forests become more degraded and more fuel is accumulated on the forest floor (Cochrane et al., 1999). A second forest surface fire event will likely burn the forest floor more severely and kill more trees (Table 1).

2.3 Data set

2.3.1 Satellite Imagery Data

Eighteen Landsat Thematic Mapper 5 (TM) images and three Landsat Enhanced Thematic Mapper (ETM+) images, acquired between June 1984 and July 2004, were used in this study (Table 2). The images were acquired through the Tropical Rain Forest Information Center (TRFIC) and the Brazilian Space Agency (INPE).

Table 2. Landsat TM/ETM+ data used in this study (orbit/point = 226/068).

Year	Landsat Sensor	Month, Day	Source
1984	TM5	June, 14	INPE
1985	TM5	July, 3	INPE
1986	TM5	August, 7	INPE
1987	TM5	June, 25	INPE
1988	TM5	August, 11	INPE
1989	TM5	August, 31	INPE
1990	TM5	August, 02	INPE
1991	TM5	July, 02	INPE
1992	TM5	July, 25	INPE
1993	TM5	August, 26	INPE
1994	TM5	July, 02	INPE
1995	TM5	June, 13	INPE
1996	TM5	July, 01	TRFIC
1997	TM5	August, 5	INPE
1998	TM5	June, 6	INPE
1999	ETM+	August, 19	TRFIC
2000	TM5	June, 26	INPE
2001	ETM+	August, 8	INPE
2002	ETM+	July, 10	INPE
2003	TM5	August, 6	INPE
2004	TM5	June, 5	INPE

¹ Brazilian Space Agency

² Tropical Rain Forest Information Center

2.3.2 Forest Transect Inventory

Nineteen forest transect inventories were conducted in the study area (Figure 1; Tables 3). For the purposes of this study, information about logging and fire histories, ground cover, canopy cover and biomass was used to classify the forest degradation classes found at the field scale into four degradation classes: Non-mechanized Logging, Managed Logging, Conventional Logging and Logged and Burned (Tables 1 and 3). The forest inventories were conducted following the field protocol proposed by Gerwing (2002) to characterize degraded forest in the eastern Amazon. This method has been successfully applied to characterize biophysical properties and dynamics of degraded forests in transitional forests (Monteiro et al., 2004).

All trees with Diameter at Breast Height (DBH) greater than 10 cm were mapped along a 10 m by 500 m transect. In addition, ten sub-parcels (10 m x 10 m) were created every 50 meters along each transect. All trees were mapped within the sub-parcels and ground cover and canopy gaps were estimated using a hemispherical lens and densiometer. Above ground biomass was estimated using allometric equations available in the literature (Gerwing, 2002; Monteiro et al., 2004), adapted specifically by Gerwing (2002), for degraded forests and estimating vine biomass.

2.4 Methodology

Table 3. Classification and disturbance history of the forest transects of the study area.

Class	Transect Number	Latitude	Longitude	Year of the First Forest Degradation Event	Time since first Logging (years)	Time since last Logging (years)	Number of Times Logged	Volume Harvested (m ³ /ha)	Number of times Burned
Intact	11	-11.546110	-54.933040	-	-	-	-	-	-
Intact	12	-11.540960	-54.931850	-	-	-	-	-	-
Intact	13	-11.540550	-54.923930	-	-	-	-	-	-
Intact	14	-11.579852	-55.200937	-	-	-	-	-	-
Non-mechanized Logging	1	-11.407170	-55.011950	1999	2	2	1	10	-
Non-mechanized Logging	2	-11.432190	-55.095040	1996	5	5	1	10	-
Non-mechanized Logging	6	-11.391950	-55.016940	1999	2	2	1	10	-
Non-mechanized Logging	9	-11.443970	-54.924020	1990	11	10	2	25	-
Non-mechanized Logging	10	-11.443660	-54.914810	1987	14	10	2	25	-
Managed Logging	15	-11.5910674	-55.1730850	2000	4	4	1	38	-
Managed Logging	16	-11.5068618	-55.2838944	2001	3	3	1	32	-
Managed Logging	17	-11.555747	-55.205766	2002	2	2	1	40	-
Managed Logging	18	-11.562731	-55.284380	2003	1	1	1	40	-
Managed Logging	19	-11.588599	-55.302101	2004	0	0	1	25	-
Conventional Logging	7	-11.721690	-54.866760	1997	4	4	1	10	-
Conventional Logging	8	-11.697990	-54.915840	1993	8	8	1	10	-
Logged and burned	3	-11.367190	-55.010760	1990	2	2	1	25	1
Logged and burned	4	-11.376690	-55.013770	1999	2	2	1	25	1
Logged and burned	5	-11.342810	-55.047980	1999	2	2	1	25	1

2.4.1 Pre-Processing: image registration, atmospheric correction and inter-calibration

The images were registered and radiometrically inter-calibrated in order to allow the detection of forest change over time. The Landsat ETM+ image acquired in 1999 was georeferenced using twenty-five control points extracted from NASA GeoCover 2000 Mosaic (<https://zulu.ssc.nasa.gov/mrsid/>). Next, the 1999 georectified Landsat image was used as the reference image to register the images acquired on the other dates (Table 2). The registration was based on the triangulation algorithm and nearest neighborhood resampling available in The Environment for Visualizing Images 4.0 software (ENVI; Research Systems, Boulder, CO), using at least 14 image control points. The Root Mean Squared (RMS) varied from 0.53 to 0.97, which assures that the changes detected over time were not contaminated by misregistration (Verbyla and Boles, 2000).

The Landsat ETM+ image from 1999 was first radiometrically corrected using the gains and offset provided in the image metafile. Next, an atmospheric correction was performed using Atmospheric Correction Now 4.0 (ACORN: Analytical Imaging & Geophysics, Boulder, CO). Visibility and water vapor parameters of the atmospheric correction model were determined by a trial-and-error sensitivity analysis of a dark object reflectance (a lake). The final parameters were estimated when the expected reflectance values of the dark object were found. The fixed water vapor was 40 millimeters, and image atmosphere visibility 25 kilometers.

The other images (Table 2) were inter-calibrated to the reflectance image using a relative radiometric calibration approach (Roberts et al., 1998; Furby and Campbell, 2001). This technique assumes that the atmosphere is uniform over the study area, and that invariant ground targets can be found over time. Invariant targets representing forest, second growth, green pasture, bare soil and water were selected for each image pair formed by the 1999 reference image and an uncalibrated image. A linear regression was estimated using the pixel mean values, extracted from a 3 by 3 pixel area, of the invariant targets for each band. These coefficients normalize the uncalibrated images to the 1999 reference image, converting Digital Numbers of the uncalibrated images to reflectance.

2.4.2 Endmember Selection

Image endmembers representing vegetation, soil and NPV were extracted from the reference reflectance image. Shade was assigned zero percent reflectance at all wavelengths. The pixel-purity-index (PPI), available in ENVI 4.0 (Boardman et al., 1995) was used to identify image endmember candidates. Five image subsets (500x500 pixels), representing the variety of land cover types found in the images, were used as input for the PPI algorithm. The PPI result was used to identify the pixel location in the original image and extract the spectral curves of these pixels. The final image endmembers were selected based on the pixel location in the Landsat reflectance spectra with the aid of an n-dimensional visualization tool available in ENVI. The pixels located at the extremes of the data cloud of the Landsat spectral space were selected as candidate endmembers. The final

endmembers were selected based on the spectral shape and image context (e.g., soil spectra are mostly associated with unpaved roads and NPV with pasture having senesced vegetation).

2.4.3 Spectral Mixture Analysis

Spectral Mixture Analysis – SMA – (Adams et al., 1993) assumes that the image spectra are formed by a linear combination of n pure spectra, such that:

$$R_b = \sum_{i=1}^n F_i R_{i,b} + \varepsilon_b \quad (1)$$

for

$$\sum_{i=1}^n F_i = 1 \quad (2)$$

where R_b is the reflectance in band b , F_i the fraction of endmember i , $R_{i,b}$ is the reflectance for endmember i , in band b , and ε_b is the residual error for each band. The SMA model error is estimated for each image pixel by computing the **RMS** error, given by:

$$\text{RMS} = \left[n^{-1} \sum_{b=1}^n \varepsilon_b \right]^{1/2} \quad (3)$$

Mixture models were applied to each date using the inter-calibrated image endmembers, except the reference image, which was the one used to extract the endmembers. The mixing model results were evaluated as proposed by Adams et al. (1993). First, the RMS images were inspected and models with RMS values greater than 5% were discarded from the fraction change analysis. Next, fraction images

were evaluated and interpreted in terms of field context and spatial distribution. For example, high abundance of soils is mostly associated with dirt roads and high NPV is usually found in pastures. Finally, the histograms of the fraction images were inspected to quantify the percentage of pixels lying outside the range of zero to 100% and to evaluate fraction value consistency over time (i.e., intact forest shows approximately stable values over time). Only models with at least 98% of the values within zero to 100% and those that showed mean fraction value consistency over time were kept. For the models that did not pass one of these tests new invariant targets were collected to improve the image inter-calibration coefficients and a new SMA model was run until the criterion was reached.

2.4.4 Vegetation and Near Infrared Indices

Two vegetation indices and two normalized difference infrared indices (NDII) were selected for assessing if it was possible to distinguish Intact Forest from the degraded forest classes. The vegetation indices chosen were the normalized difference vegetation index (NDVI; Rouse et al., 1974), and the soil adjusted vegetation index (SAVI; Huete, 1988). These vegetation indices use reflectance measurements from Landsat band 3 (ρ_{b3}) and band 4 (ρ_{b4}), and are computed with the following equations:

$$\text{NDVI} = (\rho_{b4} - \rho_{b3}) / (\rho_{b4} + \rho_{b3}) \quad (4)$$

$$\text{SAVI} = 1.5 * (\rho_{b4} - \rho_{b3}) / (\rho_{b4} + \rho_{b3} + 0.5) \quad (5)$$

The normalized difference infrared indices (NDII) chosen are the ones proposed by Hunt and Rock (1989) to identify forest disturbances associated with water content. These NDII indices are computed using Landsat band 4 (ρ_{b4}), band 5 (ρ_{b5}) and band 7 (ρ_{b7}), and are given by:

$$\text{NDII5} = (\rho_{b4} - \rho_{b5}) / (\rho_{b4} + \rho_{b5}) \quad (6)$$

$$\text{NDII7} = (\rho_{b4} - \rho_{b7}) / (\rho_{b4} + \rho_{b7}) \quad (7)$$

2.4.5 Class Separability and Temporal Change Analyses

Using the information on logging and fire histories acquired during field research and the Landsat time-series, it was possible to identify the date prior to degradation, representing the image condition of Intact Forest. Next, reflectance and fractions of GV, NPV, Shade and Soil were extracted using 30 pixels selected randomly within a buffer region of 5 pixels along each transect. Random pixels located in logging roads and log landings were excluded from the analysis because changes from Intact Forest to clear-cut are relatively easier to identify (Souza Jr. and Barreto, 2000; Monteiro et al., 2003). Less than one percent of the random pixels were excluded following this criterion. The vegetation and infrared indices were computed using the reflectance values extracted from the 30 randomly selected pixels. This procedure allowed us to build a time-series data set of reflectance, vegetation and infrared indices and fraction values covering the time prior to degradation (i.e., degradation age equals zero) to up to four years after the event.

The next steps were to perform a class separability and temporal change analyses based on reflectance, vegetation and infrared indices, and fractions variables. The Tukey test (Ott, 1992), available in the R Language (<http://www.r-project.org/>), was used to evaluate if the Intact Forest and the forest degradation classes could be separated from each other, and to define for how long the degradation classes could be distinguished from the Intact Forest class over a period of four years. The Tukey test was run at a 99% confidence interval ($P < 0.01$).

The Tukey test performs a multicomparison of the population means of the Intact Forest and degraded forest classes, i.e., tests the mean of a population against the mean of each other population. For the purpose of the class separability analysis, the populations are represented by the data acquired prior to the degradation event representing Intact Forest, and the year right after degradation representing the degraded forest classes (Non-mechanized Logging, Managed Logging, Conventional Logging and Logged and Burned). For the purpose of the temporal statistical analysis, the populations are represented by a time variable, encompassing the year prior to the degradation process (i.e., Time=0 means Intact Forest) up to four years after degradation (Time=1, ..., 4).

Because the Tukey test requires normally distributed samples, a data transformation was applied when necessary by computing the arcsine of the square-root of the data variable (Hogg and Graig, 1994) prior to statistical analysis. The results of the multicomparison statistical analysis are reported only for the comparison of the year prior to the degradation event against each other year. The

Tukey test also allowed us to determine how many years a significant difference between Intact Forest and the degradation classes persisted over time.

2.5 Results

2.5.1 First Year Forest Degradation Separability

Four classes of degraded forests were identified and characterized at the field scale: Non-mechanized Logging, Managed Logging, Conventional Logging and Logged and Burned (Table 1). The reflectance, vegetation and infrared indices and fraction means of Intact Forest were compared relative to each class of degraded forest, and between the other degraded forest classes. Figures 2 and 3 show the results of the class separability analysis, discussed for each type of data set below one year after the event (Also, Time=1 in Table 4).

a) Reflectance

Mean spectral reflectance +/- one standard deviation is plotted for Intact Forest and the degradation classes in Figure 2a. Qualitative inspection of these spectra indicates high overlap in the Landsat spectral bands making the distinction of these classes challenging.

Statistically, the Tukey test ($P < 0.01$) revealed that spectral differentiation of Managed Logging, Conventional Logging and Logged and Burned classes from Intact Forest was possible in the visible part of the spectrum (bands 1-3) for the year the degradation took place (Time=1; Table 4). Non-mechanized Logging, however,

showed only a significant change from Intact Forest in band 1. Overall, the differentiation among the other degraded forest classes was also possible in the visible region, except between Non-mechanized and Managed Logging, which did not show significant change in reflectance in the visible region.

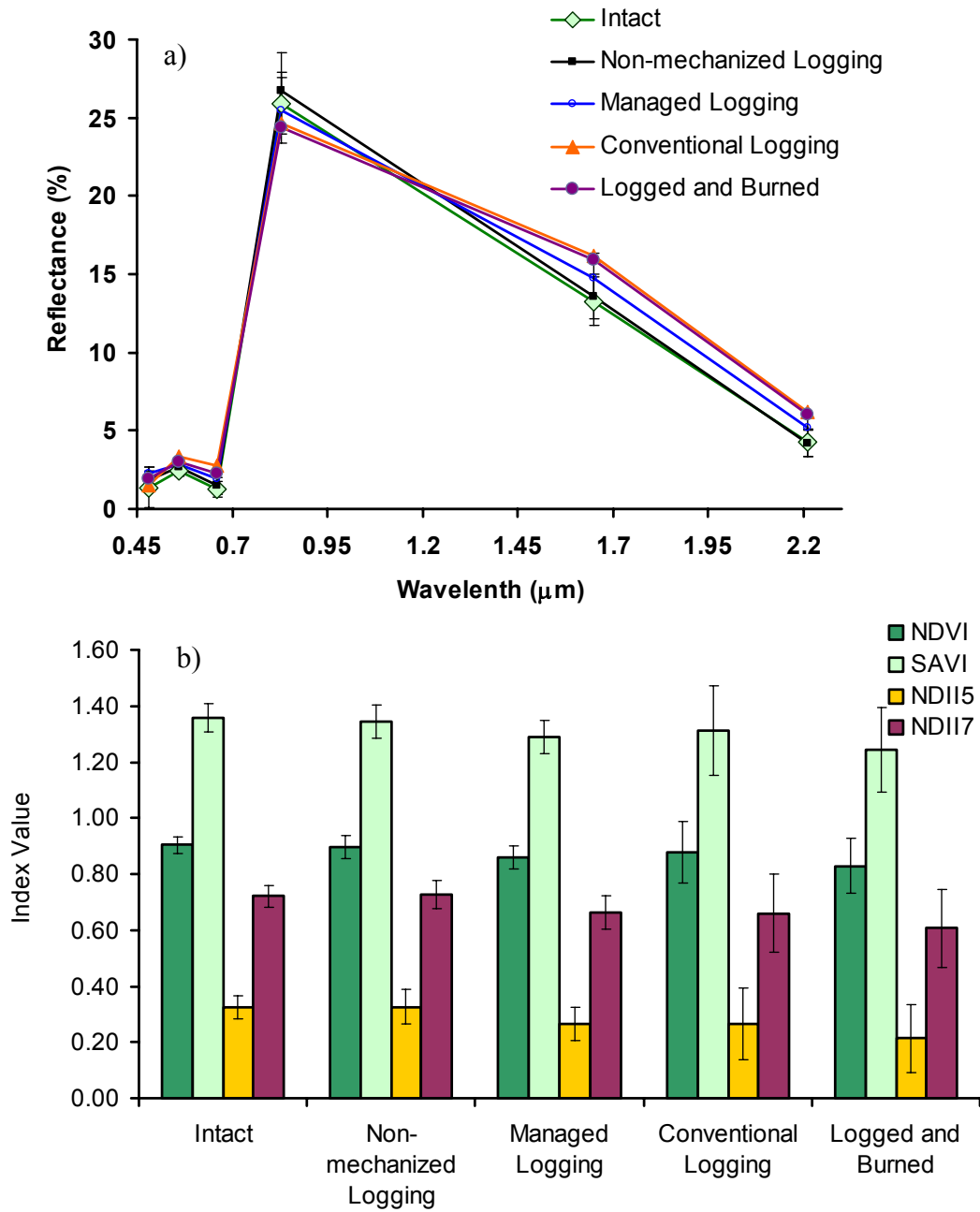
According to the statistical test, it was possible to differentiate Intact Forest from the degraded forest classes, and between each other degraded forest classes, in the near- and mid-infrared spectral region using one or two bands. Non-mechanized Logging could not be distinguished in this part of the spectrum from Intact Forest. In the infrared region, only Managed Logging and Logged and Burned classes showed significant statistical differences from Intact Forest in bands 3, 4 and 5. Conventional Logging class showed a significant difference only in band 5 (Figures 2a; Table 4).

A general trend of increasing the mean forest reflectance (1-2%) as a function of degradation intensity was observed in the visible part of the spectrum (Figure 3a). In the near-infrared region, band 4 showed a decrease (1-3%) in mean reflectance as a function of degradation intensity, whereas in the short-wave-infrared mean reflectance increased (1-3%; Figure 3a).

b) Vegetation Indices

The spectral vegetation indices, which rely on high spectral contrast between red and near-infrared bands, did not differentiate Non-Mechanized Logging from Intact Forest, due to a high overlap between these classes in these two spectral regions (Figure 2a-b; Table 4). However, Managed Logging, Conventional Logging and Logged and Burned classes showed a significant difference from Intact Forest and

between each other with NDVI and SAVI (Figure 2b; Table 4). Nonetheless, no significant difference was observed between each other degraded forest classes.



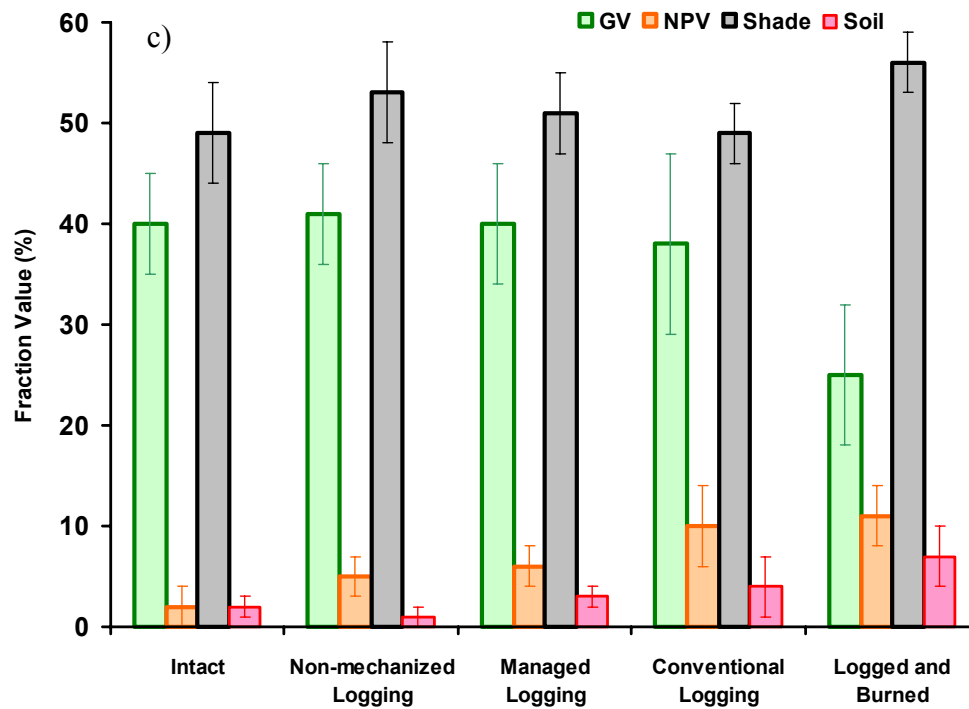


Figure 2. Means and standard deviations (vertical error bar) of intact forest and degraded forests classes as measured by Landsat bands: (a) reflectance; (b) vegetation and infrared indices; and (c) fraction images.

The infrared indices showed a general decreasing trend as a function of degradation intensity (Figures 2b and 3b). Non-mechanized Logging could not be distinguished from Intact Forest and from the other degraded forest classes. However, Managed Logging, Conventional Logging and Logged and Burned showed significant differences from Intact Forest and from each other with the Tukey test (Table 4).

Table 4. Means and standard deviation of fractions, reflectance and indices of forest degradation classes through time. Numbers in bold face denote significant differences between Intact Forest (Time=0) and degraded forest classes (Time=1,..., 4) at $P < 0.01$ utilizing a Tukey test.

(a)

Class	Time	GV (%)	NPV (%)	Soil (%)	Shade (%)	B1 (%)	B2 (%)	B3 (%)	B4 (%)	B5 (%)	B7 (%)	NDV I	SAVI	NDII5	NDII7
Non-Mecanized Logging	0	39	8	2	52	0.63	2.52	1.38	25.93	13.33	4.27	0.90	1.35	0.32	0.72
		(5)	(2)	(1)	(4)	(2.1)	(0.5)	(0.5)	(2.3)	(1.4)	(0.7)	(0.03)	(0.05)	(0.04)	(0.04)
	1	41	6	3	53	1.83	2.64	1.47	26.74	13.55	4.20	0.90	1.34	0.33	0.73
		(5)	(3)	(2)	(5)	(0.6)	(0.5)	(0.5)	(2.4)	(1.4)	(0.9)	(0.04)	(0.06)	(0.06)	(0.05)
	2	43	7	2	48	2.36	3.31	1.84	28.64	14.07	5.07	0.88	1.32	0.34	0.70
		(8)	(3)	(1)	(6)	(3.1)	(1.3)	(0.7)	(3.5)	(1.3)	(1.0)	(0.04)	(0.06)	(0.07)	(0.05)
	3	42	6	3	50	0.63	2.54	1.20	26.19	13.72	4.45	0.91	1.37	0.31	0.71
		(5)	(2)	(1)	(4)	(2.0)	(0.3)	(0.6)	(2.2)	(1.3)	(0.8)	(0.04)	(0.06)	(0.04)	(0.04)
	4	47	5	1	46	1.28	2.63	1.39	27.42	13.44	4.37	0.90	1.36	0.34	0.73
		(6)	(2)	(1)	(7)	(0.5)	(0.7)	(0.7)	(2.2)	(1.4)	(0.6)	(0.04)	(0.06)	(0.04)	(0.03)

(b)

Class	Time	GV (%)	NPV (%)	Soil (%)	Shade (%)	B1 (%)	B2 (%)	B3 (%)	B4 (%)	B5 (%)	B7 (%)	NDV I	SAVI	NDII5	NDII7
Managed Logging	0	40	5	2	50	1.62	2.70	1.47	27.01	13.41	4.26	0.90	1.34	0.34	0.73
		(2)	(3)	(1)	(3)	(0.5)	(0.3)	(0.4)	(1.4)	(1.2)	(0.6)	(0.03)	(0.04)	(0.04)	(0.04)
	1	40	6	3	51	2.26	2.87	1.92	25.49	14.77	5.16	0.86	1.29	0.27	0.66
		(6)	(2)	(1)	(4)	(0.5)	(0.4)	(0.5)	(2.1)	(1.5)	(0.9)	(0.04)	(0.06)	(0.06)	(0.06)
	2	47	6	2	45	1.66	2.66	1.53	25.97	13.76	4.61	0.89	1.33	0.31	0.70
		(6)	(2)	(1)	(5)	(0.7)	(0.5)	(0.6)	(1.9)	(1.3)	(0.7)	(0.04)	(0.06)	(0.05)	(0.05)
	3	48	5	3	45	1.09	2.49	1.41	26.53	13.47	4.54	0.90	1.35	0.33	0.71
		(4)	(2)	(1)	(3)	(0.5)	(0.6)	(0.7)	(1.6)	(1.7)	(0.8)	(0.05)	(0.07)	(0.05)	(0.05)
	4	40	6	3	50	1.51	2.88	1.80	26.26	13.38	4.44	0.87	1.31	0.33	0.71
		(5)	(2)	(1)	(4)	(0.4)	(0.5)	(0.5)	(1.8)	(1.5)	(0.8)	(0.03)	(0.05)	(0.05)	(0.04)

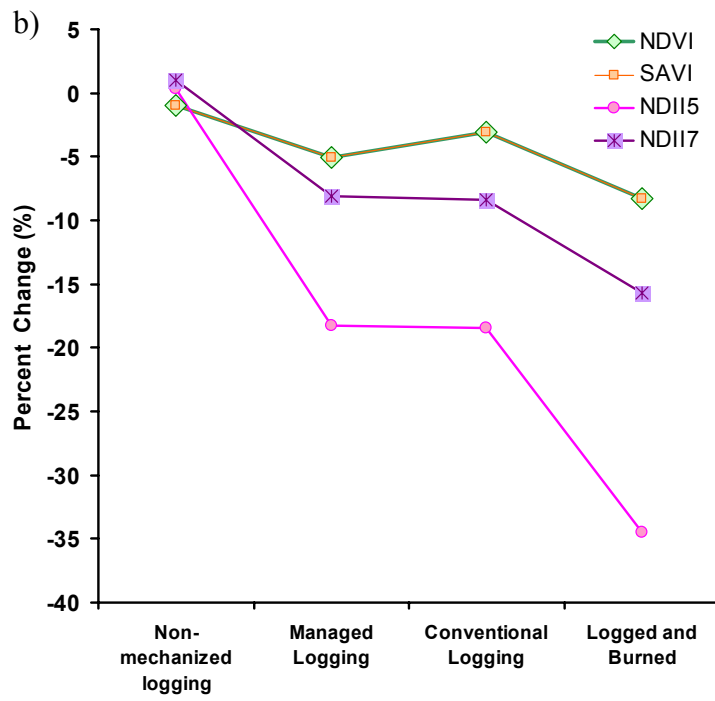
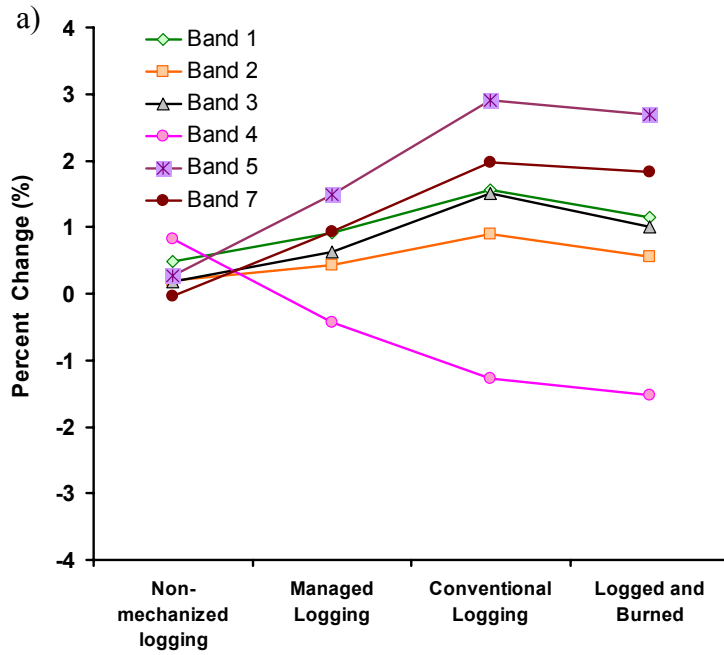
Table 4. Cont.

(c)

Class	Time	GV (%)	NPV (%)	Soil (%)	Shade (%)	B1 (%)	B2 (%)	B3 (%)	B4 (%)	B5 (%)	B7 (%)	NDV I	SAVI	NDII5	NDII7
Conventional Logging	0	45 (3)	3 (2)	2 (1)	50 (3)	1.72 (0.7)	2.11 (0.3)	0.98 (0.5)	24.62 (2.1)	12.72 (1.1)	3.92 (0.7)	0.92 (0.02)	1.38 (0.04)	0.33 (0.05)	0.73 (0.05)
	1	38 (9)	10 (4)	4 (3)	52 (4)	1.50 (1.9)	3.34 (1.3)	2.80 (1.8)	24.65 (2.8)	16.19 (3.6)	6.21 (2.6)	0.88 (0.11)	1.31 (0.16)	0.27 (0.13)	0.66 (0.14)
	2	38 (7)	5 (2)	3 (2)	54 (5)	0.62 (1.9)	2.63 (0.6)	1.70 (0.9)	25.66 (2.9)	14.36 (2.4)	4.95 (1.5)	0.89 (0.05)	1.34 (0.08)	0.31 (0.06)	0.70 (0.07)
	3	35 (6)	8 (2)	3 (2)	54 (5)	1.08 (0.5)	2.33 (0.7)	1.42 (0.8)	25.87 (2.7)	13.48 (2.0)	4.42 (1.5)	0.92 (0.05)	1.37 (0.07)	0.34 (0.06)	0.73 (0.07)
	4	41 (5)	5 (2)	3 (1)	52 (4)	2.45 (0.4)	2.58 (0.6)	1.56 (0.8)	26.66 (2.6)	13.99 (2.1)	4.85 (1.3)	0.87 (0.03)	1.31 (0.05)	0.30 (0.04)	0.69 (0.05)

(d)

Class	Time	GV (%)	NPV (%)	Soil (%)	Shade (%)	B1 (%)	B2 (%)	B3 (%)	B4 (%)	B5 (%)	B7 (%)	NDV I	SAVI	NDII5	NDII7
Logged and Burned	0	37 (5)	5 (2)	1 (2)	57 (4)	1.40 (1.9)	2.46 (0.5)	1.33 (0.7)	26.10 (2.1)	13.66 (2.4)	4.50 (1.5)	0.90 (0.04)	1.36 (0.06)	0.32 (0.07)	0.71 (0.07)
	1	25 (7)	11 (3)	7 (3)	56 (3)	1.95 (1.1)	3.01 (0.8)	2.29 (1.4)	24.38 (2.3)	15.96 (3.4)	6.06 (2.6)	0.83 (0.10)	1.24 (0.15)	0.21 (0.12)	0.61 (0.14)
	2	36 (4)	8 (2)	5 (2)	51 (3)	2.72 (0.5)	3.32 (0.6)	2.84 (0.9)	23.36 (2.9)	17.73 (2.7)	7.41 (2.0)	0.78 (0.08)	1.17 (0.12)	0.14 (0.10)	0.52 (0.12)
	3	51 (5)	8 (2)	2 (1)	40 (4)	1.88 (0.6)	2.83 (0.4)	1.82 (0.6)	26.59 (3.5)	16.41 (2.1)	5.91 (1.0)	0.87 (0.05)	1.30 (0.07)	0.24 (0.07)	0.63 (0.07)
	4	48 (5)	6 (2)	3 (1)	43 (5)	1.14 (0.5)	2.64 (0.6)	1.50 (0.7)	28.62 (3.3)	15.48 (1.8)	5.16 (0.7)	0.90 (0.05)	1.35 (0.07)	0.30 (0.04)	0.69 (0.04)



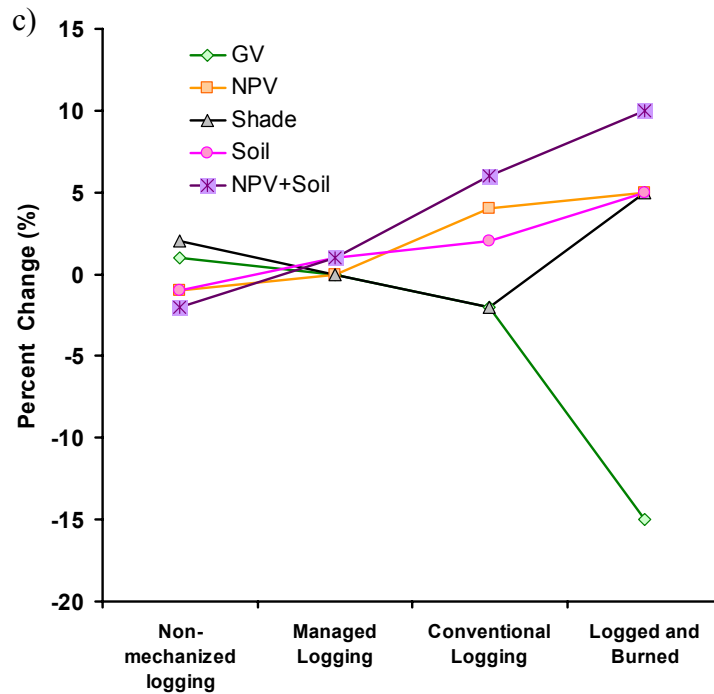


Figure 3. Delta change of (a) reflectance, (b) vegetation and infrared indices and (c) fraction images, computed by subtracting the mean value of Intact Forest from the mean value of each degraded forest class.

c) Fraction Images

The GV fraction was not significantly different between Intact Forest and Non-mechanized Logging and Managed Logging. These three classes, however, were significantly different from Conventional Logging and Logged Burned (Figure 2c). Conventional Logging and Logged Burned could also be separated from each other with the GV fraction. The NPV; Soil and Shade fractions showed results similar to the GV fraction, except that the Shade fraction showed a significant difference

between Intact Forest and Non-mechanized Logging, and Soil showed a significant difference between Intact Forest and Managed Logging (Table 4; Figure 2c).

The fraction images showed a higher absolute change between Intact Forest and the forest degradation classes (Figures 2c and 3c), when compared to the changes detected by the reflectance bands and the vegetation and infrared indices (Figure 2a-b; Figure 3a-b). The GV fraction decreased non-linearly with degradation intensity (Figure 3c). A significant change in mean of about 3% was observed between Intact Forest and Conventional Logging class, and of 15% between Intact Forest and Logged and Burned (Figure 3c; Table 4).

The Shade fraction changed less than 5% from Intact Forest to the most degraded forest class – Logged and Burned. Changes in means and statistically significant differences were observed in NPV for Conventional Logging and Logged and Burned classes. The mean NPV fraction increased by about 5% between the Intact Forest and the Conventional Logging classes, and between the Intact Forest and Logged and Burned classes (Figures 3c; Table 4). The Soil fraction showed a similar change, but smaller than the change exhibited by the NPV fraction. When NPV and Soil are combined, the changes between Intact Forest and the degraded forest classes become much greater (Figure 3c).

2.5.2 Multi-year Forest Degradation Separability

The temporal analyses covered the year prior to the degradation process (i.e., Intact Forest; Time=0) up to four years after the degradation process (Time=1,...,4). Time represents the number of years after the last forest degradation event took

place. Finally, the mean values, in Table 4 faced in bold indicate statistically significant changes from the Intact Forest condition (Time=0) relative to any other year (Time=1,..., 4) obtained with the Tukey test.

a) Reflectance and Indices

Two years after degradation, Non-mechanized Logging showed an increase in mean reflectance in the visible and infrared regions, significantly different from the Intact Forest mean reflectance (Table 4a). This increase in reflectance generated changes in the vegetation and infrared indices in the second year, but only the changes in means of NDVI and SAVI were statistically significant for Non-mechanized Logging in the second year. No significant changes in reflectance and in the indices were observed for the third and fourth years in Non-mechanized Logging, except for band 4, which showed a significant increase (Table 4a).

Managed Logging showed only two significant temporal changes in mean reflectance for bands 1 and 4, in the third and second years (Table 4b). Neither the vegetation indices nor the infrared indices showed temporally significant changes in mean values according to the Tukey test results for Managed Logging (Table 4b).

The Logging class showed some significant temporal changes in mean reflectance and mean index values. Bands 2, 3, 5 and 7 showed significant differences from Intact Forest two years after logging took place (Table 4c). Significant differences were observed in bands 1 and 4, for three and four years after logging, due to an increase in mean values that might be associated with forest

regeneration. Finally, only the vegetation indices showed significant changes due to logging disturbance for the fourth year (Table 4c).

Changes in Logged and Burned areas were significant for most of the reflectance bands for all the years following the degradation process. Among the indices, only the NDII5 index showed a significant difference between Intact Forest and Logged and Burned in the fourth year (Table 4d).

b) Fraction Images

Non-mechanized Logging showed a significant increase in GV mean from the Intact Forest mean in the second, third and fourth years after logging. A significant decrease in NPV mean, relative to the Intact Forest mean, occurred in the third and fourth years for this class. The Shade fraction showed a significant decrease in mean in the second and fourth years (Table 4a).

Managed Logging showed a significant change between Intact Forest and Non-mechanized Logging for the GV fraction in the second and fourth years. The results indicate that no significant change in GV and Shade means occurred in the first year, when the degradation took place. However, an increase in GV and a decrease in Shade were observed in the second and third years, which is likely to be associated with forest canopy closure after logging. The NPV fraction, however, did not show any significant change between Intact Forest and Managed Logging for all the years. Finally, Soil and Shade fractions were significantly different between these two classes for all the years (Table 4b).

The Conventional Logging class showed a significant difference in mean for GV, NPV and Shade fractions for all the years. The Soil fraction was significantly different from Intact Forest only in the first year (Table 4c).

The Logged and Burned class is affected by two degradation processes – selective logging and burning. Because these are heavily degraded forest environments, significant changes in all fractions were revealed with the Tukey test (Table 4c). Mean GV fraction decreased after burning followed by an increase in GV mean in the following years. The NPV mean showed an opposite pattern compared to GV mean, with an increase in mean in the first year followed by a decrease in NPV mean in the subsequent years. In the second year after burning, the Shade fraction became important for distinguishing Intact Forest from Logged and Burned forest due to a decrease in mean value (Table 4c).

2.5.3 Optimal Temporal Resolution

Non-Mechanized Logging is more difficult to distinguish from Intact Forest than the other types of disturbances in the first year. GV and Shade fractions varied inversely over time for this class (i.e., an increase in GV is followed by a decrease in Shade; Figure 4a). Because this type of selective logging does not greatly impact the forest in the year when the forest disturbance took place, the significant changes observed might be associated with canopy closure after logging. Therefore, the optimal temporal resolution for detecting this type of logging is between two to three years, when canopy closure is more likely to happen, reducing canopy roughness and, as a result, decreasing shade content. But, because this type of low impact

logging does not build roads and log landings, its differentiation from other types of disturbances (e.g., blow down winds) becomes much harder using the forest regeneration signal.

Managed Logging is more likely to be detected with reflectance bands and vegetation and infrared indices in the first year. The Soil fraction was the only SMA result that showed significant change in the first year for this class. However, a higher magnitude change in GV and shade fractions means were observed in Managed Logging when compared with the changes observed in Non-mechanized Logging (Figure 4a-b). Therefore, the regeneration of Managed forests is more likely to be detected in the second and third years than the actual low disturbance in the first year. In addition, the roads and log landing built in managed forests can be used to differentiate Managed Logging from other types of forest disturbances. After the fourth year no change relative to Intact Forest can be observed.

Conventional Logging and Logged and Burned areas can be detected in the first year with all reflectance bands, indices and fractions. However, regeneration changes in the Conventional Logging areas, in the subsequent years, are more likely to be detected using fraction images. The Conventional Logging class can be distinguished from Intact Forest in the first year because of a decrease in GV and an increase in NPV (Figure 4c). After the second year, an increase in GV and decrease in NPV is observed. However, the temporal time-series shows a second decrease in GV and increase in NPV means in the third year (Figure 4c). Such a pattern may be due to a second harvesting operation (recurrent logging), which is common in the study area. The temporal fraction pattern of Logged and Burned areas shows a more

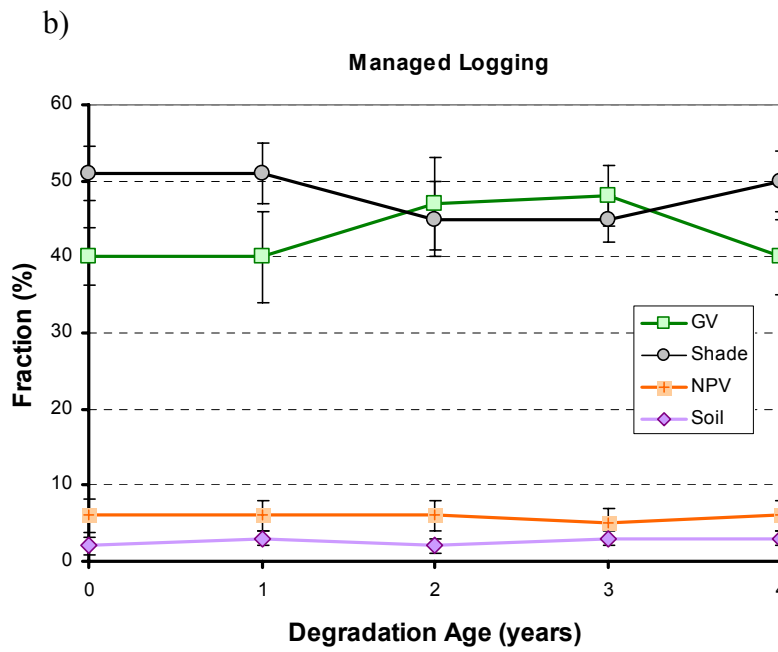
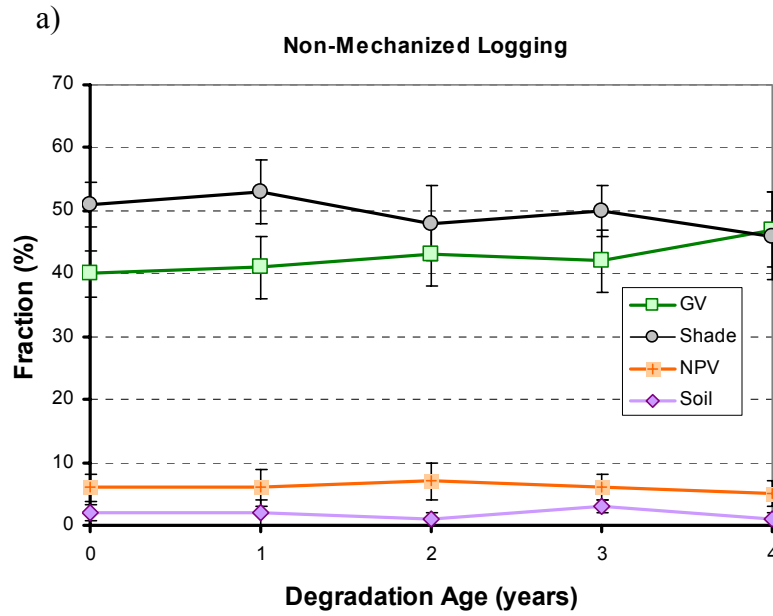
dramatic decrease in GV and increase in NPV mean values in the first year after degradation (Figure 4d). The NPV signal is still high in the second year and after the third year GV increases and NPV decreases. Therefore, the optimal temporal resolution for detecting disturbances in Conventional Logging and Logged and Burned environments is one year; regeneration, however, can be detected in Logged and Burned areas up to four years

The time-series results indicate that intensive and unplanned logging, and logging followed by burning can be detected in the first year. Up to the second year, detection becomes a challenge due to forest regeneration. Less intensive forest impacts, such as those caused by non-mechanized logging and managed logging are more difficult to detect even in the year after degradation took place. The regeneration signal of these low intensity types of logging becomes significant in the second and third years. But, the detection of logging infrastructure is important to distinguish this low impact logging from other types of forest disturbance.

2.6 Discussion

2.6.1 Degraded Forest Mapping Potential

The fraction images derived from SMA have more advantages in differentiating types of degraded forests than reflectance data and vegetation and infrared indices. First, the fraction images showed higher absolute changes in



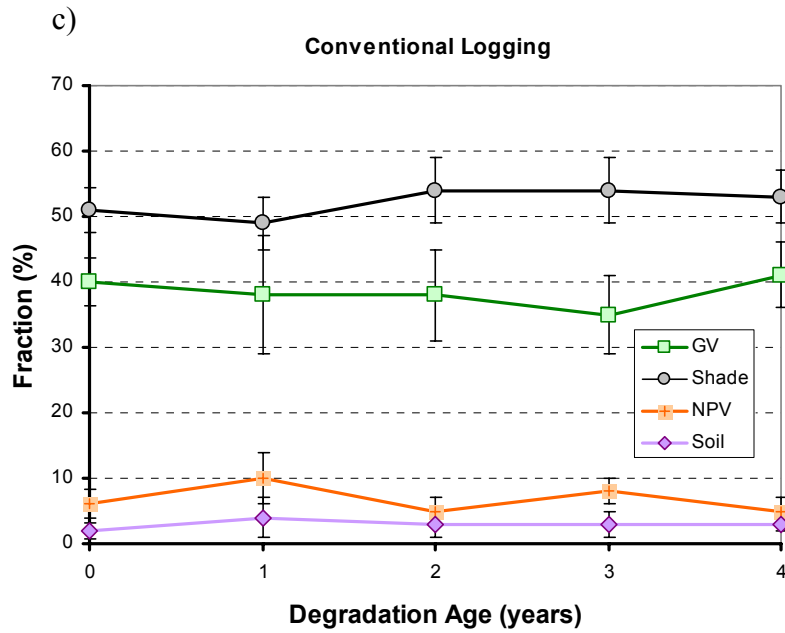


Figure 4. Change in fractions mean fraction values trough time for: (a) Non-mechanized Logging, (b) Managed Logging, (c) Conventional Logging and (d) Logged and Burned.

mean values between Intact Forest and the other degraded forest classes than the other types of data. Second, temporal changes were better revealed using fraction images. Third, the fractions have a more intuitive physical link with field data. Additionally, fraction images have been successfully used to map selective logged and burned forest areas. For example, Cochrane and Souza Jr. (1998) reported that the NPV fraction showed the greatest separability of sub-classes of burned forests and Souza Jr. et al. (2003) demonstrated that the NPV fraction was an important variable for differentiating Intact Forest from degraded forest in a decision tree classifier. Finally, other studies have shown that damage associated with selective logging is difficult to identify and map using Landsat reflectance data (Stone and Lefebvre, 1998; Asner et al. 2002).

Fraction temporal changes revealed in the statistical comparisons described above can be observed visually using a color composite of fraction images (Figure 5). When displaying NPV, GV and Soil as Blue, Green and Red, respectively, it is possible to identify and potentially map degraded forest classes. NPV is the most prominent fraction change in the degraded forest environment and is easily observed in this type of color composite.

One important issue that should be taken into consideration when interpreting forest degradation signatures in this type of color composite is the time of image acquisition versus the time when degradation event took place. For example, the Managed Logging areas of Transects 15 and 17, do not exhibit an NPV signature in 1999, because no selective logging had taken place in that year (Figure 5a). In the

following year, only Transect 15 showed an increase in NPV due to selective logging, but no increase in NPV was observed in Transect 17 (Figure 5b). To explain why this is possible one must consider the time of both harvesting and image acquisition. The Landsat image for the year 2000 was acquired immediately after harvesting took place in the area of Transect 15, but before harvesting occurred near Transect 17 (Figure 5b). In the next image, acquired in 2001, the NPV signal in Transect 15 area is no longer as visible, but the NPV content has increased in Transect 17 relative to the images acquired in 1999 and 2000. This type of temporal lag between image acquisition and harvesting is important for building change detection classifiers for mapping degraded forest.

The NPV fraction signature was more visible and persistent in Logged and Burned environments (Figure 5e-h). In the area of Transects 3, 4 and 5, selective logging took place in 1999 followed by intensive forest burning in 2000. NPV increased more drastically in burned areas and its signature was still visible in 2001. In 2002, the NPV signature disappeared, followed by an increase in GV and decrease in Shade.

2.6.2 Linking Field Measurements with Fraction Images

Forest biophysical properties acquired with the forest transect for Intact Forest and the degraded forest classes are summarized in Table 5. The results obtained with the SMA agree with the field measurements. GV fraction tends to decrease as a function of degradation intensity. At the field scale this change in GV can be explained by a decrease in the amount of intact vegetation and canopy cover.

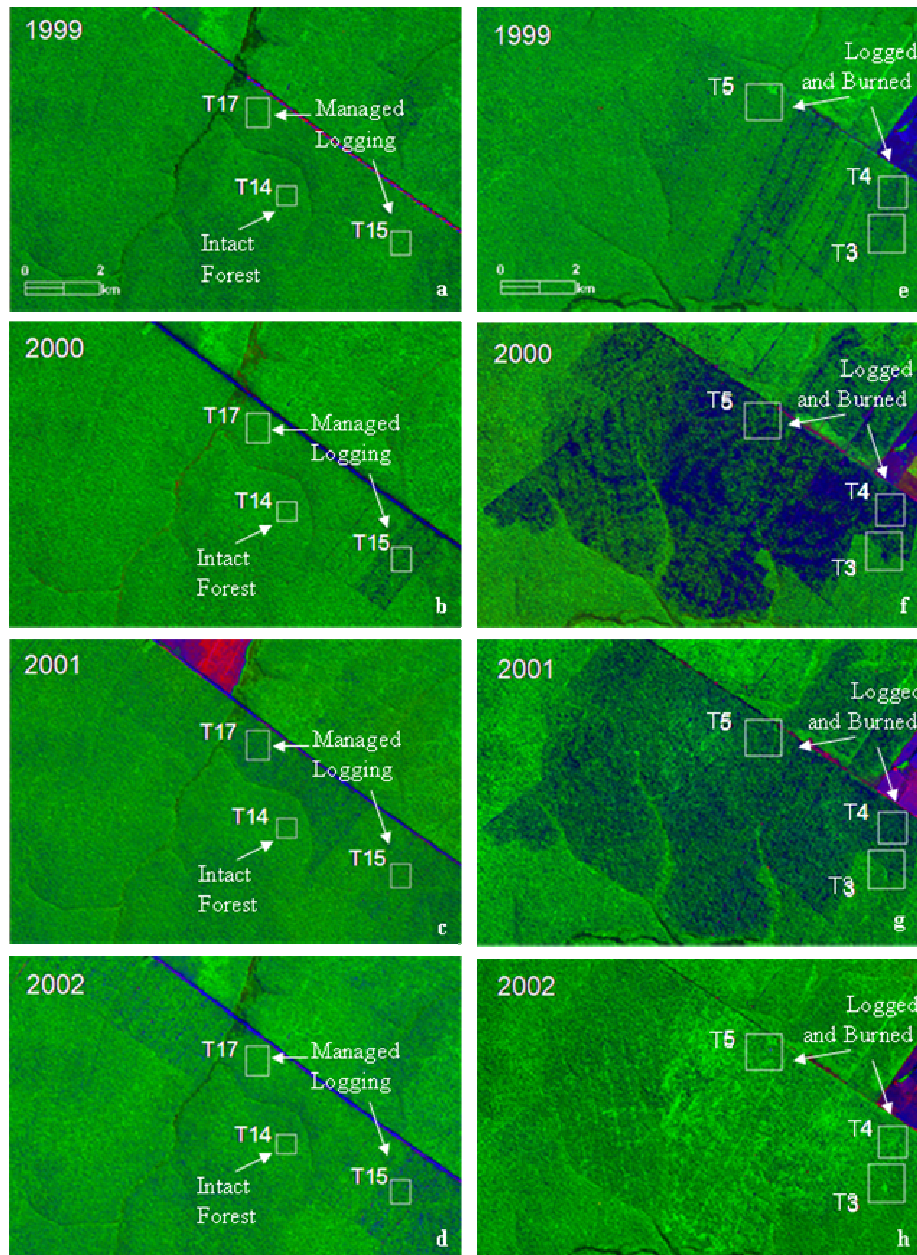


Figure 5. Examples of forest degradation processes and temporal changes as detected using fraction images derived from SMA (Red = Soil, Green = Green Vegetation, Blue = NPV).

The field results show that the mean of intact vegetation proportion drops from 95% in the Intact Forest to 50% in Logged and Burned areas (Figure 2c; Table 5). The canopy cover also decreased from Intact Forest (93%) to Logged and Burned (67%).

The proportion of forest area affected by disturbed soil and wood debris increases as a function of the degradation intensity. This pattern also agrees with the pattern captured by Soil and NPV fractions (Figure 2c; Table 5). At the field level all these ground disturbances are significant for differentiating Intact Forest from the degradation classes. However, because the ground cover is not always imaged by satellite sensors, the distinction of these classes from Landsat is not always possible using these field properties.

NPV fraction has an inverse relationship with biomass measurements made in degraded forests in the Eastern Amazon (Souza et al., 2003). In the study area, the biomass estimates obtained with the field transects also show a trend in decreasing biomass with an increase in NPV as a function of degradation intensity (Figure 2c; Table 5). Even though it is not the objective of this paper to evaluate if these correlations are statistically significant, the results indicate that there is a potential for using the NPV fraction images to estimate biophysical properties of degraded forests in open forest environments as well.

2.6.3 Monitoring Forest Degradation: practical application and challenges

One potential application of the fraction change detection technique is the discrimination between managed and unplanned logging. Currently, there is an

increasing need to monitor areas under forest management in the Amazon region. First, the Brazilian government has improved the control of selective logging in the region by requesting detailed information on the location of forest plots that will be subject to timber harvesting and requiring specific management practices following logging (Casa Civil, 2004). Second, the logging private sector has become more interested in forest certification, which requires high standard management practices (Lentini et al., 2003). Finally, the Brazilian government has been evaluating the possibility of providing long-term concessions in National Forest areas for logging companies interested in timber harvesting (Veríssimo et al., 2002). Therefore, low cost, timely and reliable information on forest disturbances is required to monitor the forest areas authorized by the government and/or certified for conducting forest management.

The fraction change technique presented in this chapter has the potential to be used to indicate if an area is following the management practices required by the Brazilian government and/or by the certification institutes. For example, both the GV and NPV fractions showed significant differences from Intact Forest to Managed Logging, but showed higher significant differences and more pixels showed changes in fraction values from Intact Forest to Conventional Logging and Logged and Burned areas. In other words, the fraction change technique has the potential for differentiating managed logging areas from unplanned logging areas. Therefore, a forest monitoring program could use the fraction change technique to verify if the areas that have received government authorization and/or forest certification to

manage forest areas for timber harvesting are following the management prescriptions.

There are, however, two main challenges to implementing a remote sensing program for monitoring forest management plans in the Amazon region. The first has to do with technical remote sensing issues. Reflectance retrieval, radiometric inter-calibration and SMA, particularly dealing with the need to find the correct set of endmembers, are not trivial tasks. Second, processing and interpreting the fraction data requires training the end-users who will be in charge of such a forest monitoring system.

2.7 Conclusion

Statistical multi-temporal analysis of reflectance, vegetation and infrared indices and fraction images, derived from SMA, showed that fraction images are more sensitive to changes in transitional forest environments due to selective logging and burning than the broad-band indices tested here. Low intensity logging, such as Managed Logging and Non-mechanized Logging are more difficult to distinguish from Intact Forest but a regeneration signal - caused by understory vegetation growth and canopy closure - becomes significant in the second and third year due an increase in GV and decrease in Shade. The time-series results showed that changes in GV and NPV fractions were higher when Intact Forest was changed to Conventional Logging and to Logged and Burned environments in the first year following the degradation event. In the Logged and Burned Forests, the NPV signal was more persistent,

showing a burned signature through the second year after forest burning. Therefore, both GV and NPV can be used in change-detection classifiers for identifying and mapping Conventional Logging and Logged and Burned forests in the Brazilian Amazon, with images no more than one year apart.

Table 5. Biophysical properties of the Intact Forest class and of the degraded forest classes estimated from the forest inventories.

Biophysical property	Intact Forest (n=4)	Non-mechanized Logging (n=5)	Managed Logging (n=5)	Conventional Logging (n=2)	Logged and Burned (n=3)
Ground cover (%)					
Intact vegetation	95 (5)	83 (9)	50 (11)	59 (3)	50 (19)
Woody debris	4 (5)	10 (11)	29 (7)	17 (8)	39 (28)
Disturbed soil	0	7 (2)	17 (6)	24 (12)	5 (7)
Canopy cover (%)	93 (5)	87 (4)	97 (1)	92 (0)	67 (5)
Aboveground live biomass (t ha⁻¹)	306 (44)	250 (20)	219 (31)	277 (44)	166 (45)

^aMeans presented with S.D. noted parenthetically.

CHAPTER III: Combining Spectral and Spatial Information to Map Canopy Damages from Selective Logging and Forest Fires²

3.1 Introduction

Remote sensing techniques for mapping forest degradation caused by selective logging and the forest fires are critically needed in the Brazilian Amazon. In these regions, ongoing deforestation has fragmented remaining forests and exposed the remnants to increasing levels of timber extraction and an alarming frequency of uncharacteristic forest fires (Cochrane, 2003). Several techniques for mapping selectively logged or burned areas have been proposed, but none has proven satisfactory as a general tool for detecting the type and severity of forest degradation. Visual interpretation of Landsat Thematic Mapper (TM) images was the first technique proposed to map selective logging (Watrín and Rocha, 1992); it provided some of the first remote sensing based estimates of the area affected by selective logging in the Brazilian Amazon (Santos et al., 2002; Matricardi et al., 2001). Visual interpretation is possible when logging ‘scars’ are visible on the images. However, these logging “scars” only persist for one to two years after logging (Souza Jr. et al., in press a). Furthermore, visual interpretation is challenging when the logging intensity is low as is the case, for example, with mahogany harvesting (Veríssimo et

² Accepted for publication: Souza Jr. et al., (in press b).

al., 1995) or non-mechanized logging. Finally, visual interpretation is time consuming and can have a human bias.

Conventional digital image processing techniques such as minimum distance and maximum likelihood classifiers have also been evaluated for mapping selective logging in the Amazon (Stone and Lefebvre, 1998) as have texture and reflectance analyses (Asner, et al. 2002). These techniques are prone to error due to the spectral ambiguity between selectively logged areas of various ages and extraction intensities and intact forest.

SMA overcomes some of the problems of visual interpretation and conventional image processing techniques. The soil fraction derived from SMA enhances the detection of the log landings and logging roads, which have been recognized as the spatial signature of mechanized logging in tropical forests (Souza Jr. and Barreto, 2000; De Wasseige and Defourny, 2004). The total forest area affected by selective logging, which integrates the clear-cut forest to build roads and log landings, forest island that were not harvested and canopy damaged forest (Souza Jr. and Roberts, 2005), can be estimated from log landings using an estimated tree harvesting radius (Souza Jr. and Barreto, 2000; Monteiro et al., 2003). If forest damage data are available, this area mapping technique can be used to estimate the impact of selective logging on the forest. However, this approach does not provide spatial information about the location of the forest canopy damages. To overcome this limitation, Asner *et al.* (2002) proposed using gap fraction data derived from Green Vegetation (GV) fraction images obtained with SMA as a means to estimate forest canopy damage

associated with selective logging. The gap fraction approach cannot separate selective logging gaps from canopy gaps generated by natural forest disturbances (e.g. treefalls, windthrows, lightning strikes), and is likely to overestimate the area affected by selective logging in the Amazon region. Finally, the non-photosynthetic vegetation (NPV) (Roberts et al., 1993) fraction has been used to quantify levels of forest degradation caused by burning (Cochrane and Souza Jr., 1998).

The Soil, GV and NPV fractions have been used independently, underutilizing the information provided by SMA models. Decision tree classification was proposed to integrate the fractions of GV, Soil and NPV to classify degraded forest environments due to selective logging and burning (Souza Jr. et al., 2003). However, this approach is only useful for mapping highly degraded forests which have been subject to recurrent logging and burning.

In this study, I present a robust technique to map canopy damage caused by selective logging and burning that overcomes the problems described above. First, a novel spectral index is proposed to enhance the identification and detection of forest degradation that combines GV, NPV, Shade and Soil fractions derived with SMA. Second, a contextual classification algorithm (CCA) integrates the spatial information of log landings and roads with the proposed fraction index images to unambiguously separate canopy damage due to selective logging and associated burning from canopy damages due to natural disturbance. Fires are not considered natural disturbances in this study due to the extreme rarity of such fires in these forests (Cochrane, 2003). Forest fires are becoming increasingly common in

fragmented and logged forests, however, the spatial distribution of these fires (Cochrane, 2001) and association with human land use (Cochrane et al., 1999; Cochrane et al., 2004) clearly indicate their anthropogenic origins.

3.2 Study Area

The proposed techniques were tested in the vicinity of Sinop County, located in the state of Mato Grosso, Brazil (Figure 1). Transitional forest, between ‘cerrado’ and dense forest, is the predominant vegetation type in the study region. These transitional forests are characterized by 93% canopy cover, a tree density of 422 trees ha⁻¹, and a total aboveground live biomass of 326 tons ha⁻¹ (Monteiro et al., 2004). The diversity and density of timber species in these transitional forests are smaller than in dense forests. The topography varies from flat to undulating terrain, on Latosol soils. The average annual precipitation is 2,000 mm (RADAMBRASIL, 1981).

Selective logging in this area is characterized by the selective harvesting of only high quality timber species. The harvesting intensity ranges from 10 to 40 m³/ha and conventional logging operations are predominantly unplanned in terms of forest management (Monteiro et al., 2004). Four types of selectively logged forest were identified in the field: Non-mechanized Logging, Managed Logging, Conventional Logging and Logged and Burned (Table 1). Selectively logged forests are a complex mosaic of three environment types: i) undisturbed forest islands that were not affected by logging operations, often due to difficult access resulting from

topography and rivers, or because of a lack of commercial timber species; ii) cleared forest for logging roads and trails used for machine movements (skidders and trucks) and log landings used to temporarily store the harvested timber; and iii) forests with canopies damaged by tree-felling and extraction during logging operations. Forest fires are frequent in the study region and are strongly associated with prior selective logging (Cochrane et al. 2004). The synergism between selective logging and forest fires increases the extent and severity of forest burning and results in extensive forest degradation (Cochrane et al., 1999; Monteiro et al., 2004). Detection and mapping of selectively logged and burned forests in the resulting forest mosaic is difficult and further complicated by the rapid canopy closure and undergrowth that occur after logging or burning.

3.3 Data Set

3.3.1 Forest transect inventory

Nineteen 0.5 ha forest transect inventories, conducted in September 2001 (n=14) and August 2004 (n=5), were used to characterize the different classes of degraded forests found in the study areas (Figures 1 and 6). Additionally, information about logging and fire histories, ground cover, canopy cover and biomass were used to test the sensitivity of the proposed fraction-based index for distinguishing the forest degradation classes, Non-mechanized Logging, Managed Logging, Conventional Logging and Logged and Burned (Table 1).

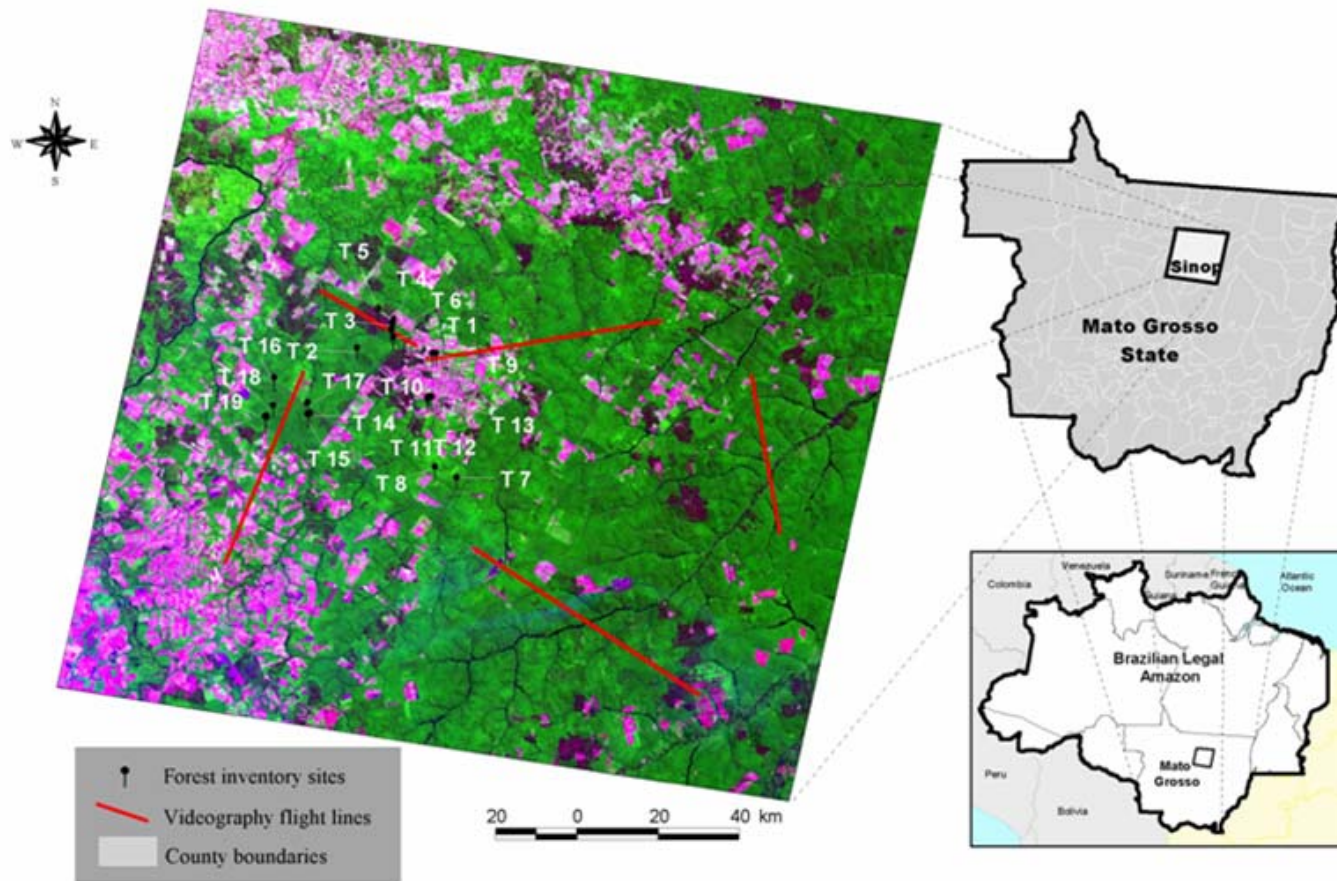


Figure 6. Map of the study area showing the location of the forest transects and of the aerial videography transects.

Table 3 lists the year that forest degradation took place and the disturbance history of the forest transects conducted in the study area. The forest inventories were conducted following the field protocol proposed by Gerwing (2002) to characterize degraded forest in the eastern Amazon. This method has successfully been applied to characterize biophysical properties and dynamics of degraded forests in transitional forests (Monteiro et al., 2004) like those in the study region. The forest inventory procedure required measuring all trees with Diameter at the Breast Height (DBH) greater than 10 cm along a 10 m by 500 m transect. Ten sub-parcels (10 m x 10 m) were established every 50 meters along each transect where all trees were mapped and ground cover and canopy cover fractions were estimated. Above ground biomass estimates were made using allometric equations available in the literature (Gerwing, 2002). The biophysical information extracted from the transect inventories are summarized in Table 5.

3.3.2 Satellite Imagery Data

Landsat TM 5 and Landsat Enhanced Thematic Mapper (ETM+) images, bands 1-5 and 7, acquired between 1984 and 2004 were used in this study (Table 2). The images were acquired through the Tropical Rain Forest Institute Center (TRFIC) and the Brazilian Space Agency (INPE).

3.4 Methodology

3.4.1 Image Processing

a) Image Registration and Radiometric Calibration

The Landsat ETM+ image acquired in 1999 in Sinop (226/68) was georeferenced using several control points extracted from NASA GeoCover 2000 Mosaic (<https://zulu.ssc.nasa.gov/mrsid/>). Next, the georectified Landsat image was used as the reference image to register the images acquired for the other dates (Table 2). The registration utilized a polynomial algorithm and nearest neighborhood interpolation, available in the Environment for Visualizing Images – ENVI - 4.0 software (ENVI; Research Systems, Boulder, CO). A minimum of 14 image control points were used and the maximum root-mean-square error allowed was 1 pixel.

b) Atmospheric correction and Inter-calibration

The reference image was converted from encoded digital number (DN) to reflectance. To perform this task, the reference image was converted to radiance using the gains and offset provided in the image metafile. Next, atmospheric correction was performed using Atmospheric Correction Now 4.0 (ACORN: Analytical Imaging & Geophysics, Boulder, CO). Visibility and water vapor parameters of the atmospheric correction model were determined by a trial-and-error sensitivity analysis of a dark object reflectance (a lake). The final

parameters were estimated when the expected reflectance values of the dark object were found. The fixed water vapor for Sinop was 40 millimeters, and the image atmosphere visibility was 25 km.

The other images (Table 2) were inter-calibrated to the reflectance image using a relative radiometric calibration approach (Roberts et al., 1998; Furby & Campbell, 2001), regressing encoded radiance against reflectance in the reference image. This technique assumes uniform atmosphere over the image scene, and that invariant ground targets can be found in the reference and the uncalibrated images. To account for spatially variable atmospheric contamination due to haze and smoke, the Carlotto (1999) technique was applied to those images that had significant contamination prior to relative radiometric calibration. The Carlotto technique is based on the assumption that smoke and haze only adversely impact the visible bands, leaving the NIR and short-wave Infrared bands unchanged. Statistics are calculated for the entire image, in which average values for TM bands 1, 2 and 3 are calculated for each unique combination of TM bands 4, 5 and 7. After calculating these statistics, the original values for TM bands 1, 2 and 3 for a specific combination of bands 4 to 7 are then replaced with the scene averages for that combination. This approach, developed by Carlotto (1999) has the effect of homogenizing contamination throughout a scene – thus clear sky portions of the image gain a slight amount of contamination, while contamination is significantly reduced in areas under smoke or haze.

Typical invariant targets used included intact forest, second growth, green pasture, bare soil and water. Second growth and green pasture were only used as invariant targets for images that were no more than two years apart from the reference image date. The slopes and intercepts for the relative radiometric inter-calibration were obtained from a linear regression that was estimated using the pixel mean values, extracted from a 3 by 3 pixel area, of the invariant targets for each band. These coefficients normalize the uncalibrated images to the reference images, converting Digital Numbers of the uncalibrated images to reflectance.

3.4.2 Spectral Mixture Analysis - SMA

The Landsat TM/ETM+ reflectance data of each pixel were decomposed into fractions of GV (green vegetation), non-photosynthetic vegetation (NPV), Soil and Shade through Spectral Mixture Analysis – SMA. (Adams et al., 1993). The SMA model assumes that the image spectra are formed by a linear combination of n pure spectra, such that:

$$R_b = \sum_{i=1}^n F_i R_{i,b} + \varepsilon_b \quad (8)$$

for

$$\sum_{i=1}^n F_i = 1 \quad (9)$$

where R_b is the reflectance in band b , $R_{i,b}$ is the reflectance for endmember i , in band b , F_i the fraction of endmember i , and ε_b is the residual error for each band. The

SMA model error is estimated for each image pixel by computing the **RMS** error, given by:

$$\text{RMS} = \left[n^{-1} \sum_{b=1}^n \varepsilon_b \right]^{1/2} \quad (10)$$

The identification of the nature and number of pure spectra (i.e., endmembers), in the image scene is imperative for a successful application of SMA models. Four mixed endmembers are expected in degraded forest environments, GV, NPV, Soil and Shade. Image endmembers representing GV, NPV and Soil were extracted from the reference reflectance image. Shade was assigned zero percent reflectance at all wavelengths. The pixel-purity-index (PPI), available in ENVI 4.0 (Boardman et al., 1995) was used to identify image endmember candidates. Five image subsets (500x500 pixels), representing the variety of land cover types found in the images, were used as inputs for the PPI algorithm. The PPI result was used to identify the pixel location in the original image and extract the spectral curves of these pixels. The final image endmembers were selected based on the pixel location in the Landsat reflectance spectra with the aid of an n-dimensional visualization tool available in ENVI. The pixels located at the extremes of the data cloud of the Landsat spectral space were selected as candidate endmembers. The final endmembers were selected based on the spectral shape and image context (e.g., soil spectra are mostly associated with unpaved roads and NPV with pasture having senesced vegetation).

SMA models were computed for each date using the inter-calibrated image endmembers, except the reference image, which was the one used to extract the endmembers. The SMA model results were evaluated as proposed by Adams et al. (1993). First, the RMS images were inspected and models with RMS values greater than 5% were discarded from the fraction change analysis. Next, fraction images were evaluated and interpreted in terms of field context and spatial distribution. Finally, the histograms of the fraction images were inspected to quantify the percentage of pixels lying outside the range of zero to 100% and to evaluate fraction value consistency over time (i.e., that intact forest values were similar over time). Only models with at least 98% of the values within zero to 100% and those that showed mean fraction value consistency over time were kept. For the models that did not pass one of these tests, new invariant targets were collected to improve the image inter-calibration coefficients and new SMA models were run until the criterion was met.

3.4.3 Normalized Difference Fraction Index – NDFI

Selectively logged forests and burned forests have a lower proportion of GV and a higher proportion of NPV and Soil relative to intact forest (Souza Jr et al., in press; Souza Jr. et al., 2003; Cochrane and Souza Jr., 1998). The shade content of these degraded forests is also higher relative to intact forest (Souza Jr. et al., in press). In order to enhance the degradation signal caused by selective logging and burning, a Normalized Difference Fraction Index (NDFI) is proposed, computed using the fraction images obtained with SMA models by:

$$\text{NDFI} = \frac{\text{GV}_{\text{Shade}} - (\text{NPV} + \text{Soil})}{\text{GV}_{\text{Shade}} + \text{NPV} + \text{Soil}} \quad (11)$$

where GV_{shade} is the shade-normalized GV fraction given by,

$$\text{GV}_{\text{Shade}} = \frac{\text{GV}}{100 - \text{Shade}} \quad (12)$$

The NDFI values range from -1 to 1. Theoretically, the NDFI value in intact forest is expected to be high (i.e., about 1) due to the combination of high GV_{shade} (i.e., high GV and canopy Shade) and low NPV and Soil values. As the forest becomes degraded, the NPV and Soil fractions are expected to increase, lowering the NDFI values relative to intact forest. Therefore, the NDFI has the potential to enhance the detection of forest degradation caused by selective logging and burning. The NDFI has the advantage of combining, in one synthetic band, all the information that has been shown to be relevant for identifying and mapping degraded forests in the Amazon region.

3.4.4 Statistical Analysis

Based on the information on logging and fire histories, it was possible to identify the date of the forest degradation events (Table 3). The Landsat image corresponding to the forest degradation events for each transect were selected for analysis. For example, for transect 8, which was logged in 1993, the 1993 image would have been selected. Next, the geographic coordinate of the transects were used to locate the degraded forests areas in the images. Fractions of GV, NPV, Shade and Soil were extracted using 30 pixels selected randomly within the degraded area where transects

were conducted. The NDFI value of the randomly selected pixels was also computed for each transect using the fraction values extracted according to Equations 11 and 12.

The final step was to perform a pair-wise class separability analyses based on the fractions and NDFI variables. The Tukey test (Ott, 1992), available in the R Language (<http://www.r-project.org/>) was used to evaluate if the Intact Forest and the forest degradation classes could be separated from each other at a 99% confidence interval ($P < 0.01$). The Tukey test performs a multicomparison by testing the mean of a population against the mean of each other population. Because the Tukey test requires normally distributed samples, a data transformation was applied when necessary by computing the arcsine of the square-root of the data variable (Hogg and Graig, 1994) prior to statistical analysis.

3.4.5 Contextual Classification Algorithm

The log landing locations extracted from the Soil fraction image were used as contextual information to map forest canopy damage associated with selective logging and forest burning. Because log landings are the spatial signature of selective logging (Souza Jr. and Barreto, 2000; De Wasseige and Defourny, 2004) and burned forests are associated with selective logging (Cochrane et al., 2004), this approach allows us to separate selective logging and forest fires from forest natural disturbance (e.g., blow downs and drought-deciduous trees) in tropical forests. Natural disturbances in the Brazilian Amazon affect mostly the forest canopy and soil is not exposed because the ground is covered by damaged vegetation (Nelson et al., 1994).

In order to separate canopy damages caused by selective logging and associated forest burning from other types of canopy disturbance, a contextual classification algorithm (CCA) was developed. The CCA integrates log landing and logging roads extracted from soil fraction images with the NDFI image. Log landings exhibit higher Soil fraction values than intact forest and their detection and extraction can be automated (Souza and Barreto, 2000; Monteiro et al., 2003). Logging roads show high soil values and have a linear shape. An image thresholding technique was applied to extract log landings and logging roads from the Soil fraction images. All pixels with a Soil fraction greater than 10% were extracted and used as inputs for a region labeling program available in IDL (Interactive Data Language, Research System, Boulder, CO). Next, all regions found in the region-labeled image were indexed and the area and shape of each indexed-region were calculated. Regions with area varying from one to four pixels in size were classified as log landings based on field measurements of log landings. The log landing average area for this region measured at the field scale is 1,043 m² (n=34) with a minimum and maximum of 348 m² 4,051 m², respectively (Monteiro et al., 2003; Monteiro, 2005). These areas translate to a minimum of 40% of a pixel (18x18 m), an average of slightly more than a pixel and a maximum of 4.5 pixels. Assuming a worst case scenario of a small log landing falling between four pixels, this translates to a minimum Soil threshold of 10% and areas ranging from 1 to 4 pixels. Therefore, the area and fraction threshold used to extract the log landings from the Landsat images is within the range of log landings measured in the field. Finally, a forest mask was applied to

avoid confusing log landings with other small cleared areas found in deforested areas (Souza Jr. and Barreto, 2000; Monteiro et al., 2003).

A 2D-search program, also available in IDL, was used to look for a specific range of values in the NDFI images associated with canopy damages due to selective logging and burning. First, the log landing extracted from the Soil fractions were used as the starting locations to search within the NDFI image for values ranging from 0 to 0.75 which represents the NDFI values associated with canopy damage. This range of NDFI values was defined empirically using the canopy damage data collected during the forest inventories (Figures 1 and 6, Table 3) and is associated NDFI values. Given the pixel location of a log landing region, the IDL 2D-search program extracts the NDFI value of each neighboring forested pixel adjacent to the selected log landing. If the NDFI value of the selected neighboring pixel is within the specified NDFI threshold range (i.e., between 0 and 0.75), the pixel is classified as Canopy Damage. Otherwise, the pixel is classified as Intact Forest. Next, each pixel classified as Canopy Damage provides new locations to search for new neighboring pixels and to test if their NDFI values are within the canopy damage range. The new neighboring pixels are classified as Canopy Damage or Intact Forest based on the criteria described above. This process grows canopy damage regions from the log landings until all neighboring pixels are classified as Intact Forest. Then, the algorithm jumps to the next log landing location that had not been included within a Canopy Damage region. The Canopy Damage classification is completed when all log landing locations are evaluated as described above. The

NDFI image was smoothed, prior to the application of the 2d-search program, using a 3 x 3 pixel kernel, to remove image classification speckle.

3.4.6 Accuracy Assessment

The canopy damage map generated with the contextual classifier was assessed with aerial videography images acquired in December 14 and 17 of 2000. The videography system consisted of a SONY DCR-VX1000 digital camera, a Magelan NAV5000 GPS and of a HORITA GPS3 time code generator. Image mosaics of 1 meter spatial resolution were generated to build five videography transects, covering a region of 168 km by 0.64 km (Figures 6). An example of an aerial videography mosaic is given in Figure 7.

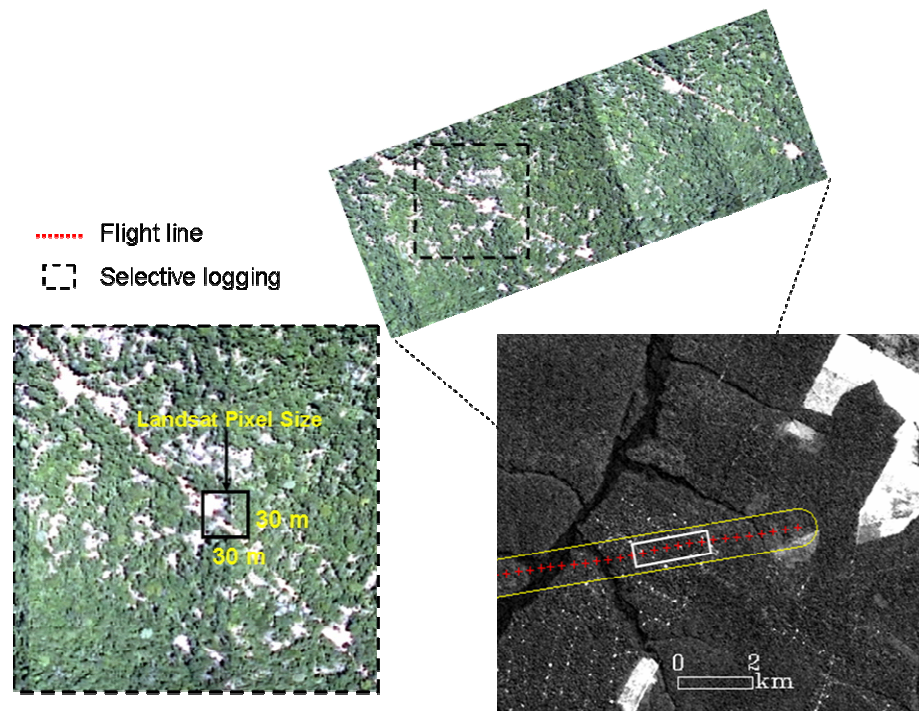


Figure 7. Example of aerial videography mosaic used as reference data for the map accuracy assessment

The videography mosaics were georeferenced using the GPS data collected during the image acquisition. The pixel location accuracy of the videography mosaic was 15 m after georeferencing, which guaranteed accurate registration with the Landsat images.

The accuracy assessment protocol included defining a sampling design, a response design, and evaluating the canopy damage map using the reference data (Powell et al., 2004). The sample design used a block sample of 5 by 5 Landsat pixels. A total of 80 block samples (i.e., 2000 pixels) were randomly selected from the Landsat, located on the videography and interpreted by an independent image interpreter. The response design used the forest and soil cover proportions and the shadow proportion within the block sample as the criteria for labeling each block sample as Intact Forest, Canopy Damage or Deforestation. The block sample was classified based on cover fractions observed in the videography as follows:

- Intact Forest: $\geq 70\%$ of forest canopy and $\leq 30\%$ of shade, 0% of soil;
- Canopy damage: 30-70% of forest canopy, 10-40 % soil plus NPV, and $\geq 50\%$ of shade;
- Deforestation: $<30\%$ of forest and $>40\%$ of soil plus NPV, and $\leq 50\%$ of shade

These classification threshold values were defined based on visual interpretation of the videography images. It is important to highlight that the shade content observed in the videography images does not correspond to the amount of shade estimated with SMA for the Landsat images pixels. The shade fraction in a Landsat

scene is a product of two components, reduced reflected radiance due to local illumination (ie, leaf angles, shaded crowns) and shadows. In contrast, the shade fraction derived from videography is strictly a measure of shadows. As a result, the two measures of “shade” will differ, with videography derived estimates typically lower. In addition, the videography was flown closer to solar noon in December, when the solar zenith is lowest in the southern hemisphere. In contrast, the Landsat data were acquired earlier in the day in June, at a higher solar zenith and thus would be expected to have a higher amount of shadowing. To account for the fact that the videography and Landsat data were acquired six months apart (December 14-17, compared to June 26, 2000 for Landsat), pixels that were subject to land cover changes in the videography reference data were removed from the accuracy assessment (5 blocks or 125 Landsat pixels) prior to calculation of the classification error matrix (Powell et al., 2004). Geocorrection errors of the block sample pixels were also corrected when necessary using land features such as roads, rivers and forest edges.

3.5 Results

3.5.1 Class Separability

Table 6 shows fractions and NDFI statistics for the Intact Forest, Non-mechanized Logging, Managed Logging, Conventional Logging and Logged and Burned, for the areas where the forest transects were conducted. The results of the pair-wise comparison of these classes using the Tukey test ($P < 0.01$) is represented

by superscript letters shown in the means of GV, NPV, Soil, Shade and NDFI (Table 6). Means with the same superscript letters showed no significant statistical differences, whereas different superscript letters indicates the opposite. For example, no significant changes in the GV means of Intact Forest (40%, symbol a), Non-Mechanized Logging (41%; symbol a) and Managed Logging (41%; symbol a) were observed among each pair of these classes (Table 6). But, when the pair-wise comparison was performed using the Tukey test between Intact Forest (40%, symbol a), Conventional Logging (38%, symbol b) and Logged and Burned (25%, symbol c) classes, significant changes in the means of the GV fraction were observed for all possible pairs among these classes (Table 6). This also implies that Conventional Logging (b) and Logged and Burned (c) can be separated from Non-mechanized Logging (a) and Managed Logging (a); and that Conventional Logging (b) can also be distinguished from Logged and Burned (c) (Table 6).

NPV and Soil, on the other hand, showed a pattern of increasing mean values from Intact Forest to the most degraded forest class (Table 6). The statistical analysis showed that NPV means of Intact Forest (a), Non-mechanized Logging (a) and Managed Logging (a) are not significantly different from among each other. The NPV means of Conventional Logging (b) and Logged and Burned (b) are also not significantly different from each other. However, Conventional Logging (c) and Logged and Burned (d) showed mean values significantly different from the mean values of Intact Forest (a), Non-mechanized Logging (a) and Managed Logging (a) (Table 6). The Soil fraction showed a similar result as the NPV fraction, except the

Managed Logging (b) and Conventional Logging (b) did not have significantly different means (Table 6).

The mean Shade fraction was slightly higher in Logged and Burned forest (56%) relative to the Intact Forest class (51%). No statistically significant change was observed among each pair of the Intact Forest (a), Non-mechanized Logging (a) and Managed Logging (a) classes (Table 6) using Shade fractions. Significant statistical changes in mean values were observed between Conventional Logging (c) and Logged and Burned (d), and between these two classes and the other classes (i.e., Intact Forest (a), Non-mechanized Logging (a), Managed Logging (a). Managed Logging (b) and Conventional Logging (b) did not show significant change in their means (Table 6).

These statistical results show that GV, NPV and Soil fractions are each sensitive to forest degradation to a certain degree. However, the NDFI which synthesizes all of these data showed more pronounced changes in mean values as a function of forest degradation intensity than the changes in the mean values of any of the individual fraction images. The pair-wise statistical analysis showed that NDFI cannot separate Intact Forest (a) from Non-mechanized Logging (a). But, all other classes [i.e., Managed Logging (b), Conventional Logging (c) and Logged and Burned (d)] showed significant statistical changes in means among each other and against Intact Forest (a) and Non-mechanized Logging (a) (Table 6).

Table 6. Means and standard deviations for Intact Forest and the forest degradation classes. Different superscript letters represent significant statistical difference among classes using the Tukey test at $P < 0.01$. For example, Intact Forest and Non-mechanized Logging showed the same letter (a) meaning that their means are not significantly different using NDFI, whereas Managed Logging (b), Conventional Logging (c) and Logged and Burned showed different letters meaning that there are significant statistical differences among them.

Class	Intact		Nonmechanized Logging		Managed Logging		Conventional Logging		Logged and Burned	
	Mean	Standard Deviation	Mean	Standard Deviation	Mean	Standard Deviation	Mean	Standard Deviation	Mean	Standard Deviation
GV	40 ^a	4	41 ^a	5	41 ^a	5	38 ^b	9	25 ^c	7
NPV	6 ^a	2	5 ^a	2	6 ^a	2	10 ^{bc}	4	11 ^{bd}	3
Soil	2 ^a	1	1 ^a	1	3 ^{ab}	1	4 ^{bc}	3	7 ^d	3
Shade	51 ^a	3	53 ^a	5	51 ^{ab}	4	49 ^{bc}	3	56 ^d	3
NDFI	0.84 ^a	0.08	0.87 ^a	0.07	0.79 ^b	0.07	0.58 ^c	0.24	0.49 ^d	0.22

The changes in mean values from Intact Forest to degraded forest classes can be better visualized in the delta change graph shown in Figure 8. This delta change graph is calculated by subtracting the mean value of Intact Forest from the mean value of each degraded forest class.

The GV fraction decreased non-linearly with degradation intensity. The most drastic changes in GV mean were observed between Intact Forest and Logged and Burned Forests (15%; Figure 8). The Shade fraction changed less than 5% from Intact Forest to the most degraded forest class – Logged and Burned. The mean NPV fraction increased by about 5% between the Intact Forest and both the Conventional Logging and Logged and Burned classes. The Soil fraction showed smaller increases in mean values than the change in mean exhibited by the NPV fraction (Figure 9).

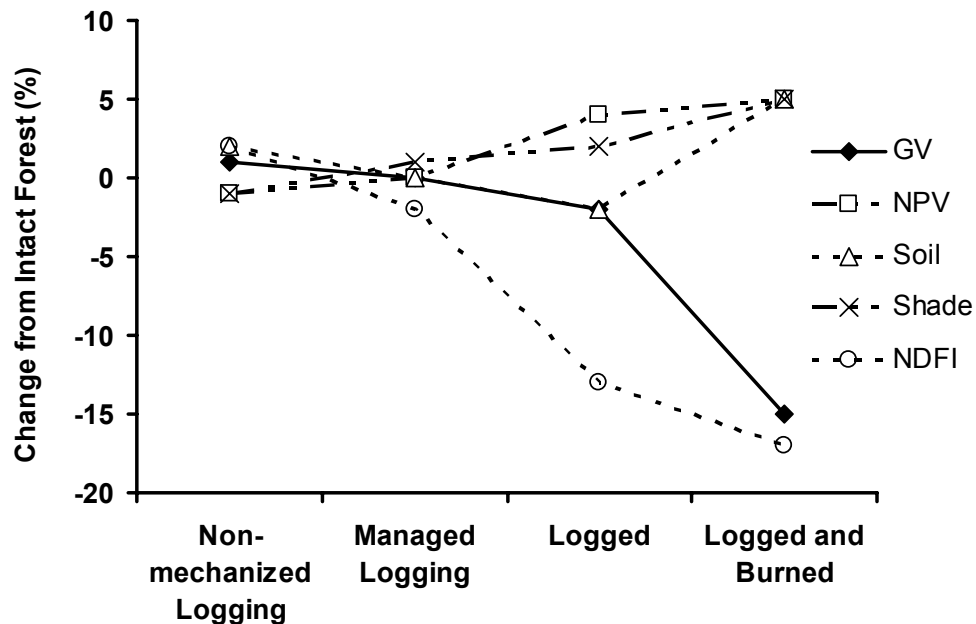


Figure 8. Delta changes of fractions and NDFI, calculated by subtracting the mean value of Intact Forest from the mean value of each degraded forest class.

The percent change of NDFI was also computed to facilitate the comparison of its performance to detect forest degradation changes relative the percent changes obtained with the fraction images. The NDFI images showed a higher percent change between Intact Forest and the forest degradation classes, when compared to the changes detected by any of the individual fraction image (Figure 8). This higher magnitude change is due to the fact that the NDFI includes all changes detected by each individual fraction in one single band. Therefore, the identification of canopy damages due to selective logging and forest burning is enhanced by the NDFI making this information useful for image classification purposes. The most pronounced enhancement can be seen in the potential for discriminating the Conventional Logging class, which typifies most logging activities in the region. None of the individual fractions showed a mean change of greater than 5% but the corresponding NDFI mean values were close to 15% different (Figure 8).

3.5.2 Forest Canopy Damage Detection

Figure 9 shows the region where transects 3, 4 and 5 were conducted, which was selectively logged in 1998 and 1999, severely burned in 2000, then allowed to regenerate over the next three years. Dark green colors in Figure 9 represent forest areas that were not subject to canopy damage due to selective logging and/or burning and as result have high NDFI values (>0.75). Orange to yellow colors are associated with forest canopy damage ($0 < \text{NDFI} < 0.75$) due to selective logging and forest burnings. Areas with negative NDFI values show up in the NDFI images in magenta

and white colors and are mostly associated with areas that were subject to clear-cutting (Figure 9).

The first selective logging event in this area happened in 1998 (Figure 9a). It is possible to observe log landings and infer the location and shape of the primary logging roads connecting the log landings. Forest canopy damage is identified as light green pixels with $\text{NDFI} < 0.75$ as indicated by the arrow in Figure 9a. Because the timber harvesting had not been completed until the image acquisition date, it is still possible to observe Intact Forest ($\text{NDFI} > 0.75$) areas among the log landings and logging roads in the southern part of the selectively logged area in 1998.

The NDFI values of the selectively logged forest in 1998 increased in the 1999 image – old logged in Figure 9b – but a canopy damage signal (i.e., $\text{NDFI} < 0.75$) of selective logging appeared right beside the area logged in 1998. In 2000, this logged forest area was subject to a severe fire event, burning approximately 5,000 hectares (Figure 9c). The NDFI values of this Logged and Burned forest are smaller than the NDFI values found in the conventionally logged forests in the previous years due to more drastic canopy damage and a higher concentration of exposed NPV and Soil (Figure 9a-b). Areas that completely lost forest canopy due to fire show up as negative NDFI values (Figure 9c). In the year following burning, the forest canopy damages can still be detected with the NDFI image (Figure 9d). In the second year after burning, the canopy damages are no longer visible with only log landings showing up (Figure 9e). Finally, in the third year the NDFI values returned to those found in intact forest (Figure 9f).

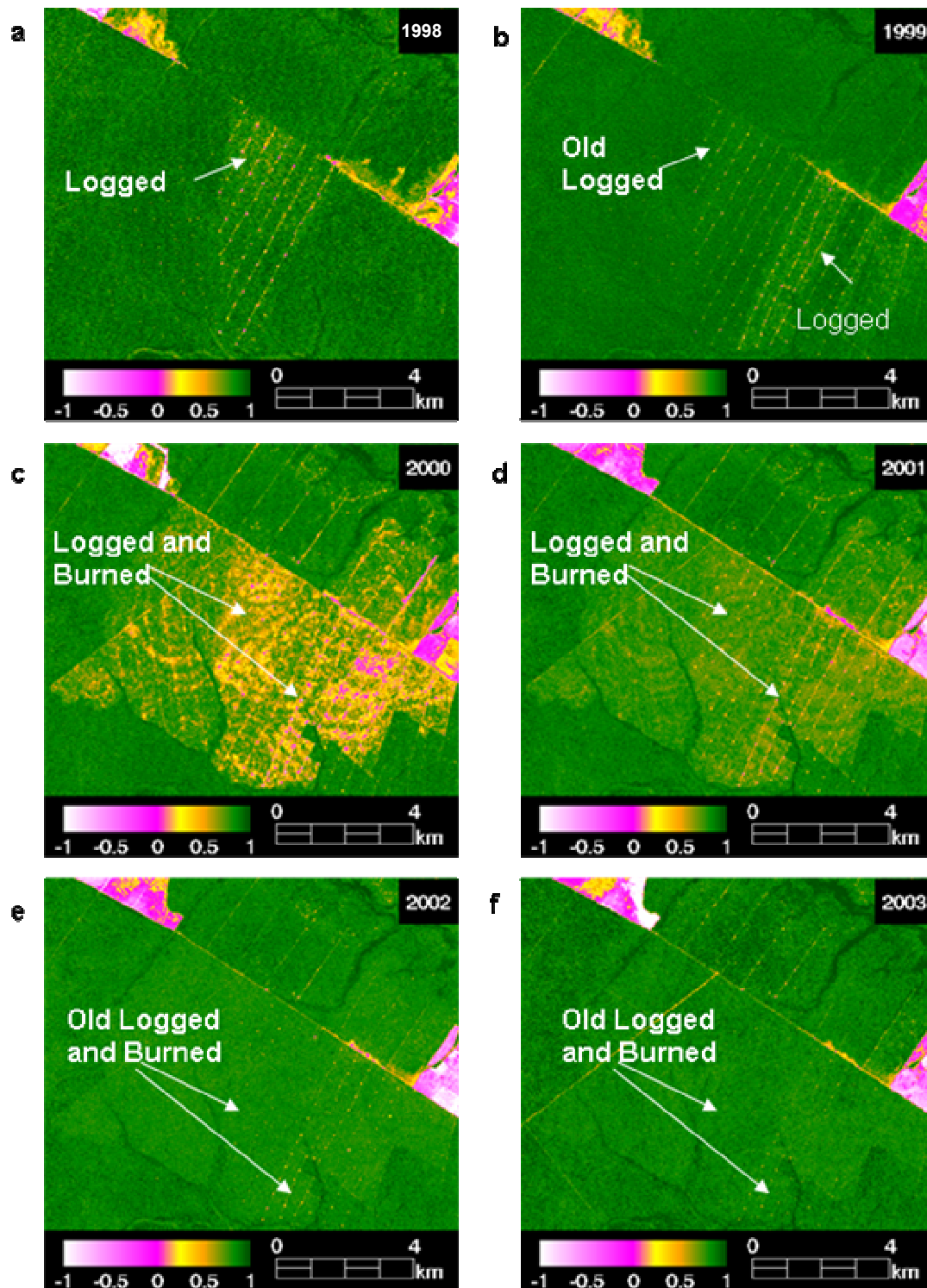


Figure 9. Examples of forest degradation processes and temporal changes as detected the NDFI band.

NDFI and individual Fraction statistics were calculated for intact forest, canopy gaps, log landings and burned areas found in the Logged and Burned forest showed in Figure 10. Mean NPV, Soil and Shade fractions increased in log landings, canopy gaps and burned forest areas relative to intact forest areas (Figure 10). On the other hand, GV was the only fraction that exhibited a decrease in canopy gaps, log landings and burned areas relative to intact forest areas. The NDFI means for these environments changed more drastically than the changes detected by any of the individual fractions. The NDFI mean in intact forest was 0.84, dropping to 0.73, 0.26 and 0.17 in canopy gaps, respectively (Figure 10). Therefore, NDFI has a greater potential for sub-classifying these types of degraded forest than individual fraction images values.

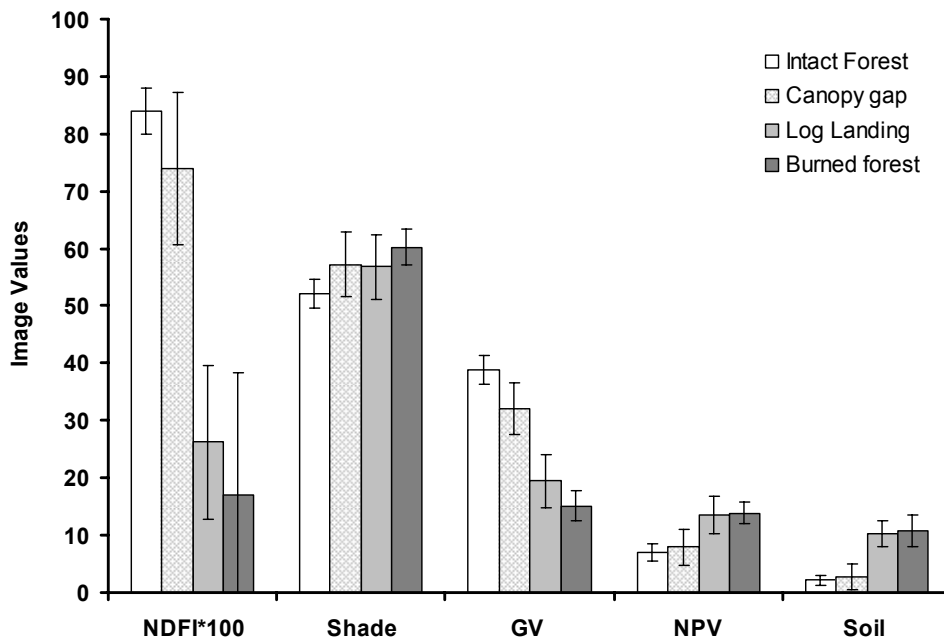


Figure 10. Fractions and NDFI means and standard deviation (vertical error bar) of the main environments found in degraded forests areas.

3.5.3 Canopy Damage Classification

The CCA detected canopy damages associated with selective logging and forest burning using the location of log landings as contextual information and the NDFI as the spectral information sensitive to canopy damages. The classification results were very accurate for the transect areas (Figure 1). The canopy damages were detected in all transects of Managed Logging, Conventional Logging and Logged and Burned classes. In the Non-mechanized Logging, however, the CCA algorithm did not detect canopy damage because the forest pixel showed NDFI values above the detection threshold and no log landing existed in these areas. Cleared areas for building log landings and logging roads were detected and mapped within the Managed Logging transect areas, but tree fall gaps were less frequently identified because of the reduced canopy damage characteristic of forest management practices used in these forests (Johns et al., 1996). In the Conventional Logging transect sites, the canopy damage area was much greater than that detected in the Managed Logging transect sites. This is to be expected due to the more intensive canopy damage associated with unplanned logging operations. All Logged and Burned transect areas, which show the most severe canopy damage impacts, were mapped accurately with the CCA classifier.

It was not the objective of this study to perform a time-series classification, so only the full classification results for 2000, which corresponds to the year that the aerial videography data were acquired. In the study area (about 30,000 km²), 65%

was classified as Intact Forest, 22% as non-forest (i.e., deforested areas and water bodies) and 13% was classified as canopy damaged areas.

Examples of canopy damaged areas detected with the CCA classifier, outside the transect areas, are shown in Figure 11. Selectively logged areas that have an irregular spatial arrangement of log landings and logging roads are usually associated with more damage than unplanned harvesting operations. Managed logging operations are characterized by a more regular arrangement of log landings and roads. The CCA values for unplanned logging areas showed a much higher proportion of canopy damage, relative to intact forest, than the proportions from managed logging areas (Figure 11a,b). Forest areas that were subjected to the more drastic impacts of logging and burning have virtually all of the canopy area mapped as damaged (Figure 11c).

The overall accuracy of the CCA classifier was 90.4% and the user's accuracy of the canopy damage class was 94% (Table 7a). Most of the error, revealed in the error matrix, is associated with the classification of reference canopy damage data as forest (23%). This misclassification is expected due to the land cover mixing between intact forests, canopy damaged forests and areas subjected to clear-cut (i.e., log landings and logging roads) that typify selectively logged forests. The canopy damage map accuracy has also been assessed using the shade-normalized GV fraction as the search image to detect canopy damage (threshold ranging from 50 to 75%). The overall accuracy dropped from 90.4% using NDFI to 86.8% using the shade-normalized GV to detect canopy damage (Table 7b). The user's accuracy of

the canopy damage class obtained with the shade-normalized GV (92.0%) was virtually the same as the one obtained using the NDFI image (94.0%). But the user's accuracy of the forest class was 6% lower using shade-normalized GV (Table 7b).

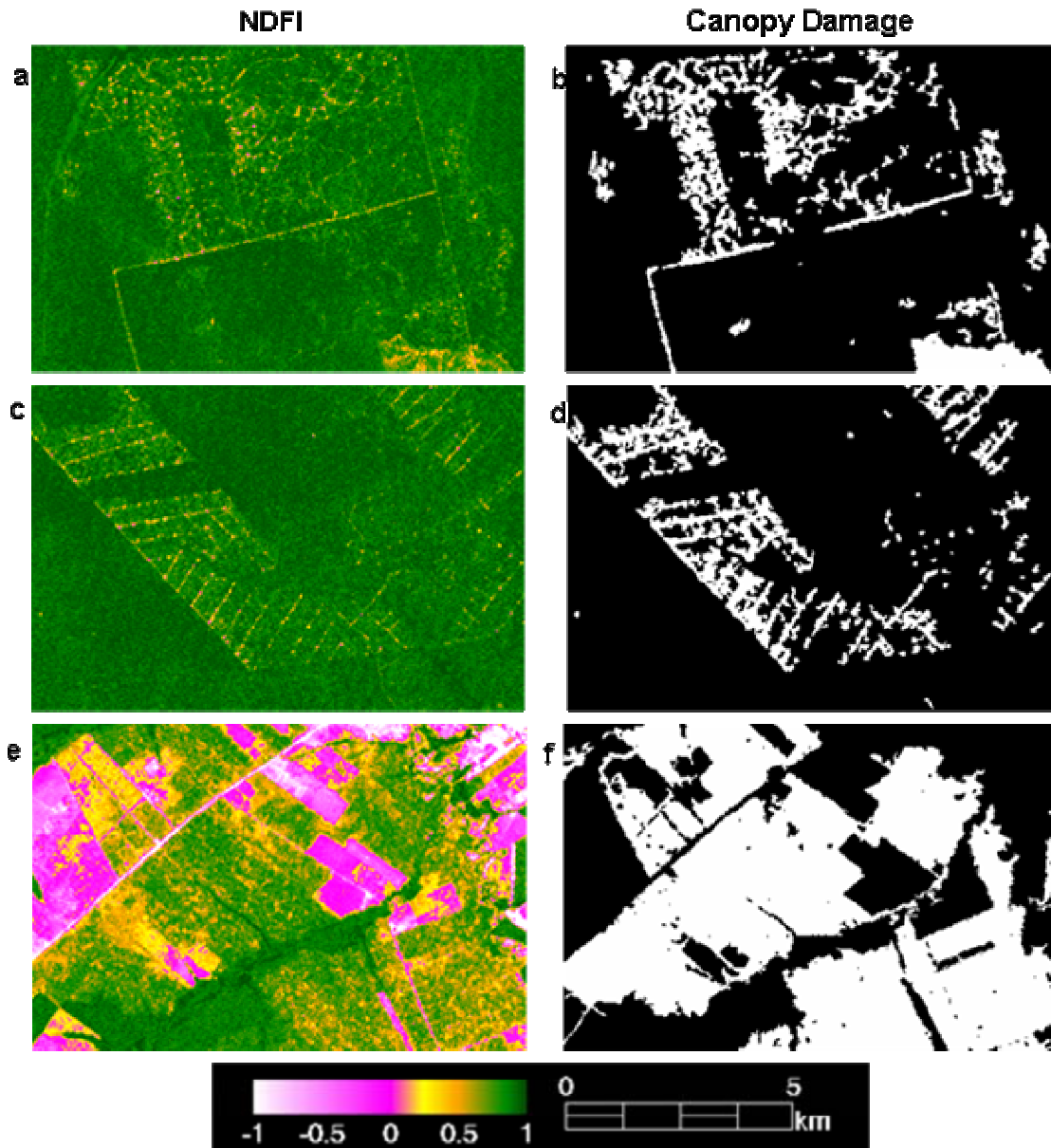


Figure 11. Canopy damage classification examples obtained with the CCA classifier.

Table 7. Accuracy assessment results of the CCA classifier: a) using the NDFI as the search image for CCA; b) using GV as the search image for CCA.

a) NDFI accuracy assessment

Classified Pixels	Reference Pixels				Users Accuracy (%)
	Non-forest	Forest	Canopy Damage	Total	
Non-forest	454	0	17	471	96.4
Forest	6	625	117	748	83.6
Canopy Damage	40	0	616	656	93.9
Total	500	625	750	1875	

Producers Accuracy (%) 91.0 100.0 82.0

Overall Accuracy = (1695/1875) = 90.4%

Kappa Coefficient = 0.85

b) Shade-normalized GV accuracy assessment

Classified Pixels	Reference Pixels				Users Accuracy (%)
	Non-forest	Forest	Canopy Damage	Total	
Non-forest	454	0	17	471	96.4
Forest	6	625	185	810	77.0
Canopy Damage	40	0	548	594	92.0
Total	500	625	750	1875	

Producers Accuracy (%) 91.0 100.0 73

Overall Accuracy = (1627/1875) = 86.8%

Kappa Coefficient = 0.80

* The accuracy error matrix obtained after removing 5 blocks of canopy damage reference data that were subjected to land cover changes within the period of Landsat image and videography images acquisitions, and after geo-correcting five block samples, also of this class, as proposed by Powell et al. (2004).

The detection of log landings is crucial for a successful implementation of the CCA classifier. Recent log landings can be easily identified in selectively logged forest and were accurately mapped. In severely logged and burned forest, however,

not all log landings could be mapped. However, this did not represent a problem in these areas because very large contiguous canopy damaged areas are associated with these forests and only a few log landings are required as start locations for the 2D-search program that seeks canopy damage areas.

3.6. Discussion

The NDFI and the CCA methods proposed in this study have the potential to contribute to the mapping of degraded forest associated with selective logging and burning in the Amazon region. The NDFI provides higher sensitivity to detected canopy damage than individual fraction values derived from SMA. The CCA classifier utilizes the location of log landings – the spatial signature of selective logging – to look for canopy damaged areas, enabling the distinction between natural and anthropogenic forest disturbances. Because most forest fires occur in logged forests (Cochrane, 2003), this methodology can also detect and map forest canopy damage due to forest fires.

The detection and mapping of forest canopy damage due to logging and forest fires is intimately related to the detection of log landings and to the damage intensity. The detection and mapping of Non-mechanized Logging is not possible because this type of logging does not build log landings and generates low canopy damage. But, this type of selective logging in the Amazon region is associated with less than 5% of the timber production in the region (Lentini et al., 2003) with Conventional Logging and, to a lesser extent, Managed Logging the dominant forms. For these two types of

logging, detection and mapping of log landings are imperative to the success of the NDFI-CCA methodology. The log landing detection and mapping depends on empirical thresholds (Souza Jr. et al., 2003; Monteiro et al., 2003). The first threshold is applied to identify forested pixels with high soil fraction (i.e., Soil > 10%) associated with logging roads and log landings. Next, an area threshold is applied to map log landings (i.e., 1 to 4 contiguous pixels). These thresholds cannot be generalized to the whole Amazon region – it is likely that new thresholds have to be defined for other types of forests where selective logging is taking place such as dense and open forests. The same caution should be used when applying the NDFI threshold to other types of forests to detect canopy damages.

The NDFI-CCA approach identifies and maps a variety of canopy damages associated with selective logging including the construction of roads and log landings, tree fall gaps, and all canopy damaged areas in burned forests. Tree fall gaps and burned forest are responsible for most of the biomass impacts and forest damages in selectively logged areas (Johns et al., 1996; Gerwing, 2002). Undamaged forests within the logged forests area not mapped with the NDFI-CCA methodology. The method proposed by Souza Jr. and Barreto (2000), which uses the location of log landings and a field-calibrated harvesting radius to estimate the total area potentially impacted by logging (i.e., damaged and undamaged forests) could be integrated with the NDFI-CCA method proposed in this study. By integrating these two approaches, the proportion of canopy damage, detected with NDFI and CCA, could be calculated relative to the total logged area. Such information would be useful for local

monitoring of approved forest management plans and certified logging operations, which are expected to harvest trees with a minimal amount of canopy damage. For example, the Forest Stewardship Council (FSC) has defined a set of on-the-ground forestry operation standards to provide certification to loggers (<http://www.fscoax.org/index.html>). Currently, 1.8 million hectares of forests are certified in the Amazon region (FSC-Brazil; <http://www.fsc.org.br/>).

The NDFI-CCA method can also be integrated with existing methods to subclassify canopy damaged areas into classes of degraded forests (e.g., managed logging, conventional logging, heavily logged and burned forests). For example, a decision tree classification was used to map several classes of degraded forests in the Eastern Amazon using GV, NPV and Shade fraction images derived from SPOT 4 (*Satellite Pour L'observation de la Terre* ; Souza Jr., et al. 2003). I tested this approach in the transitional forests of Sinop, using fraction images derived from Landsat images, and found the results to be less accurate than those obtained for the dense forests of the Eastern Amazon due to confusion caused by the more open nature of these forests. However, the CCA method can be used to flag a region of forest as degraded for subsequent classification using decision trees, thereby increasing the overall accuracy of the method. There is the potential for additional improvement, by combining the NDFI image with the other fraction images, in the decision tree classification. This is an area of ongoing experimentation by our research group.

Access to cloud free images over the Amazon is critical for monitoring forest degradation. The optimal temporal resolution for detecting selective logging and burning is one year using the GV fraction and two years with the NPV fraction (Souza Jr., et al., in press a). The results indicate that the optimal temporal resolution of NDFI to detect canopy damage due to selective logging and burning is also one and two years, respectively. However, the NPV and the GV forest degradation signals are not as strong as the NDFI signal, making the detection and mapping of forest canopy damage more accurate with NDFI.

The NDFI statistics extracted for the Intact Forest transects and for the degraded forest transects are compatible with the field-measured biophysical properties (Table 5). The observed amounts of intact vegetation decreased with increasing forest degradation intensity and the corresponding amounts of detected wood debris and soils increased. The NDFI mean decreased as intact vegetation amounts decreased and the amount of wood debris and disturbed soil increased. Therefore, there is also potential to correlate canopy cover and biomass field measurements with the NDFI. More detailed studies, however, need to be conducted to demonstrate if these biophysical forest properties can be estimated with NDFI.

Further image processing improvements that would prove helpful include developing fast and generic SMA models to generate physically meaningful fraction images over the Brazilian Amazon. Such generic SMA models have been suggested by Small (2004), due to the consistent topological structure of Landsat images spectral space. Currently, available SMA automation techniques use a combination

of very large endmember spectral libraries and Monte Carlo simulation (Bateson et al., 2000; Asner et al., 2004), which are computationally prohibitive for most Brazilian government agencies. The proposed NDFI-CCA methodology should be compared with the existing methods used to map selective logging and forest fire damage.

3.7 Conclusions

The NDFI and the CCA classifier can contribute to ongoing efforts to map and monitor logging operations in the Brazilian Amazon. NDFI enhances the detection of canopy damage over existing techniques and can be used in conjunction with the CCA algorithm to unambiguously map forest canopy damage caused by selective logging and burning. Additionally, the proposed techniques can be integrated with existing image processing methods to classify the damaged forest canopy areas into sub-classes of degradation. Image processing improvements, including the development of fast and generic SMA techniques for generating consistent NDFI images across the Amazon region, will be necessary to fully automate such forest degradation analyses. This is important for practical monitoring applications by government environmental agencies and private institutions tasked with certifying logging operations.

CHAPTER IV: Long Term Forest Degradation Mapping and Change Detection in the Southern Brazilian Amazon Forests

4.1. Introduction

Tropical forests of the Brazilian Amazon have changed greatly in the past 30 years. Two key forest changes in the region are forest conversion to agriculture (i.e. deforestation) and forest degradation by such processes as selective logging and forest fires that only partially deforest an area. Forest conversion replaces the original forest cover by another land cover type (e.g., forest to pasture), whereas forest degradation changes the original forest structure and composition, but without completely removing the original forest cover. Forest can be degraded by natural phenomena (e.g. treefalls, windthrows, lightning strikes) or by anthropogenic activities. Selective logging and forest fires are the main anthropogenic disturbances responsible for forest degradation in the Amazon (Nepstad et al., 1999; Cochrane et al., 1999; Cochrane, 2003). Although natural forest fires may have historically occurred, these events have been so rare that forest tree species are almost all extremely sensitive to fire disturbance, exhibiting no evolutionary adaptations specific to fire (Uhl and Kauffman 1990). The current prevalence of forest fires in the Amazon has been clearly linked to human fire use (Cochrane 2001, Cochrane et al. 2004).

Forest conversion has been quantified using satellite remote sensing in the Amazon region by a long-term deforestation monitoring program (INPE, 2003),

providing relevant information for policy making such as the location and geographic extent of deforestation and estimates of deforestation rates (e.g., Casa Civil, 2004). Several local and regional studies have focused on the identification and mapping of deforestation (e.g., Fearnside and Salati, 1985; Fearnside 1989; Skole and Tucker, 1993; Alves and Skole 1996; Roberts et al., 2002). Pasture to second growth transitions, and second growth succession have also been the focus of several studies (e.g., Moran et al., 1994; Adams et al., 1995; Rignot et al., 1997 Nelson et al., 2000).

More recently, pioneering remote sensing techniques for mapping forest degradation have been developed (Cochrane and Souza Jr., 1998; Souza Jr. and Barreto, 2000; Monteiro et al., 2003, Souza Jr. et al., 2003), however, they are still being perfected (Souza Jr. et al., in review). Existing change detection analyses of degraded forest in the Amazon have been of limited use due to the types of imagery available, evolving techniques, and a lack of frequent enough image dates to fully characterize selective logging (Stone and Lefebvre, 1998; Souza Jr. and Barreto, 2000; Monteiro et al., 2003) and fire dynamics (Cochrane et al. 1999, Cochrane 2001). Single date, infrequent or short-term satellite acquisitions are potential sources of errors in forest degradation temporal analyses due to rapid canopy closure and regeneration of degraded forest (Stone and Lefebvre, 1998; Lambin, 1999; Souza Jr. et al., in press a).

Annual forest degradation maps would enable estimation of forest degradation rates, and an understanding of the relationships between forest degradation, deforestation (Cochrane et al., 1999; Cochrane, 2001) and selective logging

(Cochrane et al., 2004). This is key information for land cover change models that could be useful for predicting the future of the Amazon and the impacts of forest degradation on hydrological, biogeochemical and carbon cycles (Bazzaz, 1998; Giambelluca, 2002; Houghton et al., 2000). Environmental agencies could also benefit from the ability to monitor the expansion of degraded areas, facilitating enforcement of environmental protection laws.

A pioneering study that utilized a robust multi-temporal analysis of degraded forests, encompassing 20 years of Landsat images has been conducted in the Southern Amazon (Souza Jr. et al., in press). The aim of the study was to statistically define the most useful information, extracted from Landsat images (e.g., reflectance bands, vegetation indices and fraction images), for detecting forest degradation changes caused by selective logging and forest fires, as well as the optimal temporal resolution for mapping these changes. Here, I present results from a twenty year long series of annual Landsat imagery that was used to map and quantify the rates of forest degradation caused by selective logging and forest fires. Additionally, I characterize and quantify the relationship between deforestation and forest degradation in the study area by answering the following questions: How much degraded forest is subsequently deforested? What are the observed fates of the degraded forests in the study area?

4.2. Study Area

The change detection analysis was conducted in the area defined by the intersection of the all Landsat images used in this study (path 226, row 68), encompassing 28,750 km². This Landsat path/row covers the Sinop region, an important sawmill center of the state of Mato Grosso during the 1990's (Figure 1). Transitional forest between 'cerrado' and dense tropical forest is the main forest type found in this region. The topography is predominantly flat, on Latosol soils with an average annual precipitation of 2,000 mm. The dry season is characterized by several months of less than 100 mm of precipitation and typically extends from May to October (RADAMBRASIL, 1981). The main land uses in this region are agricultural (e.g. ranching and soybean cultivation) and selective logging. Selective logging extracts only a few of the most valuable trees from each hectare of forest but logging operations frequently cause extensive damage to the remaining trees and fracture the forest canopy (Uhl and Vieira, 1989). Forest burning is also common in this region, acting synergistically with selective logging to increase forest canopy damages (Monteiro et al., 2004; Cochrane et al., 2004). Conventional logging and forest fires are the main causes of forest degradation in the region, reducing on average the forest canopy cover by 33% and the live biomass by 45%. (Souza Jr., et al., *in press*).

4.3 Data set

Eighteen Landsat Thematic Mapper 5 (TM) images and three Landsat Enhanced Thematic Mapper (ETM+) images were used in this study (Table 1). The imagery

was acquired during the dry season of each year between 1984 and 2004. Limiting imagery dates to the dry season minimizes any potential misclassification of forest degradation due to seasonal changes. The number of days between image acquisitions varied from 299 to 433 days, with an average of 359 days (Table 1). For annual rate calculations of deforestation and forest degradation, the change increments quantified between satellite image dates were normalized to 365 days (i.e., the change detect between two consecutive dates divided by the number of days and multiplied by 365).

4.4. Methodology

The forest conversion and forest degradation change detection analyses consisted of three image processing stages: pre-processing, canopy damage classification and forest change detection (Figure 12). The image processing techniques of each stage are described in detail in the subsections below.

4.4.1 Pre-processing

a) Georeferencing and Registration

Image registration is an important step in remote sensing change detection because pixel misregistration can introduce error in the quantification of land cover changes. First, the Landsat ETM+ image acquired in 1999 was georeferenced using 30 image control points extracted from NASA GeoCover 2000 Mosaic (<https://zulu.ssc.nasa.gov/mrsid/>). Next, the georectified Landsat image was used as

the base image for registering the remaining images (Table 2). A minimum of 14 image control points were used and the maximum root-mean-square error allowed was 1 pixel in the image registration process. The RMS varied from 0.53 to 0.97, which assures that the changes detected over time were not contaminated by misregistration (Verbyla and Boles, 2000). The software Environment for Visualizing Images – (ENVI 4.0; Research Systems, Boulder, CO) was used for these tasks (Figure 13).

b) Atmospheric Correction

The 1999 Landsat reference image was converted from encoded digital number (DN) to reflectance. First, the reference image was converted to radiance using the gains and offset provided in the image metafile. Next, the radiance image was converted to reflectance using the software Atmospheric Correction Now 4.0 (ACORN:Analytical Imaging & Geophysics, Boulder, CO). The atmospheric parameters that cannot be estimated from the Landsat bands were estimated using a trial-and-error sensitivity analysis of a dark object reflectance (a lake). The estimated water vapor and the image atmosphere visibility were 40 millimeters and 25 km, respectively, for the reference image (Figure 12).

c) Image Inter-calibration

The other images (Table 2) were inter-calibrated to the reflectance image using a relative radiometric calibration approach (Roberts et al., 1998; Furby & Campbell, 2001), regressing encoded radiance against reflectance in the reference image. This

technique assumes uniform atmosphere over the image scene, and that invariant ground targets can be found in the reference and the uncalibrated images. To account for spatially variable atmospheric contamination due to haze and smoke, the Carlotto (1999) technique was applied to those images that had significant contamination

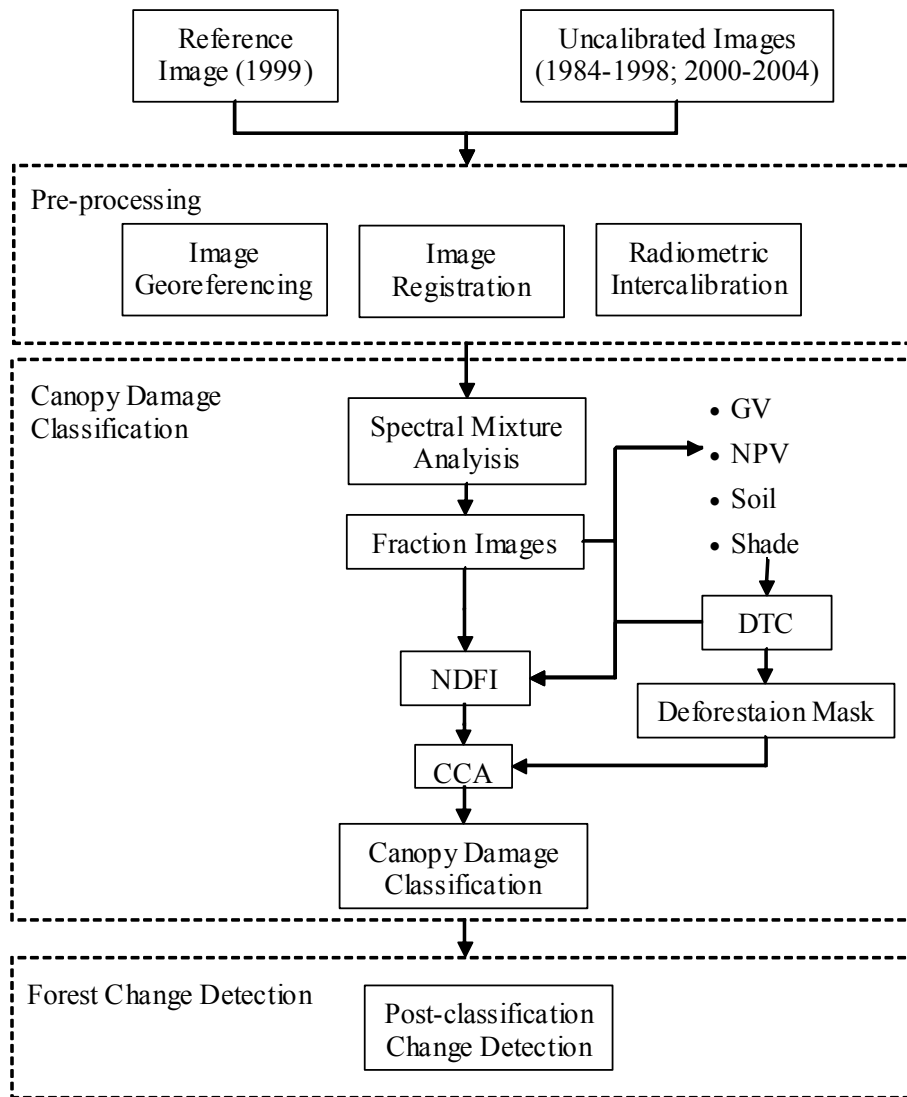


Figure 12. Image processing chain conducted in the forest change detection analyses.

prior to relative radiometric calibration. The Carlotto technique is based on the assumption that smoke and haze only adversely impact the visible bands, leaving the NIR and short-wave Infrared bands unchanged. Statistics are calculated for the entire image, in which average values for TM bands 1, 2 and 3 are calculated for each unique combination of TM bands 4, 5 and 7. After calculating these statistics, the original values for TM bands 1, 2 and 3 for a specific combination of bands 4 to 7 are then replaced with the scene averages for that combination. This approach, developed by Carlotto (1999) has the effect of homogenizing contamination throughout a scene – thus clear sky portions of the image gain a slight amount of contamination, while contamination is significantly reduced in areas under smoke or haze.

Typical invariant targets used included intact forest, second growth, green pasture, bare soil and water. Second growth and green pasture were only used as invariant targets for images that were no more than two years apart from the reference image date. The slopes and intercepts for the relative radiometric inter-calibration were obtained from a linear regression that was estimated using the pixel mean values, extracted from a 3 by 3 pixel area, of the invariant targets for each band. These coefficients normalize the uncalibrated images to the reference images, converting Digital Numbers of the uncalibrated images to reflectance (Figure 12).

4.4.2 Canopy Damage Classification

Fraction images derived from Spectral Mixture Analysis – SMA – (Adams et al., 1993) perform better than reflectance bands and vegetation indices in detecting forest

degradation caused by selective logging and forest fires (Souza Jr., et al., in press a). The Normalized Difference Fraction Index – NDFI was chosen as the spectral index for the analysis because it synthesizes all fraction images, derived from SMA, into a single band that enhances the detection and mapping of canopy damage (Souza Jr. et al., in press b; and Chapter III for details). For these reasons, fraction images and NDFI were chosen for mapping deforestation and canopy damage prior to the forest change detection analysis.

SMA was applied to decompose the Landsat TM/ETM+ reflectance data of each pixel into fractions of green vegetation (GV), non-photosynthetic vegetation (NPV), Soil and Shade. Detailed information on how these models were computed and validated for these Landsat imagery data sets can be found in Chapters II and III. Once the fractions are obtained, the NDFI can be computed as:

$$\text{NDFI} = \frac{\text{GV}_{\text{Shade}} - (\text{NPV} + \text{Soil})}{\text{GV}_{\text{Shade}} + \text{NPV} + \text{Soil}} \quad (13)$$

where GV_{shade} is the shade-normalized GV fraction given by,

$$\text{GV}_{\text{Shade}} = \frac{\text{GV}}{100 - \text{Shade}} \quad (14)$$

The NDFI values range from -1 to 1. Forests of the study area have high NDFI values (i.e., > 0.75) and degraded forests showed moderate to low NDFI values (i.e., $0.4 < \text{NDFI} < 0.75$) (see Chapter III for details).

The land cover types of interest for this study were: forest, clear-cut and forest with canopy damage. A decision tree classification (DTC) of fraction images and NDFI was used to create the base land cover map from the 1984 Landsat image that

was then used in the multi-temporal forest change analysis. Visual inspection of the DTC results, in conjunction with fraction color composite (R=Soil, G=GV, B=NPV), was performed to locate classification errors. Classification errors were then corrected manually. Common errors included small areas of green pasture or agriculture fields being misclassified as forest. The final 1984 classification base map had the following classes: Forest, Clear-cut and Non-forest (i.e., water and wetlands). The Non-forest class was used as a mask for all other images acquired after 1984 because I am not interested in quantifying changes associated within this class.

The forest canopy damage class was mapped separately for each individual image using a contextual classification algorithm – CCA – (Souza Jr. et al., in press b). The locations of log landings, which are the storage area scraped clear of vegetation by loggers, are extracted from the Soil fractions (Souza Jr. and Barreto, 2000; Monteiro et al., 2003). The CCA integrates the log landing locations with the NDFI image in a 2D-search program that looks for the range of values (0 to 0.75) in the NDFI images that are associated with canopy damages caused by selective logging and forest fires in this region (Souza Jr., et al., in review). In addition, large negative differences in NDFI values (i.e., < -0.75) detected between each pair of image dates (i.e., recent NDFI minus old NDFI) were used to map recently deforested areas and update the base land cover map (Figure 12).

4.4.3 Forest Change Detection

The change detection analysis was done using an algorithm designed to detect and quantify the following forest changes: Forest to Clear-cut, Forest to Canopy Damage, Canopy Damage to Forest, and Canopy Damage to Clear-cut (Figure 13). Next, annual rates of deforestation and of forest degradation - represented by the forest canopy damage class – were computed by normalizing the changes estimated between the acquisition intervals of each pair of images to 365 days (Table 1).

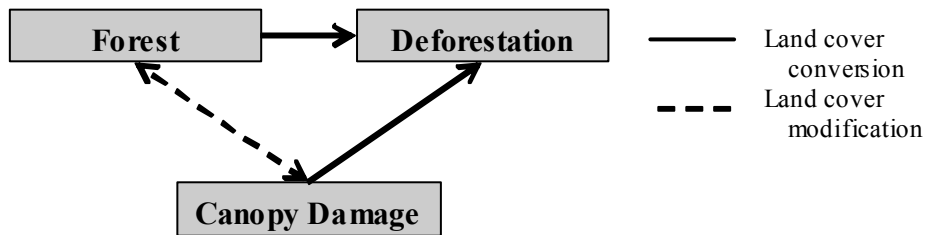


Figure 13. Forest Change detected with the multi-temporal analysis.

4.5. Results

4.5.1 Image Classification

By 1984, 8.8% of the study had already been deforested while virtually none of the forest showed canopy damage. However, by 2004, deforestation had increased to 28.2% of this region and 15% of the remaining forests showed canopy damage from recent logging and forest fire (Figure 14). Of the remaining forest (71.8% of the image), 15% had detectable canopy damage caused by selective logging and fires.

Because forest canopy damage caused by selective logging and forest fires recovers within one to two years (Souza Jr. et al, in press a), the area mapped as Forest for individual years did not show a constant decrease, but a pattern of shrinking and expanding over time (Figure 14). Canopy Damage mapped in one year is likely to be mapped as Forest in the next year if the damaged forest is not further degraded by fire or converted to pasture and agriculture fields. For example, in 2000, Forest was 65% of the study area and the Canopy Damage was 12%. In 2001, the area classified as Forest increased to 70% because much of the Canopy Damage area mapped in 2000 had recovered and was mapped as Forest (Figure 14).

The classifications also revealed that the area annually affected by forest degradation – classified in the study as Canopy Damage – varies from year to year and is substantial in many years (Figure 14). On average 3.7% of the forested area was classified as Canopy Damage each year. Seven years showed forest areas with Canopy Damage above the average over the twenty-year time period (1993, 1996, 1998, 2000, 2001, 2003 and 2004). In the years 2000 and 2004 the Canopy Damage was more than 10% of the study area (i.e., > 15% of the total forest area). These statistics are for single date classifications and do not take into account older degraded forests which may have intact canopies but which are not compositionally or structurally equivalent to intact forest. Therefore, truly intact forest that has not been degraded by selective logging and forest fires, might be much smaller than the 60% of the study area classified as Forest in 2004. Only a multi-temporal change

detection analysis can reveal how much forest area is actually free from disturbance over the last 20 years.

4.5.2 Forest Change Detection

Four forest change classes were detected and quantified with the multi-temporal analysis: Forest to Clear-cut; Forest to Canopy Damage (i.e., forest degradation); Canopy Damage to Clear-cut; and Canopy Damage to Forest (i.e., regeneration) (Figure 13). The area percent change of these class transitions was computed, relative to the study area, for each pair of dates (Table 8). Overall, the percentage of forest area that changed to Canopy Damage each year was, on average, two times larger than the area deforested (Table 8). The Forest to Canopy Damage change was three times larger than Forest to Clear-cut in three periods (1988-1989, 1995-1996, 2003-2004). From 1997 to 1998 and from 1999 to 2000, forest change to Canopy Damage was very high, damaging an area larger than 1,400 km² (5% of the study area; Table 8).

On average, about 89% of the Canopy Damage class was mapped as Forest in the subsequent year. The remaining 11% was either deforested or subjected to a recurrent degradation event in the following year. The degraded forests (i.e., Canopy Damage class) contribute on average 16% of the total deforestation, representing on average 10% of the area annually affected by forest degradation. It is important to highlight that the forest change statistics presented on Table 8 do not include the percentage of old degraded forests converted by deforestation (Table 8). Because degraded forests can change to Forest within one to two years (Souza et al., in press

a), some of the Forest to Clear-cut changes may certainly be due to Canopy Damage that changed to Forest and then changed to Deforestation. A more detailed change detection analysis was performed to account for the percentage of old degraded forests that were converted by deforestation.

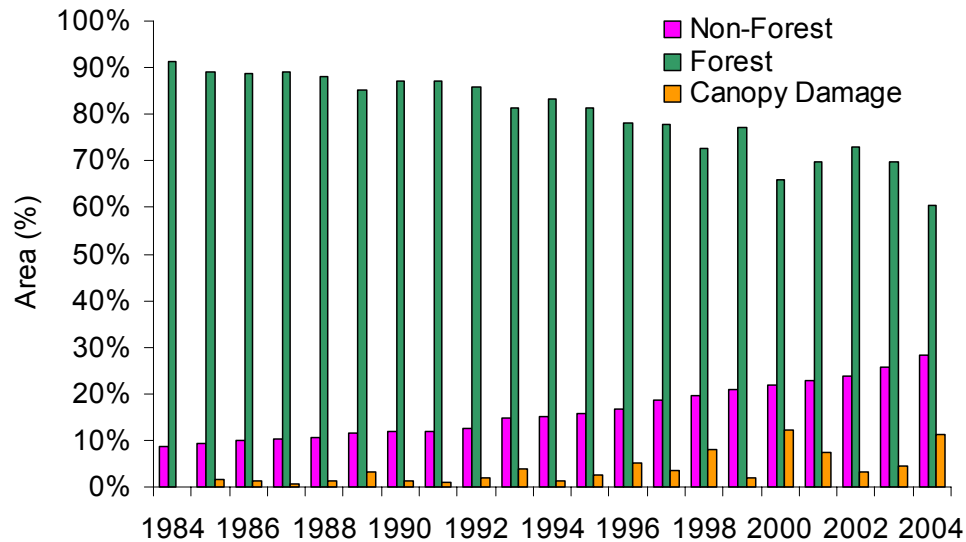


Figure 14. Areal percent of Forest, Canopy Damage and Non-forest quantified in the forest change detection analysis.

4.5.3 Deforestation and Forest Degradation Rates

The annual rates of deforestation and forest degradation (i.e., Forest to Canopy Damage) are presented in Figure 15. The average annual deforestation rate was less than 1% from 1984 to 2004. From 1992 to 1993 and 2002 to 2003, the deforestation rate was twice the average annual deforestation rate and from 2003 to 2004, the rate increased by three-fold relative to the average annual deforestation rate (Figure 15).

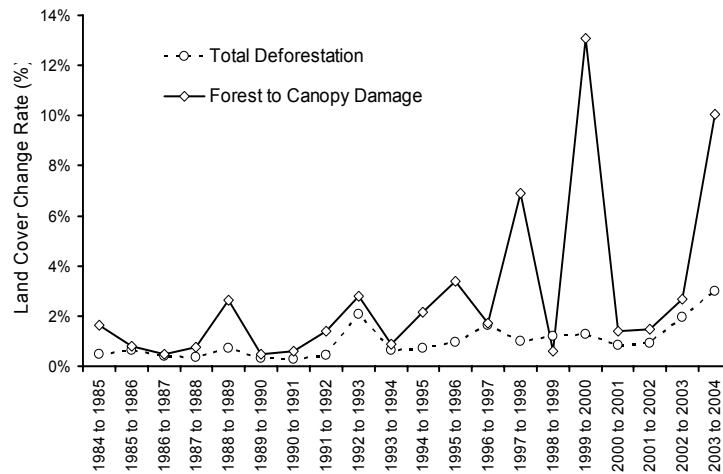


Figure 15. Annualized deforestation and forest degradation rates.

The annual rate of forest degradation in the study area was always greater than the deforestation rates, except from 1998 to 1999 which showed a deforestation rate (1.2%) two times greater than the forest degradation rate (0.6%; Figure 15). The average annual forest degradation rate was 2.8%, almost three times the average annual deforestation rate. Six peaks of forest degradation were identified (1988-1989, 1992-1993, 1995-1996, 1997-1998, 1999-2000, 2002-2003 and 2003-2004). Only the forest degradation peak from 1992 to 1993 showed a high corresponding deforestation peak. Three very high forest degradation rate peaks were detected (1997-1998, 1999-2000 and 2003-2004 (Figure 14). Most of the forest degradation mapped in these years showed Canopy Damage area associated with forest fires. When examining historical climate records most of these forest degradation peaks coincided with or are immediately after El Niño years (source:

<http://www.elnino.noaa.gov/>).

Table 8. Percentage of Forest and Canopy Damage changes quantified in the forest change detection analysis relative to the study area.

Time Interval (year)	Number of Days between Image Acquisition	Forest to Clear-cut (%)	Canopy Damage to Clear-cut (%)	Total Deforestation (%)	Forest to Canopy Damage (%)	Canopy Damage to Forest (%)
1984 to 1985	379	0.5	0.0	0.5	1.7	0.0
1985 to 1986	394	0.6	0.1	0.7	0.9	1.3
1986 to 1987	318	0.3	0.0	0.3	0.4	0.8
1987 to 1988	406	0.4	0.0	0.4	0.9	0.3
1988 to 1989	380	0.6	0.1	0.7	2.7	0.5
1989 to 1990	332	0.2	0.1	0.3	0.4	2.5
1990 to 1991	330	0.2	0.0	0.2	0.5	0.8
1991 to 1992	383	0.4	0.0	0.4	1.5	0.6
1992 to 1993	391	1.9	0.4	2.2	3.0	0.5
1993 to 1994	306	0.5	0.0	0.5	0.7	3.2
1994 to 1995	341	0.6	0.1	0.7	2.0	0.7
1995 to 1996	378	0.8	0.1	1.0	3.5	1.0
1996 to 1997	394	1.1	0.7	1.8	1.8	2.5
1997 to 1998	301	0.7	0.1	0.8	5.7	1.2
1998 to 1999	433	1.1	0.3	1.4	0.7	6.5
1999 to 2000	307	1.0	0.1	1.1	11.0	0.5
2000 to 2001	402	0.6	0.3	0.9	1.5	6.2
2001 to 2002	332	0.7	0.2	0.8	1.3	5.2
2002 to 2003	386	1.8	0.3	2.1	2.8	1.4
2003 to 2004	299	2.3	0.2	2.5	8.2	1.1

4.5.4 Canopy Damage Age and Frequency

The time series data set were used to generate a complete Canopy Damage age map by combining all the individual annual Canopy Damage maps and assigning degraded forest pixels the year of the first degradation event. The Canopy Damage age map allowed us to identify and quantify the amount of old degraded forest (i.e., degraded more than one year ago) that was converted by deforestation. This type of analysis is useful for overcoming the difficulties in detecting the percentage of old degraded forests converted to deforestation, discussed in the section 4.5.2, and provides a better estimation of the percentage of intact forest in the region.

Figure 16 shows two subsets (15km x 15 km) of the study area with examples of Canopy Damage age maps of forest areas that were predominantly degraded by selective logging (Figure 16a) and forest fires (Figure 16b). These examples show that most of the forest area was degraded between 1984 and 2004. The Canopy Damage mapped in 2004 (i.e., dark blue areas in Figure 16) represents less than 10% of the total area affected by forest degradation. The cumulative Canopy Damage area represents 23% of the study area, or 32% of the total forest area mapped in 2004. The single-date classification for 2004 mapped 11% of the study area as Canopy Damage (15% of the forest area). Therefore, single-date classification underestimates the cumulative Canopy Damage area by 8%, but when considering the average area mapped as Canopy Damage (3.7%) over the twenty-year period, the underestimation would certainly be much higher for other years.

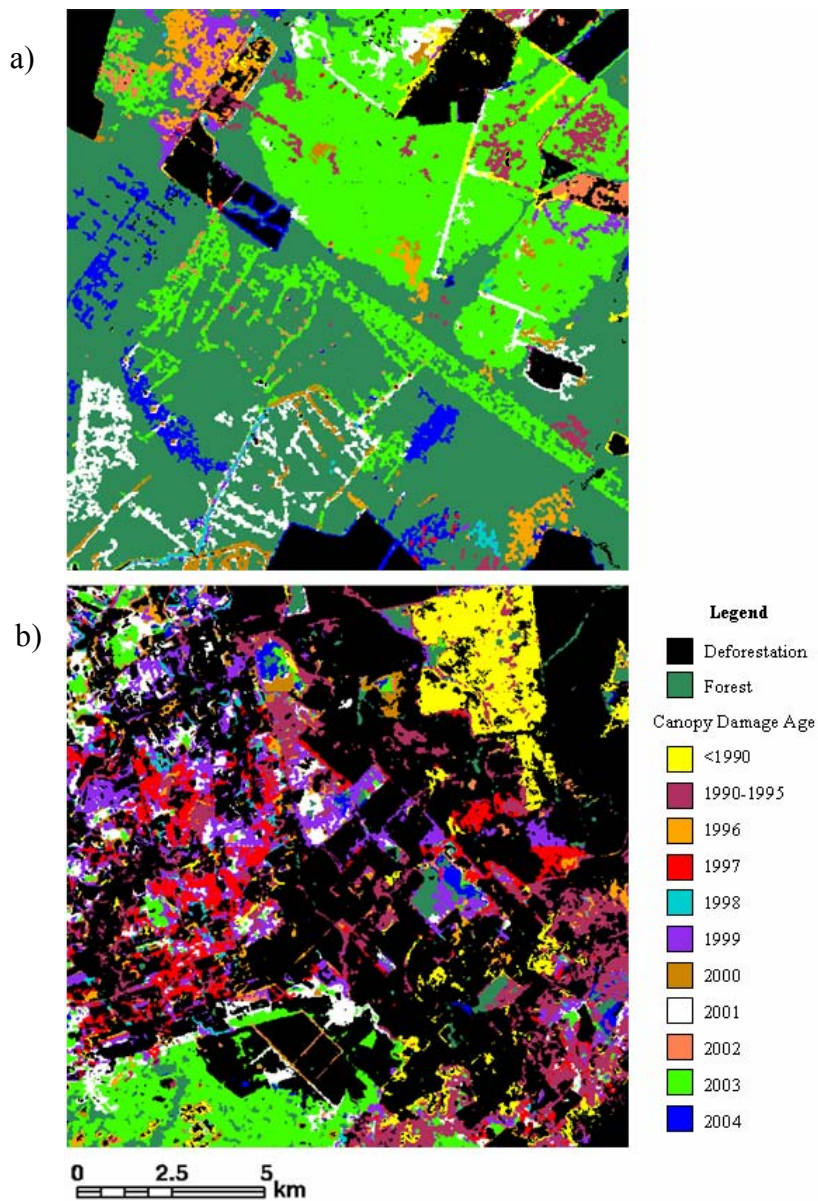


Figure 16. Canopy Damage age map of two sub-sets (15 km x 15 km) of the study area. In (a) selective logging damage is more common and in (b) forest fires are the major causes of canopy damages.

The number of times a forest was classified as Canopy Damage was also computed (Figure 17). Fifty percent of the total forest area mapped as Canopy

Damage during the twenty-year time period occurred only once. Forest degradation events were detected twice for 20% of the total Canopy Damage area, and the remaining 30% were subjected at least to three degradation events (Figure 17). These results show that selective logging and forest fire recurrence are common in this region affecting 50% of the degraded forests.

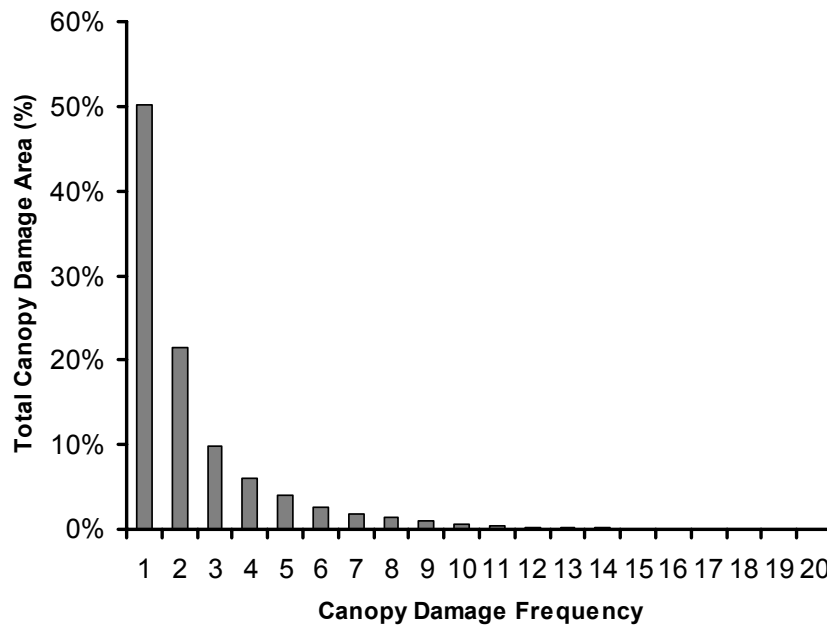


Figure 17. Average areal percentage of the Canopy Damage class converted by deforestation as a function of how many times the forest had been degraded.

Traditional change detection analysis calculates change statistics for each pair of images. Because degraded forests due to selective logging and forest fires change back to forest spectral signatures within one to two years (Souza Jr. et al, *in press*), this type of change detection approach does not allow for the estimation of how long it takes for a degraded forests to be converted by deforestation. The canopy age map

was also used to overcome this type of problem. First, the first pair of Canopy Damage maps (i.e., from 1984 and 1985) were combined to generate the first Canopy Damage age map and changes of the Canopy Damage to Deforestation were computed. At this stage, only one-year Canopy Damage areas existed. Then, the first Canopy Damage age was updated with the next Canopy Damage map (i.e., 1986) and the Canopy Damage to Deforestation conversion was calculated. At this second stage, two classes of Canopy Damage age existed: one year (i.e., Canopy Damage in 1985) old and two year old (i.e., Canopy Damage in 1984); and two estimates of one year old Canopy Damage to Deforestation (i.e., from 1984 to 1985 and from 1985 and to 1985). This process of updating the Canopy Damage age map with the subsequent year maps continues and the change statistics are computed until the last image date is reached. The result is a very large change detection matrix with several estimates of Canopy Damage to Deforestation for each Canopy Damage age that were averaged and summarized on Figure 18.

The Canopy Damage age time series analysis revealed that, on average, over the twenty year period only 5% of the degraded forests were converted by deforestation to pasture or agriculture one year after the degradation event (Figure 18). Most of the degraded forest conversion occurs in the second year accounting for an average of 20% of the total area converted. About 55% of the degraded forests were converted by deforestation between the third and tenth years, and degraded forests with more than 10 years contribute, on average, with 25% (Figure 18).

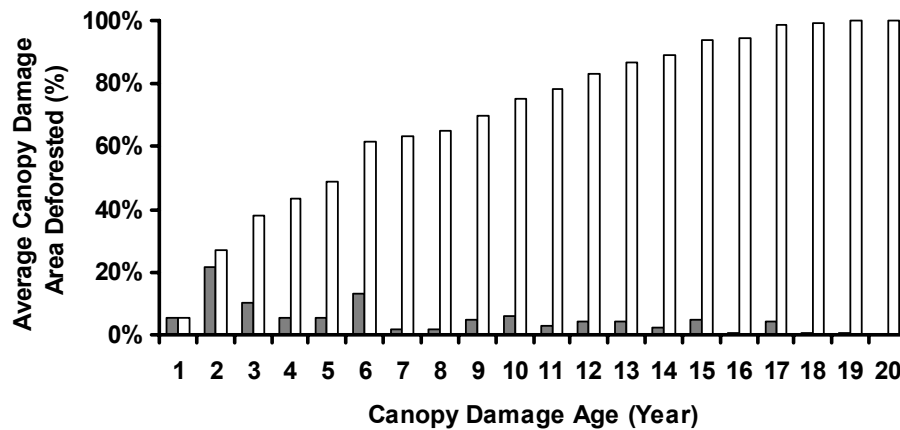


Figure 18. Average Canopy Damage area converted by deforestation as a function of degradation age. The grey regions represent the percentage of degraded forest converted by deforestation, while the white one the cumulative percentage of degraded forest converted by deforestation.

4.6. Discussion

There are several change detection techniques that can be used to quantify land forest cover changes (e.g., image differencing, post-classification change detection, multi-date unsupervised classification; Coppin and Bauer, 1995). Image differencing, which is computed as the difference between a recent and an old image, has also been tested. Image thresholds are defined and applied to the difference image to classify forest areas that did not change from those that were subject to changes between the time interval. Both GV and NDFI images were used as variables in the image-differencing algorithm. This technique has the disadvantage of detecting both natural and anthropogenic changes. Misclassification of natural canopy damages as

anthropogenic canopy damage might also happen with multi-date unsupervised change detection. Because the CCA uses contextual information from selective logging (i.e., log landings) to map canopy damage areas, canopy damages associated with natural forest changes are not mapped. Therefore, post-classification change detection is more suitable because it uses classified images that contain the forest whose changes I am interested in quantifying.

The remote sensing techniques presented in this study have the potential to be extended to other areas in the Amazon region. There are, however, some challenges to reproducing these techniques in this region. First, not all regions have optical satellite images available every year (Asner, 2001). Another important issue associated with time-series analysis has to do with the generalization of classification rules that can be ported through time and across regions. Atmospheric correction plays an important role in the success of generalized classifiers (Woodcock et al., 2001). The radiometric normalization techniques perfected by Roberts et al. (1998) coupled with the haze correction proposed by Carlloto (1999) can be used to minimize the atmospheric noise. One remaining challenge to the application of CCA for detecting canopy damage on very large areas, such as the Amazon region, has to do with the SMA. Physically meaningful SMA models, which are required for NDFI computation, depend on the right selection of endmembers. Small (2004) has demonstrated that generic endmembers can be found in the Landsat ETM+ reflectance space which makes it a promising tool for overcoming the challenges to generate consistent fraction images over the entire Amazon basin.

4.7. Conclusions

The long term remote sensing of canopy damage detection and change analyses showed that forest degradation surpasses, on average, deforestation rates by three-fold in the Sinop region. I have also demonstrated that deforestation and forest degradation are independent events and, therefore, must be accounted for separately to capture the total forest area under anthropogenic pressure; that single date canopy damage classification partially captures the amount of degraded forests; and finally that recurrent logging and forest fires events were detected in 50% of the degraded forests. The techniques for mapping canopy damage associated with anthropogenic forest degradation and the change detection techniques presented in the study have the potential to be applied in other tropical forests, contributing to the understanding of the real state of these forested areas.

CHAPTER V: Generic Spectral Mixture Analysis and Decision Tree Classification for Monitoring Forest Changes in the Brazilian Amazon

5.1. Introduction

Our research group has been engaged in a project to develop automated image classification techniques for mapping land cover changes in the Brazilian Amazon as part of the Large Scale Biosphere-Atmosphere Experiment in Amazonia – (LBA). Two broad types of land cover changes can be found in the region: land-cover conversion and land-cover modification. Deforestation and second growth are examples of land cover conversion whereas selective logging and forest fires are examples of land modification. The former examples represent a complete change of the original land cover since forest is converted to pasture or agricultural fields. The latter examples represent a partial modification of the original land cover because the original forest structure and composition is temporarily or permanently changed, but is not replaced by other type of land cover.

An image processing chain to process Landsat images to map land-cover types has been developed and tested in two distinct regions in the Brazilian Amazon- Marabá in the State of Pará, Eastern Amazon (Roberts et al., 1998); and in large areas of the State of Rondônia, Southeast Amazon (Roberts et al., 2002). The following land cover types were mapped in these two regions: Primary Forest,

Pasture, Green Pasture, Second Growth, Water, Urban and Rock/Savanna. The image processing chain to map these land cover types is: i) retrieve reflectance; ii) select image and reference endmembers; iii) perform radiometric intercalibration; iv) spectral mixture analysis – SMA; and v) decision tree classification – DTC. In addition, a protocol for map accuracy assessment has been proposed which uses aerial videography detailed mosaics as reference and correct the sources of map accuracy errors (Powell et al., 2004).

The image processing chain described above has also been tested to map land cover modification associated with forest degradation in two other regions in the Brazilian Amazon: Paragominas also in the State of Pará, Eastern Amazon (Souza Jr. et al., 2003); and Sinop in the State of Mato Grosso, Southern Amazon (Souza Jr. et al, in press a). The techniques, particularly SMA and DTC, have improved the detection and mapping of forest changes associated with selective logging and burning. Finally, a novel spectral index based on the fraction images derived with SMA has also been proposed and revealed to be more effective in enhancing the detection and mapping of forest degradation in the Amazon region (Souza Jr. et al., in press b; Chapter III).

The research progresses described above to map land cover conversion and land cover modification in the Amazon region represent a great step towards the development of an automatic and generic image classification approach for monitoring the Amazon region. By generic classification I mean, an algorithm that is both spatial and temporally robust, based on a standardized set of data and

classification rules that can be used to map land cover changes within the same environmental conditions through time. Generic classification to monitor forest conversion has been proposed in the literature (Woodcook et al., 2001), but has not been tested thoroughly in the Amazon region.

Fraction images derived from SMA are physically interpretable and have been used to identify and map land-cover changes in the Amazon (Adams et al., 1995; Roberts et al., 1998, 2002; Souza Jr. and Barreto, 2000; Souza Jr. et al. 2003; Lu et al., 2003; Numata et al. 2003). The greatest challenge regarding the use of fraction images in generic classification has to do with the generation of standardized fractions through time and space. The problem of temporal standardization has been solved previously with the use of reference endmembers and the application of radiometric inter-calibration techniques (Roberts et al., 1998, Roberts et al., 2002). One difficulty with this approach is the acquisition of reference endmembers which requires a well-calibrated spectral library representative of the land-cover types found in the areas of interest. An alternate approach based on the exploration of the spectral topology space has been proposed to define a standard set of image endmembers that can be used to generate spatially consistent fractions worldwide (Small, 2004).

Among the image classification techniques, DTC has already been tested successfully in large areas in the Amazon region using time-series of fraction images (Roberts et al, 2002; Souza Jr., et al., 2003). DTC has several advantages when compared with other image classification algorithms. First, DTC is a non-parametric

classifier which means it requires no a priori data distribution model (Friedl and Brodley, 1997), unlike a maximum likelihood classifier which requires normally distributed data (Richard and Jia, 1999). The decision rules generated by a DTC are more intuitive and more easily interpreted by both image analyst and final users (Murthy, 1998). This is not the case for neural networks, which may outperform DTC, but works as a black box (Richard and Jia, 1999). Another important attribute of the DTC is that the decision rules provide knowledge about the variables used in the classification (Murthy 1998).

DTCs, on the other hand, are very sensitive to the training sample used to generate the decision rules. As a result, any small change to the training data will generate a different set of rules for classifying the data (Breiman et al., 1984; Murthy, 1998). Another potential problem with the DTC is that the decision rules are created by a recursive partition algorithm that optimizes the data partition from the top to the bottom of the tree. Therefore, there is no guarantee that the terminal nodes, which are the nodes that define the classification, are the optimum partitions for classifying the data set (Breiman et al., 1984). Genetic algorithms – which mimic biological evolution mechanisms – have been used to overcome the data training sensitiveness and the top-to-bottom node optimization problem of DTC. Examples of genetic DTC include Sörensen and Janssens (2003), who used genetic DTC in data mining applications; Angenelli et al. (2001) who used it to extract information from scanned documents; and Delise who used it (source: [108](http://ai-</p></div><div data-bbox=)

depot.com/Tutorial/DecisionTrees.html) to improve the classification of environmental risk levels of chemical compounds.

Here I propose a generic classification approach for monitoring the Brazilian Amazon forests. The generic classification utilizes a standardized set of fraction images obtained with image endmembers defined based on the topology of the Landsat spectral space as proposed by Small (2004). The classification rules are obtained using a genetic algorithm to generate DTC rules. The generic classification was applied to 40 Landsat scenes covering several sawmill centers in the Brazilian Amazon (Figure 19). The sections below describe the methods used to generate standard fraction images for the Amazon region and the algorithm used to run genetic decision trees.

5.2 Methods

5.2.1 Spectral Mixture Analysis – SMA

a) Background

SMA decomposes a spectral mixture into fraction of purer material, known as endmembers, which are expected to be found within the instantaneous field of view (IFOV). SMA has been applied extensively in the Amazon region to generate fractions images that are further used as variable in image classification (Adams et al., 1995; Roberts et al., 1998 and 2002; Souza et al., 2003; Lu et al., 2003) or to estimate biophysical properties of vegetation and soils (Asner et al., 2003; Numata et

al., 2003; Souza et al., 2003). Most of the studies used scene-specific image, endmembers making direct comparison of fractions difficult.

Reference endmember spectra have been proposed to standardize the fraction results over large areas (Roberts et al, 2002). However, reference endmember spectra are not available for most of the Amazon regions and also depend on the selection of image endmembers to calibrate the reference endmember spectra to the image data spectra (Roberts et al., 1998). Bateson et al. (2000) have proposed an automated SMA approach that utilizes a very large endmember spectral library – endmember bundles – to generate fractions; and Asner et al. (2004a, 2004b) used it in a Monte Carlo simulation approach in mixture models. This technique generates a range of all possible values of each fraction for each pixel. Mean fraction images have been used to characterize land-cover composition (Asner et al., 2003) and to detect forest changes associated with selective logging (Asner et a., 2004b). The Monte Carlo SMA has the disadvantage of being computationally intensive and does not provide one single standard fraction value. The mean fraction images that have usually been used as the standard fraction generated by the Monte Carlo SMA approach (Asner et al., 2003) may not be the best fractional decomposition of mixed pixels.

Small (2004) showed that it is possible to obtain standard global endmembers from the Landsat n-dimensional spectral space. The methodology proposed by Small (2004) was applied to determine generic image endmembers of green vegetation (GV), non-photosynthetic vegetation (NPV) and soil to generate standard fraction images of these endmembers over the Brazilian Amazon. These endmember were

used successfully to identify, map and monitor forest changes associated with selective logging, forest fires and deforestation in the Southern Brazilian Amazon (Souza Jr. et al., in press a; in press b; Chapters II and III, respectively). In addition, a novel spectral index computed with these fractions has been developed to enhance detection and mapping of forest changes and degradation (Souza Jr., et al. in press b; Chapters III and IV).

b) Generic Endmembers for the Amazon Region

Generic image endmembers for Landsat images were obtained following the methods summarized in Figure 20. Most of the techniques shown in Figure 20 are described in detail in the previous chapters. First, the images were georectified using image control points extracted from Shuttle Radar Topographic Mission (SRTM) images. Next, the images contaminated by haze were corrected using a technique proposed by Carlotto (1999), followed by atmospheric correction. Four image subsets (500 x 500 pixels) were selected in the reflectance images to run the PPI algorithm to find the pixels that describe the convex hull of the n-dimensional Landsat spectral space. All data extracted using the PPI of each image were combined and visualized using scatter matrix plots (Figure 21). The scatter matrix made it possible to define the best set of scatter plots for identifying the generic image endmembers. The best pairs of bands were bands three and four, four and five and five and seven (Figure 22). Six types of endmembers were identified: GV, NPV, soil, shade, sand and urban (Figure 22). Finally, NDFI was computed for each

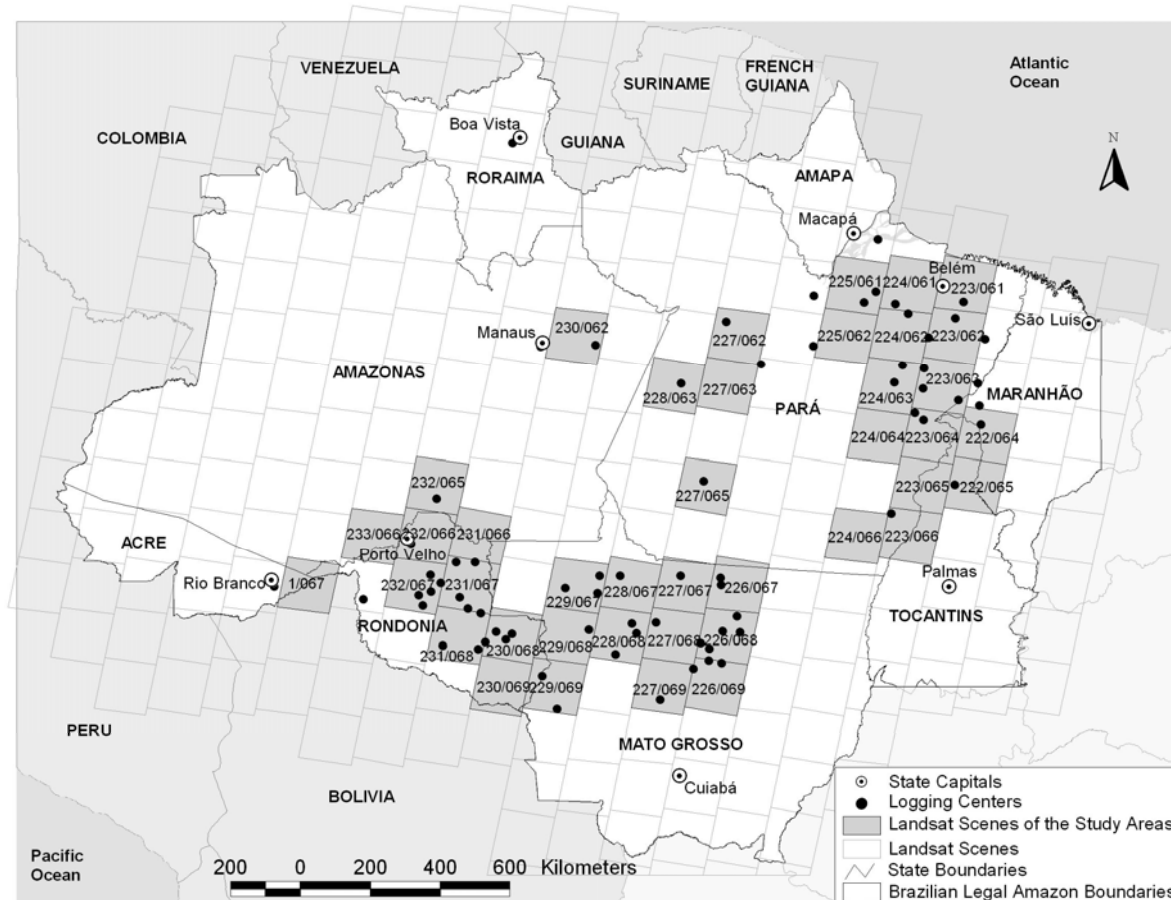


Figure 19. Landsat scenes processed with the standard image endmembers to generate fraction images.

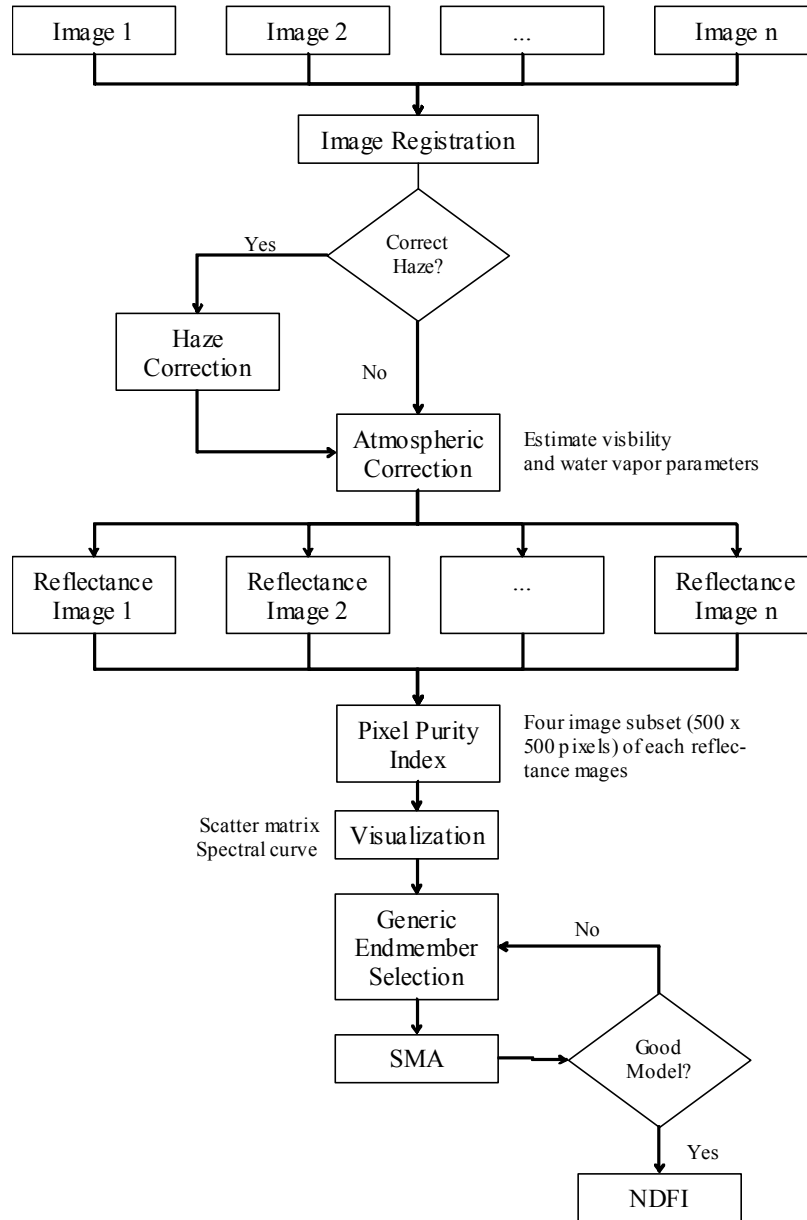


Figure 20. Image processing chain to generate standard fraction and NDFI images over the Amazon region.

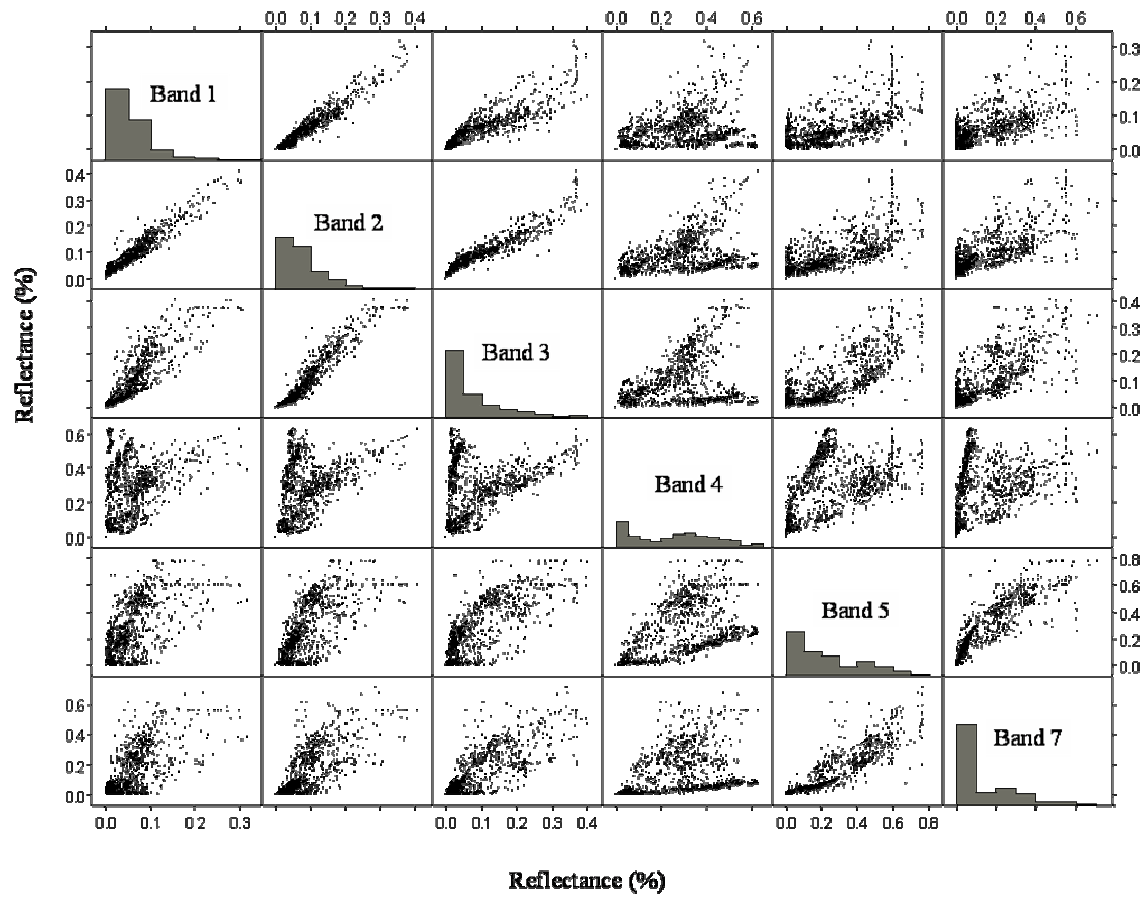


Figure 21. Scatter plot matrix showing the PPI results.

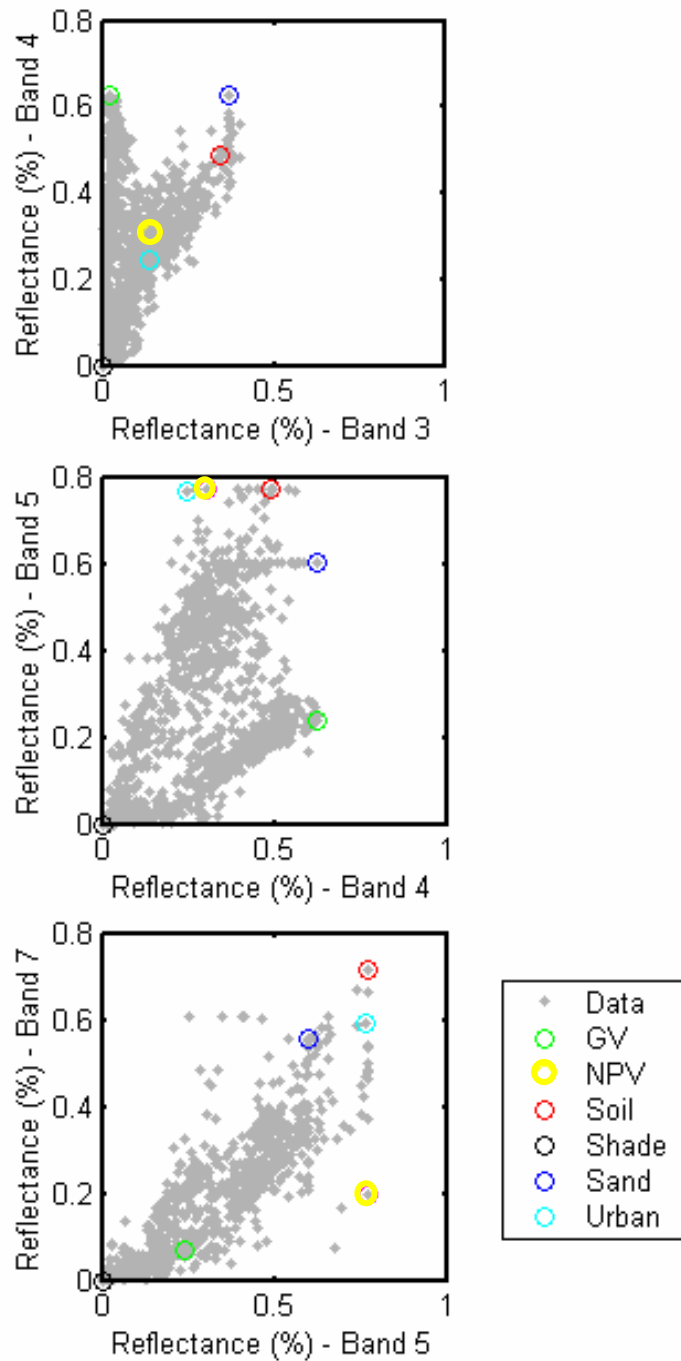


Figure 22. Image scatter plots used to identify standard image endmembers for the Brazilian Amazon.

Landsat image shown in Figure 19 using GV, NPV, Soil and Shade standard endmembers

5.2.2 Genetic Decision Tree Classification

a) Decision Trees

Decision trees generate hierarchical classification rules obtained through a recursive partition process of classification training samples (Friedl and Brodley, 1997; Murthy, 1998). The decision tree structure is composed of classification or partition rules, nodes, branches and classes (Figure 23). The classification rules are composed of one variable (V_i), an operator ($<$ or \geq) and a numeric value that represents the optimal binary partition, or split, of the variable V_i . Two types of nodes can be found: internal and terminal nodes. The internal nodes contain the classification rules that partition the data to the right when V_i is greater or equal to the partition value; and to the left when V_i is smaller than the partition value. By convention, the classification rules are presented with the smaller sign ($<$). The internal nodes are connected by branches from the top of the tree (i.e., root node) to the terminal nodes that contain the classes that will be assigned to the data set (Figure 23).

The decision trees can be symmetric or asymmetric. Asymmetric trees are more common, but for the purpose of presenting the tree component and properties a symmetric tree example is presented (Figure 23). The tree level ($l=0,1,2,\dots,n$) defines the depth of the tree. The number of nodes at each level l is given by 2^l . For

example, there is only one internal node at the first level ($l=0$; $2^0=1$), two in the second level ($l=1$; $2^1=2$) and so on.

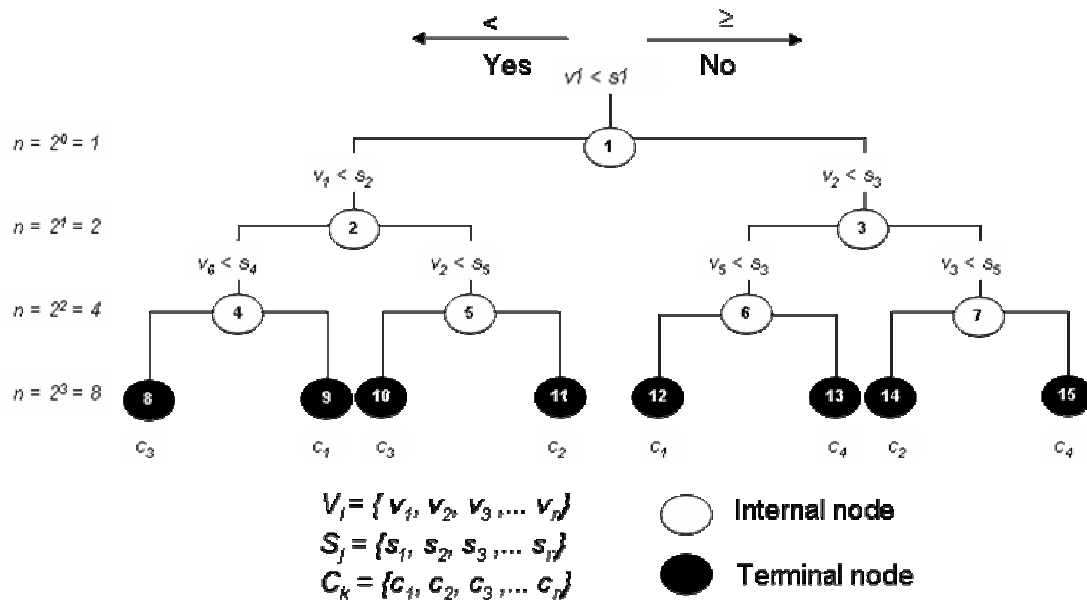


Figure 23. Binary decision tree classification components and structure.

The data partition of each internal node happens when an optimal binary splitting value is found. A recursive partition algorithm is applied until the classification criterion is obtained. There are several methods applied to stop the recursion process from reaching the classification, i.e. the terminal node, including the minimum node size, data deviance and tree complexity (Murthy, 1998). Even though there are several binary partition recursive algorithms, they all have one characteristic in common: the binary partition is optimized from the top to the bottom of the tree. This means that the first nodes are more optimized to split the data set where the

deep node rules have sub-optimal splitting rules. The top-to-bottom splitting optimization has been considered one of the greatest disadvantages of decision trees because optimal classification rules are not obtained with this process (Lawrence et al., 2004). If the first level's internal nodes were sub-optimally generated, the terminal nodes might be more optimal, thus generating better classification rules.

Decision trees are also highly sensitive to the quality of the classification training data. Data noise and small changes in the data set will generate complete different classification rules). Finally, a decision tree requires classification training samples of equal size (Murthy, 1998). The next subsection presents a promising approach for overcoming these decision tree problems.

b) Genetic Decision Tree Classification Algorithm

Genetic algorithms are computer programs that mimic biological evolutionary mechanisms (Russel and Norvig, 2003). There are five major steps to implement genetic algorithms: 1) random selection, 2) evaluation, 3) selection of the best individuals, 4) mutation and 5) final selection (Figure 24). The genetic decision tree classification algorithm (GDTCA), implemented to overcome the decision tree problems described in the sub-section 5.2.2.a, is based on the following steps:

Step 1: generation of one hundred random decision trees based on uniform random selection of 50 to 70 percent of a very large classification training sample (i.e., more than 1000 pixels per class).

Step 2: evaluation of the best trees based on the accuracy to classify the training samples used to generate the decision trees.

Step 3: biased selection of the twenty best trees using a linear rank fitness (LRF) index and roulette-wheel (Whitley, 1989):

$$\text{LRF} = 2 - \text{SP} + 2 (\text{SP} - 1) * (\text{Ind} - 1)/(\text{N} - 1) \quad (15)$$

where, SP is the selection pressure which gives the probability of the best tree being selected compared to the average probability of selection of all trees. Ind is the inverse rank position from the most accurate to the least accurate tree; and N is the total number of trees (N=100). For SP equals 2, then:

$$\text{LRF} = 2 * (\text{Ind} - 1)/(\text{N} - 1) \quad (16)$$

Next, the selection probability is computed for each tree:

$$P = \text{LRF}_i / \sum(\text{LRF}) \quad (17)$$

for $i = 1, \dots, N$.

Therefore, for SP equals 2 and N equals 100 (i.e., 100 trees) the best tree has Ind value of 100 and an LRF value of 2. The P value is 0.02 and the average probability of selection of all trees is 0.01, giving these trees twice the probability of selection relative to the average. Finally, the selection probability of each tree is mapped to contiguous segments of a line, such that the size of each segment of a tree is equal in size to its probability. Thus, a random number is generated using a uniform distribution function from 0 to 1 to select a tree for mutation. The tree whose segment spans the random number is selected for mutation. Twenty trees were selected for mutation.

Step 4: mutation of the twenty trees selected in step 3. For each tree selected, one internal node is selected randomly. Next, one variable V_i is selected randomly from

the list of the variables that belong to the tree selected for mutation. A new variable V_j is randomly selected from the list of all existing variables in the data set. Finally, a random splitting value is also randomly selected from the list of possible splits. The new randomly selected variable and value are combined to create a new splitting rule to substitute the original optimal splitting rule. The decision tree is reconstructed from the selected internal node to terminal nodes.

Step 5: the original one hundred trees are combined with the twenty mutated trees and the best tree is selected based on tree accuracy to classify the training sample.

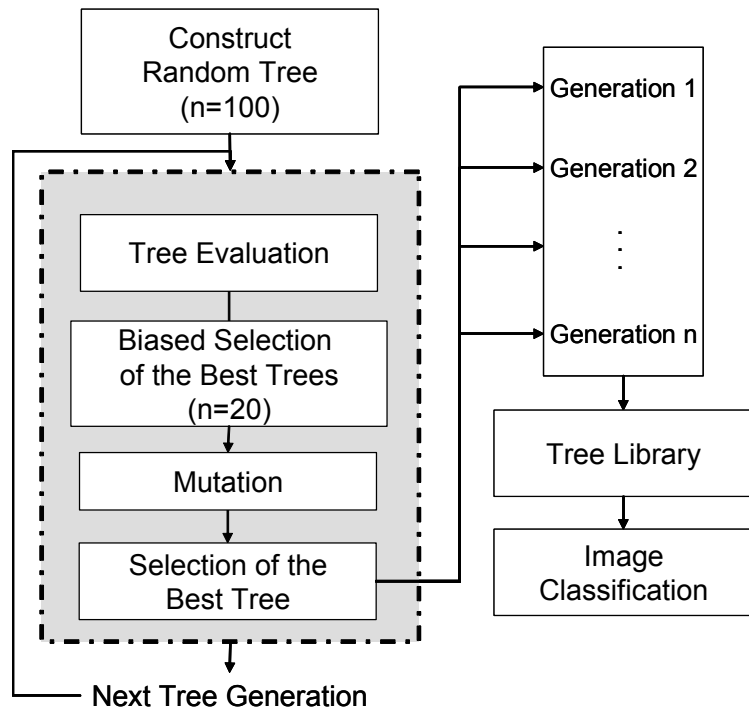


Figure 24. Genetic decision tree algorithm.

Steps one through five define one tree generation. One thousand tree generations were computed using this genetic algorithm. The GDTCA was based on the algorithm proposed by Delisle (2004). The overall assumption of the GDTCA is that a mutation process may occur that will improve the tree accuracy and that after the *Nth* generation, a more robust tree population will be created. The mutation process was implemented to make the top-level nodes sub-optimal and the bottom-level nodes optimal, overcoming one of the decision tree limitations. A second limitation overcome is that the GDTCA reduces human bias in selecting the decision tree classification training sample. The GDTCA was run using as variables the standard fraction images and the NDFI images. The best tree obtained with the GDTCA was used for classifying the Landsat images showed on Figure 19.

5.4 Results

5.4.1 Standard Fraction Images

For the purpose of monitoring the Amazon forests only GV, NPV, Soil and Shade endmembers were selected to run SMA models. Figure 25 shows these image endmembers, their respective endmember bundles obtained with the PPI results and the mean of the endmember bundles. SMA results were evaluated as described in Chapters II and III.

Fraction values of dense forests, transitional forests and open forests were extracted to test if the fractions obtained with the standard endmembers were spatially consistent. The forest polygons were selected with the aid of a regional

forest map (IBGE, 2005). The polygons were located in flat terrain to reduce topographic illumination effects. GV fractions were shade-normalized and the NDFI values were also calculated for each forest type. The means and standard deviations of these forest types are shown in Table 9.

NPV and Soil fractions showed spatially consistent fraction values for each forest type. NPV means varied from 4 to 5% in dense forests, whereas the Soil means varied from 1 to 3%. Transitional and open forests also showed small variations among the NPV and Soil means obtained with the standard endmembers (Table 9).

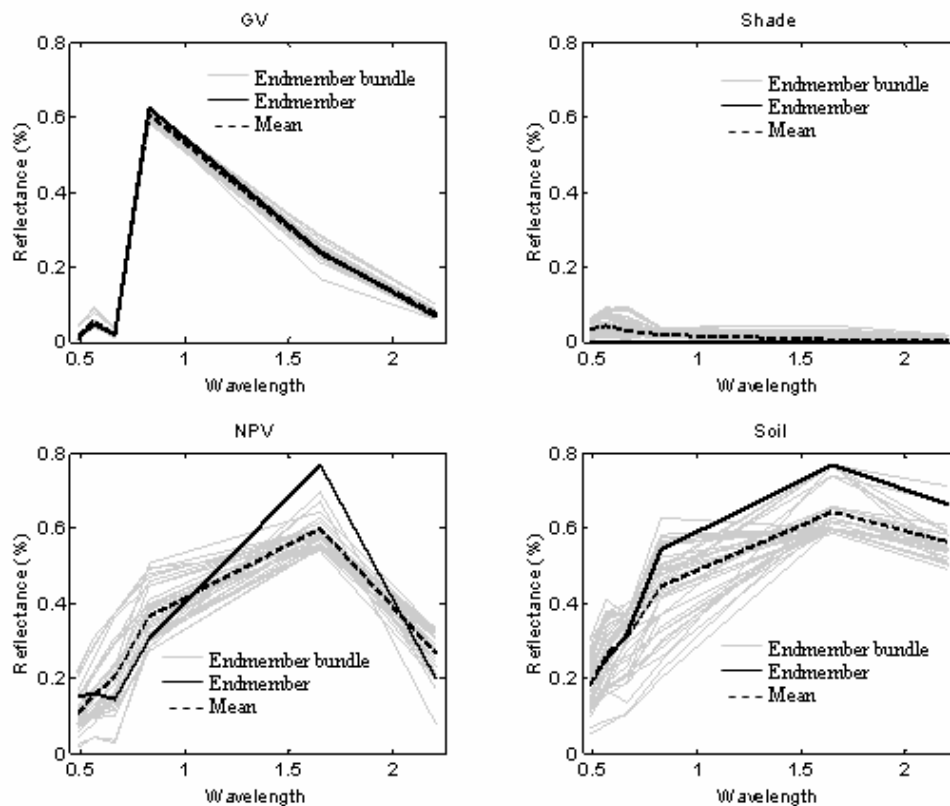


Figure 25. Image endmembers defined based on the topology of the Landsat n-dimensional spectral space. Endmember bundles of each endmember were obtained from the PPI results. The mean of each endmember bundle is plotted in a dashed line.

GV and Shade fractions showed the greatest spatial variation in mean values (Table 9). In dense forests, the GV means ranged from 44 to 52%, and the Shade fraction means varied from 38 to 52%. The spatial variation of GV and Shade was higher in open forests, reaching 12% and 10%, respectively. Transitional forests showed the most spatially consistent mean values obtained with the standard image endmembers.

The mean spatial variation of the fraction was reduced in the shade-normalized GV and NDFI (Table 9). The ranges of the shade-normalized GV means were 5% for dense forests and 4% for transitional and open forests (Table 9). The NDFI means range was 0.05 for dense and transitional forests, and 0.03 for open forests. The NDFI means shown in Table 9 for all vegetation types are above the 0.75 threshold used to detect canopy damages in the transitional forests of the Sinop region (Souza Jr., et al., in press b; Chapter III).

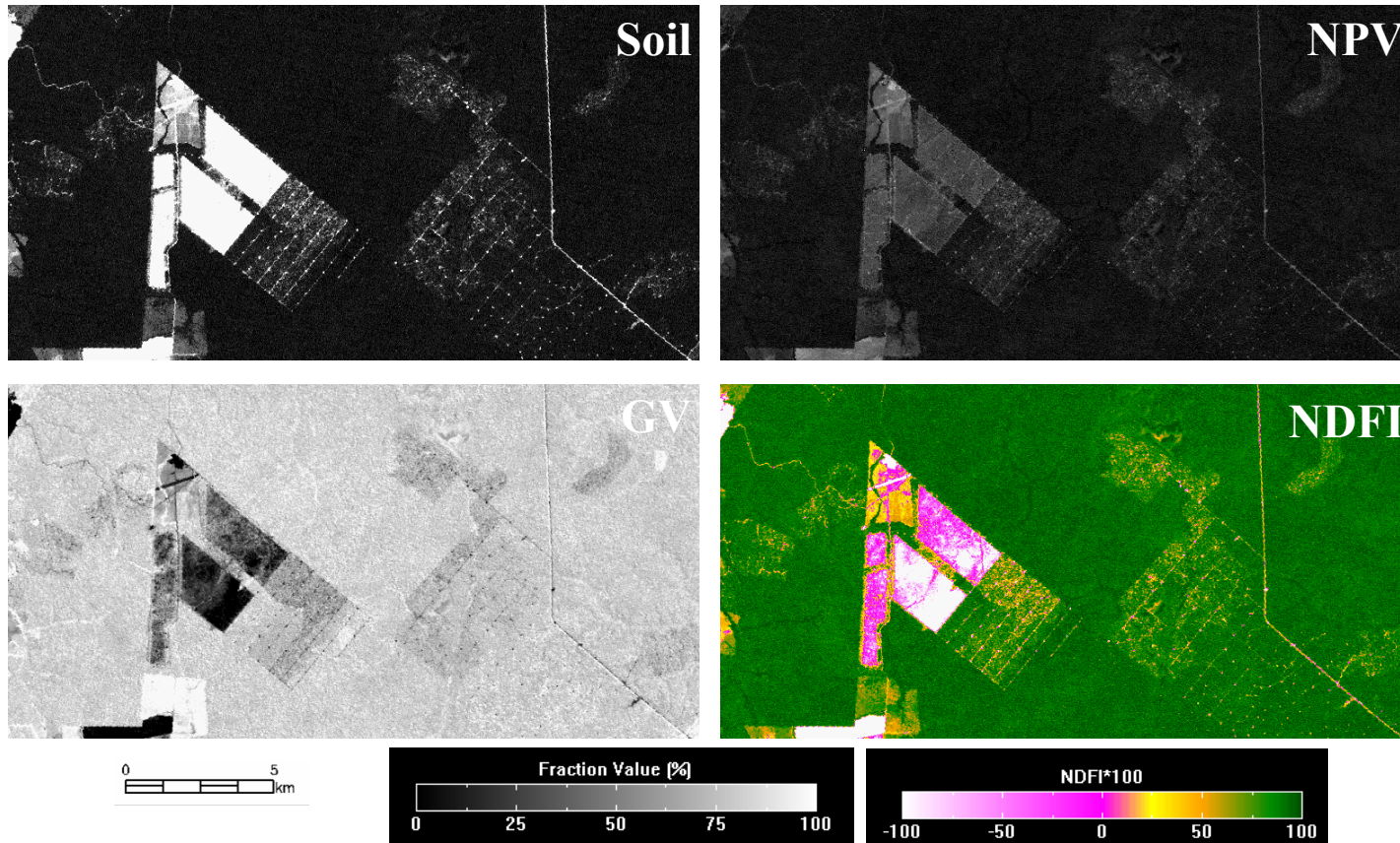
The statistical results shown on Table 9 leads to the conclusion that the standard image endmembers generated spatially consistent fractions of NPV and Soil and that shade-normalization and the use of NDFI reduced the illumination variation among the scenes. Examples of fraction color composites (R=NPV, G=GV, B=Soil) and NDFI images of four subset regions are shown for Paragominas (Figure 26a), Santarém (Figure 26b) and Ji-paraná (Figure 26c). Most of the forest canopy damages can be identified in the fraction color composites. However, old selectively logged areas are better identified in the corresponding NDFI images. In the Ji-paraná region, for example, logging roads and log landings cannot be easily identified in the

fraction color composite, but the NDFI image allowed the identification of these features (Figure 26c).

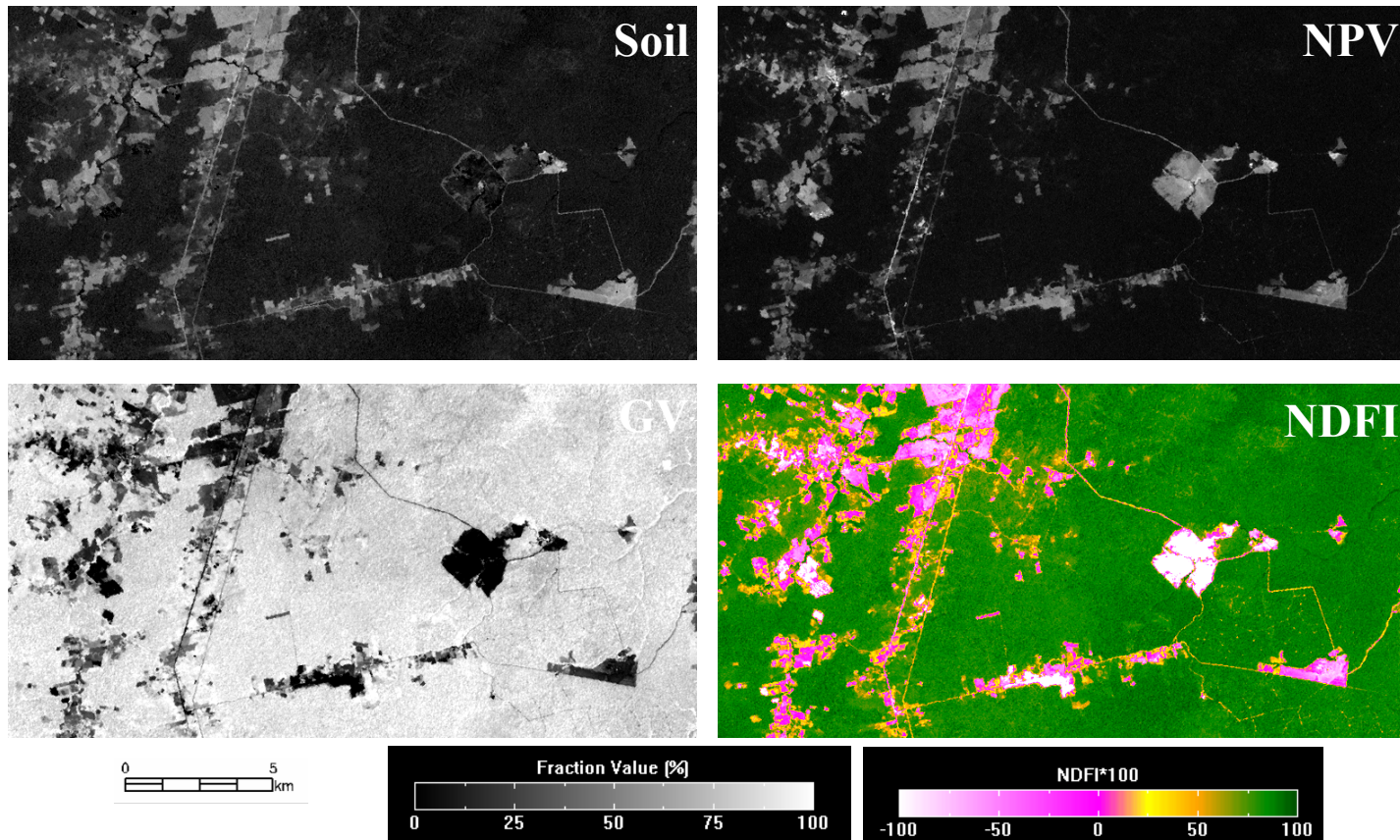
Table 9. Means and standard deviations of standard fraction images and NDFI for dense forest, transitional forest and open forest found in different regions in the Brazilian Amazon.

Forest Type	Path/Row	GV	NPV	Soil	Shade	GVn	NDFI
Dense Forest	227/62	48 (3)	4 (2)	1 (1)	47 (3)	91 (3)	0.90 (0.04)
	228/63	45 (4)	4 (2)	1 (1)	50 (4)	89 (3)	0.88 (0.04)
	230/62	44 (2)	5 (2)	2 (1)	49 (3)	86 (3)	0.85 (0.04)
	236/66	54 (3)	5 (2)	3 (1)	38 (3)	88 (3)	0.84 (0.04)
	232/65	52 (3)	4 (1)	1 (1)	43 (3)	91 (2)	0.89 (0.03)
Transitional Forest	226/67	53 (4)	1 (1)	1 (1)	45 (3)	96 (2)	0.96 (0.03)
	226/69	52 (3)	2 (1)	1 (1)	45 (3)	95 (2)	0.95 (0.02)
	227/69	51 (4)	3 (1)	1 (1)	45 (3)	93 (3)	0.92 (0.03)
	228/68	51 (3)	1 (1)	0 (1)	47 (2)	97 (2)	0.97 (0.02)
Open	227/63	44 (3)	5 (1)	1 (1)	50 (3)	89 (3)	0.88 (0.03)
	231/66	56 (4)	3 (1)	2 (1)	40 (4)	93 (3)	0.91 (0.03)

a) Paragominas, Pará State - 223/62



b) Santarém, Pará State - 227/62



c) Ji-paraná, Rondônia State - 231/67

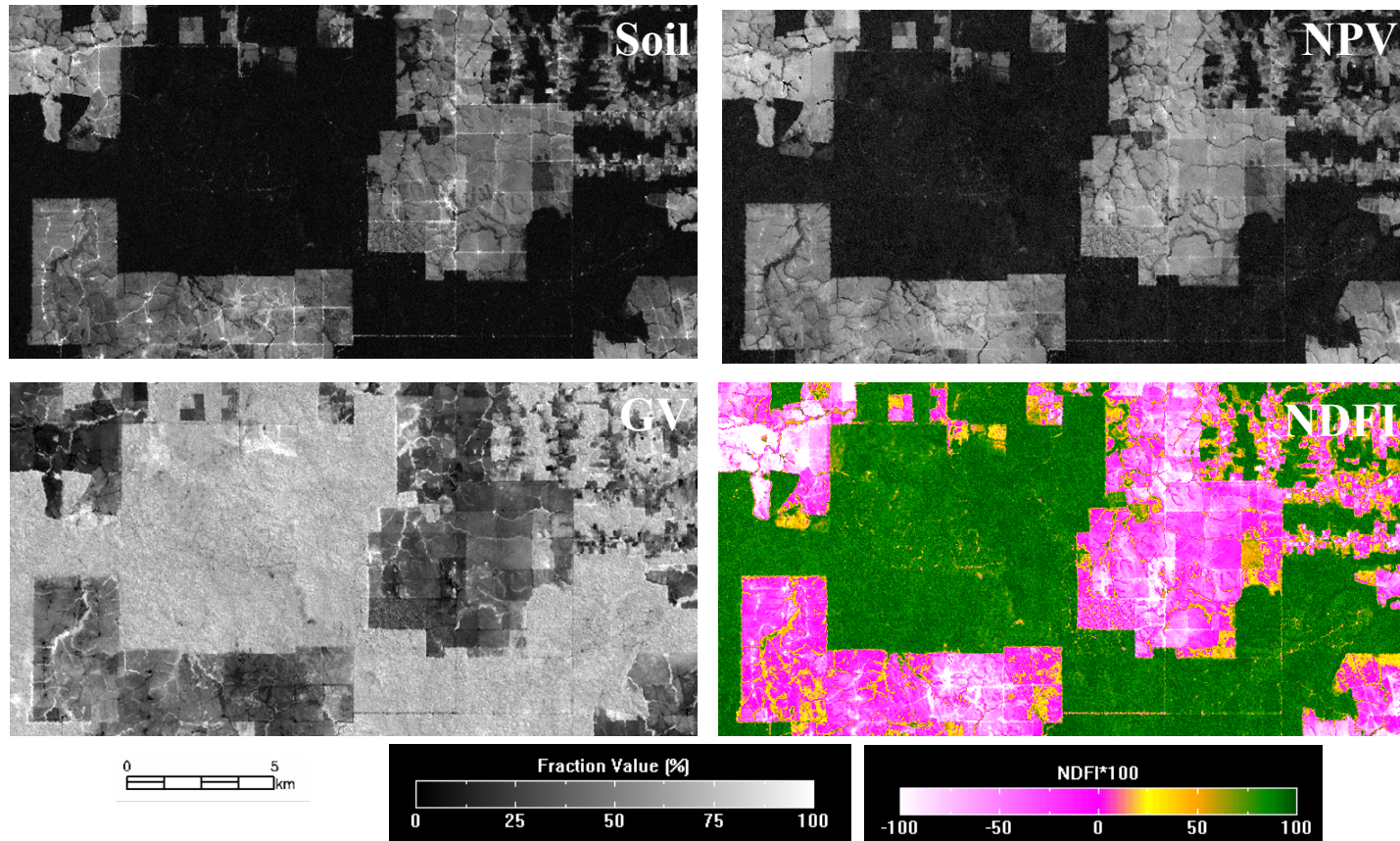


Figure 26. Examples of fraction (R=NPV, G=GV, B=Soil color composite) and NDFI images obtained with the standard image endmembers for areas Paragominas (a), Santarém (b) and Ji-paraná (c).

5.4.2 Generic Decision Tree Classification

Three types of decision tree classifications were run using the GDTCA. The first type of decision tree was constructed to generate a forest/non-forest map given that a forest mask is required for the successful application of the canopy damage classification described in Chapter III. The land-cover classes used to generate the forest mask were: forest, clear cut second growth and urban. The other two decision tree classifications aimed at sub-classifying the canopy damage areas. Another classification scheme was attempted based on the type of degradation which included the following classes: forest, logging and burning.

The accuracy values to classify the training data of the one hundred random trees used as input in the GDTCA varied from 87% to 92% for the Land Cover classification (Table 10). The mean accuracy for the Land Cover classification was 89.4%, and forty-one random trees had accuracy between 89 and 90% (Table 10). This means that most of the random trees generated for the Land Cover classification would be closer to the mean accuracy of the one hundred random trees.

The accuracy values of the one hundred random trees for the Forest Degradation and classifications varied between 75 and 80% (Table 10). The Forest Degradation classification produced the low accuracy for the random trees, with a mean accuracy of 77.4%. Most of the random trees produced accuracy near the mean accuracy value (Table 10). The chance of generating one tree with accuracy higher than the mean accuracy was small. For example, the highest accuracy constructed randomly was 91.8% for the Land Cover classification and only 5 out of 100 trees showed accuracy

in 91 to 92% range (Table 9). For a more challenging classification such as the forest degradation, only 7 trees out of one hundred showed accuracy values higher than the mean (Table 9).

Table 10. Accuracy of the random trees for land cover, forest degradation and degradation intensity.

	Land Cover Classification		Forest degradation Classification	
	Accuracy range (%)	Number of Trees	Accuracy range (%)	Number of Trees
	87-88	6	75-76	5
	88-89	29	76-77	41
	89-90	41	77-78	47
	90-91	19	78-79	6
	91-92	5	79-80	1
Mean	89.4		77.2	
Minimum	87.6		75.4	
Maximum	91.8		79.4	

The tree mutation implemented in the GDTCA improved the accuracy of the trees constructed randomly. Figure 27 shows the minimum and maximum accuracies of each tree generation and the minimum and maximum accuracies of each mutation process. The minimum accuracy increased by 5% for both Land Cover and Forest Degradation classification schemes and by 2% only for the Degradation Intensity. The improvement for the maximum accuracy of the 1000th tree generation relative to the maximum accuracy of the random trees was smaller was less than 2% (Figure 27).

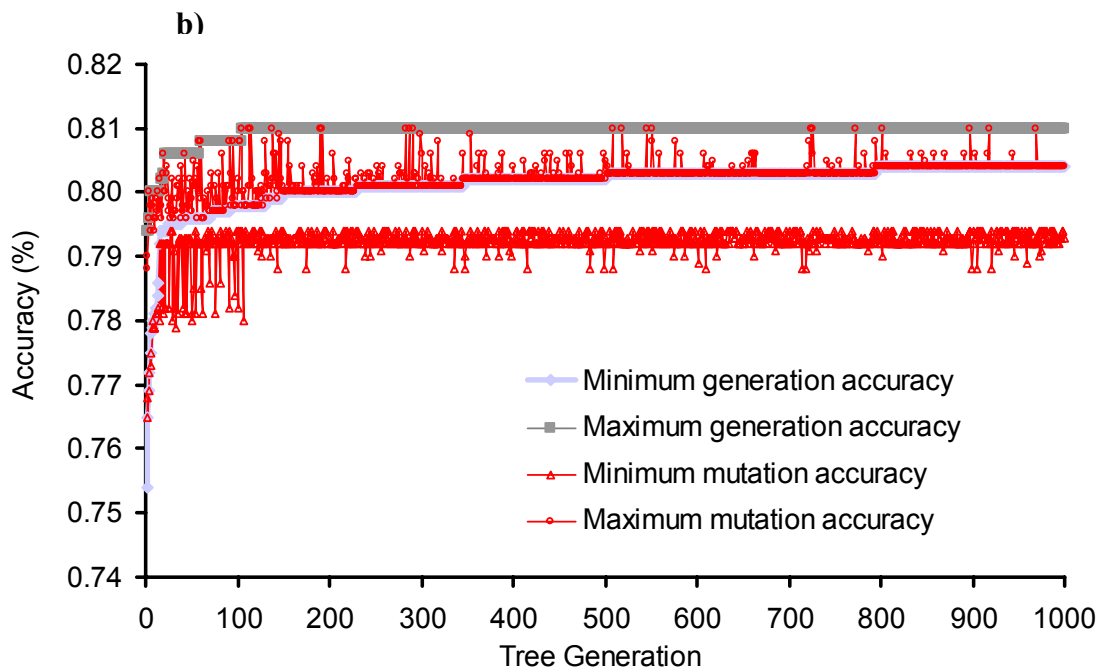
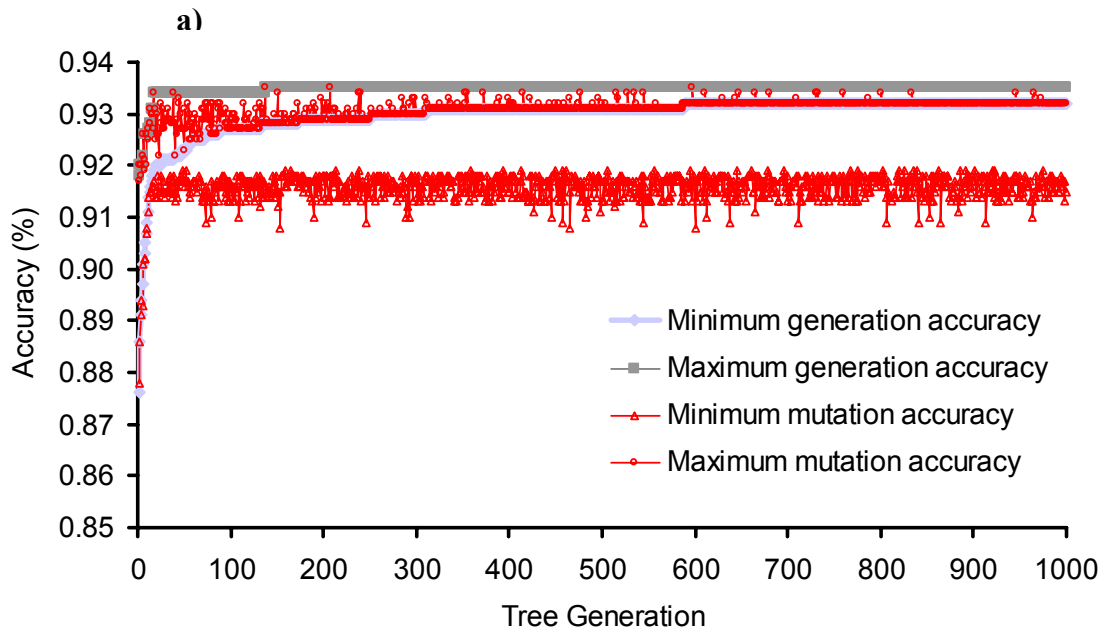


Figure 27. Accuracy of the tree generations and mutated trees for the Land Cover (a) and Forest Degradation (b) classification schemes.

5.4.3 Cross-Regional Comparison

Canopy damage caused by selective logging and forest burning happened most intensively in two regions. The first one is the NE region located in the state of Pará, encompassing the Landsat scenes (n=8) 225/61-62, 224/61-63 and 223/61-63. Two important sawmill centers are located within this region: Paragominas and Tailândia (Figure 19). Of the eight scenes covering this region, only three showed extensive signs of selective logging impacts (224/62, 223/62-63) (Figure 19). In 2001, on average 4% (i.e., 1,300 km²; 185 km x 185 km per scene) of canopy damage was detected per scene in this region. The scenes covering the lowland regions, known as *varzea* (225-223/61) showed very few logging signatures, but it is very likely that logging is happening or had happened at high intensity in this region but cannot be detected using the techniques presented in this dissertation. The reason for not detecting the logging scars is that detection is difficult in flooded forests due to the lack of soil and NPV signals. Other remotely sensed data such as microwave radar or LIDAR images could potentially detect the forest gaps caused by logging in this type of region.

The other region with large impacts of canopy damage due to selective logging is located in the South, where the Sinop county is located. This region is covered by the following scenes: 229/67-69, 228/67-68, 227/67-69 and 226/67-69 (n=11) (Figure 19). The average canopy damage area per scene in this region was 3%. The most impacted scenes are 226/68 and 226/69. The 226/69 scene is the Sinop scene used in

this research to develop the remote sensing techniques to detect canopy damage due to selective logging and forest fires (Chapters II, III and IV).

The other scenes showed low signals of canopy damage due to selective logging. These scenes are clustered into three regions: Central (n=4), SE (n=7) and SW (n=10) regions (Figure 19). In the Central region, less than 1% of the 227/62 was mapped as canopy damage and the other three scenes showed virtually no signs of selective logging spatial signature and canopy damage. In this region, logging activity started growing recently and it is expected that more signs of canopy damage due to logging will appear in the future.

In the SE and SW regions there is no sign of selective logging. For example, in the 231/67 scene, incipient canopy damage was detected with the NDFI technique (Figure 26c). The lack of signs of canopy damage associated with selective logging in these regions raises the following question: what is the source of timber for the sawmill centers located in these regions? It is likely that deforestation is the major source of timber to the sawmill industries located in the SE and SW regions that showed very low or none signs of selective logging. Deforestation is one of the sources of timber in the Amazon region and is the easiest and cheapest way to put legal timber in the market (Uhl et al., 1997). The high value timber species are usually harvested prior to deforestation, and the Brazilian Environmental Agency, IBAMA, provides authorization to commercialize them. Deforestation rates are also high in these regions (INPE, 2003).

It is important to highlight that the hypothesis that deforestation is the main source of timber to many sawmill centers located in the Amazon region disagrees with previous study conducted by Nepstad et al. (1999). These researchers used information on the total volume of timber consumed in the sawmill centers and transportation cost of timber to estimate the forest area affected by selective logging impacts. The area estimates generated in this dissertation cannot be compared directly with the forest degradation area estimated by Nepstad et al. (1999) because they were made for different years. Nepstad et al. (1999) estimated that the forest area degraded by selective logging annually was in the range of 10-15 thousand km². The estimate obtained with the NDFI-CCA approach for 2001 was about 20 thousand km² and includes canopy damages associated with selective logging and forest fires. Nepstad et al. (1999) estimate for forest fires impacts is much higher (80 thousand km²/year). Therefore, it is very likely that the total annually degraded forest area found by these researchers (90-95 thousand km²/year) is overestimated. One of the reasons why this estimate is too high is because the source of timber was not taken into consideration in their analyses. Further research that integrates socioeconomic field and maps derived from satellite images is need and might reduce the uncertainties in this subject.

5.5 Discussion

Standard fractions images of GV, NPV, Soil and Shade were generated with generic image endmembers obtained from the reflectance six-dimensional space of

the Landsat sensor. The generic endmembers generated physically meaningful fraction estimates for all the Landsat scenes processed (Figure 19). Examples of fraction images of GV, NPV and Soil for Both NPV and Soil for Paragominas, Santarém and Ji-paraná are shown on Figure 26. The fractions values were non-negative and spatially consistent (e.g., soil values were high and NPV was low on dirt roads); Soil fraction revealed the log landings and roads and the GV and NPV the canopy damaged areas. The calculation of the NDFI index using the standard fractions also produced consistent NDFI values across the Amazon region (Table 10, Figure 26).

There is a potential for defining standard reference endmembers using the standard image endmembers generated with this research. Reference endmembers are spectrally purer than the image endmembers and, theoretically, could generate more accurate fraction estimates. However, a robust spectral library is required for use in the algorithm proposed by Roberts et al. (1998) to calibrate image and reference endmembers. The available spectral library developed for the state of Rondônia (Roberts et al., 2002) was tested in the Sinop region but did not produced physically meaningful estimates of NPV (Figure 28a). Soil and NPV fractions were not spatially consistent as well. However, these problems did not happen with the standard image endmembers (Figure 28b).

Data standardization is an important step towards the implementation of generic classification techniques for monitoring tropical forests (Woodcock et al., 2001). Among the existing image classification techniques, decision trees have the potential

to generate generic classification rules to map land cover classes and to sub-classify canopy damaged forests. Finding the right set of data training to generate optimal decision tree rules is the greatest challenge in decision tree classifier (Murthy, 1998).

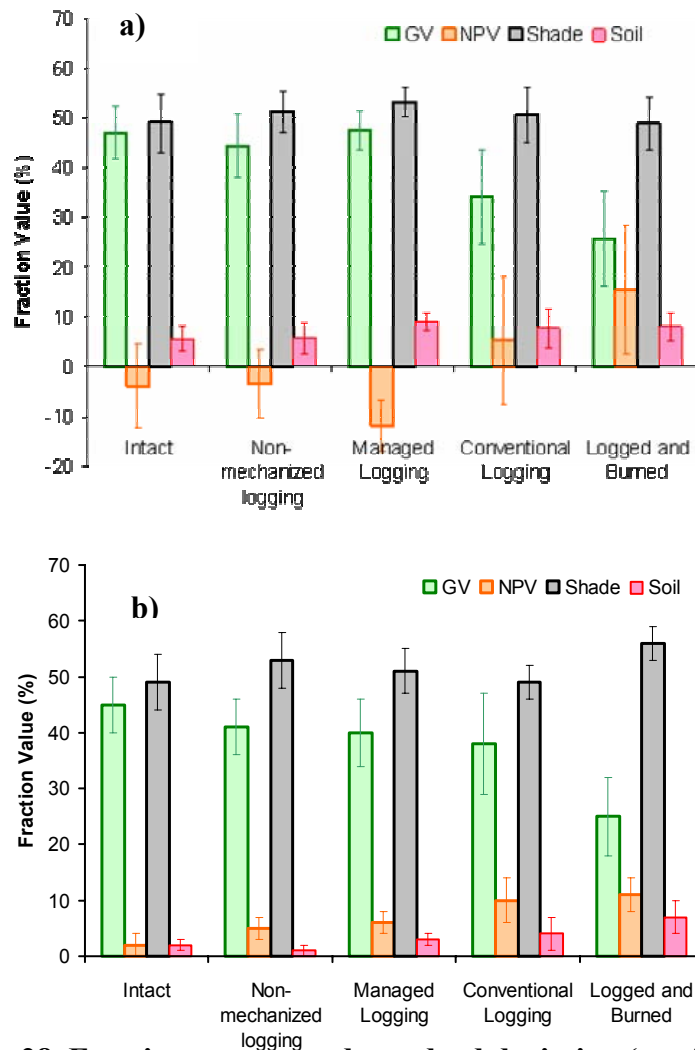


Figure 28. Fractions means and standard deviation (vertical error bar) estimated using reference endmembers (a) and standard image endmembers (b) for the Sinop transects.

The GDTCA proposed in this research helped to overcome this challenge. Overall, the genetic mutation algorithm improved the decision tree map accuracy of the three

classification schemes evaluated in this research (Figure 27). The tree mutation eventually creates a tree that is more accurate than the trees from the past generations. The accuracy improvement occurs because the mutation process eventually creates more optimal partitions in the terminal nodes. In addition, the GDTCA presented here is less human biased in the selection of training samples; the only requirement is that a very large training sample be collected to generate the initial random trees that will be used as an input in the genetic algorithm.

In order to apply the techniques successfully developed and tested in the Sinop region (Chapters III) to map forest canopy damages, a forest/non-forest map is required. The land cover classification obtained with the GDTCA algorithm made it possible to generate this type of information using a generic set of decision rules. Examples of forest/non-forest maps obtained with GDTCA are shown in Figure 30. One classification problem detected was the confusion between second growth forest and old degraded forests. These classes have similar signatures in the Landsat spectral domain and a two-step classification will be required to distinguish them out accurately. First, second growth and forest regeneration classes should be combined with the forest class. The CCA technique proposed in this research can be used to map out the forest regeneration. The pixels of the combined second growth and forest regeneration classes that were not mapped by the CCA algorithm would be classified as second growth forest since log landings are not found in this type of environment. Another improvement in the Land Cover GDTCA is to include cloud and shadow classes in the classification scheme. The Landsat images used to

extracted training samples for the GDTCA were cloud free and for this reason these classes were not include in the GDTCA training sample. However, this will not represent a problem because both cloud and shadow have been successfully mapped with decision trees in the Amazon region (Roberts et al., 1998; 2002) and could be easily incorporated to the GDTCA.

The GDTCA accuracy in sub-classifying canopy damaged forest degradation classes (e.g., logged, burned and clear cut) was 81% (Figure 28; Table 10). Because selective logging and burning may result in the same level of canopy damages and act synergistically, degrading the forests, it was not possible to sub-classify these two classes accurately. Figure 30 shows an example of an area that was both conventionally logged and burned, sub-classified into these classes. The forest degradation can be easily identified in a fraction color composite (R=NPV, G=GV, B=Soil; Figure 30b). The dark purple areas in the fraction color composite were classified as clear cut and the light purple as burned forests. The dark green areas in the fraction color composite were classified as logged forest (Figure 30a).

The canopy damage sub-classification were compared with the transect data collected in the Sinop region. The results agree with the type of degradation event observed during the forest inventory. These canopy damage sub-classification schemes were applied to other Landsat scenes and similar results were observed. However, more detailed field studies are required to validate the results presented in this dissertation.

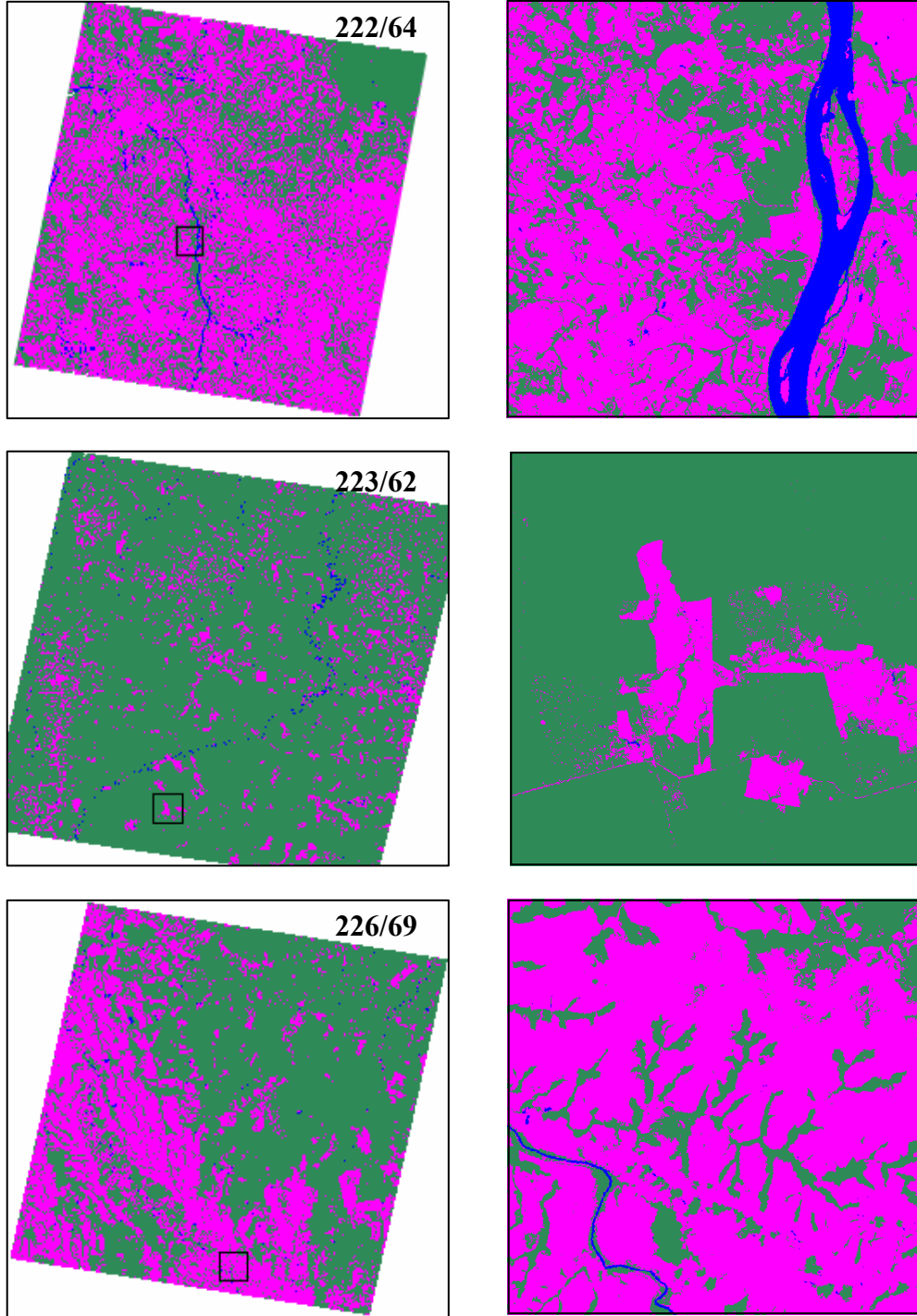


Figure 29. Examples of forest (green) and non-forest (magenta) maps obtained with the GDTCA. The Landsat scene is shown on the left; and on the right the sub-area indicated with the black box.

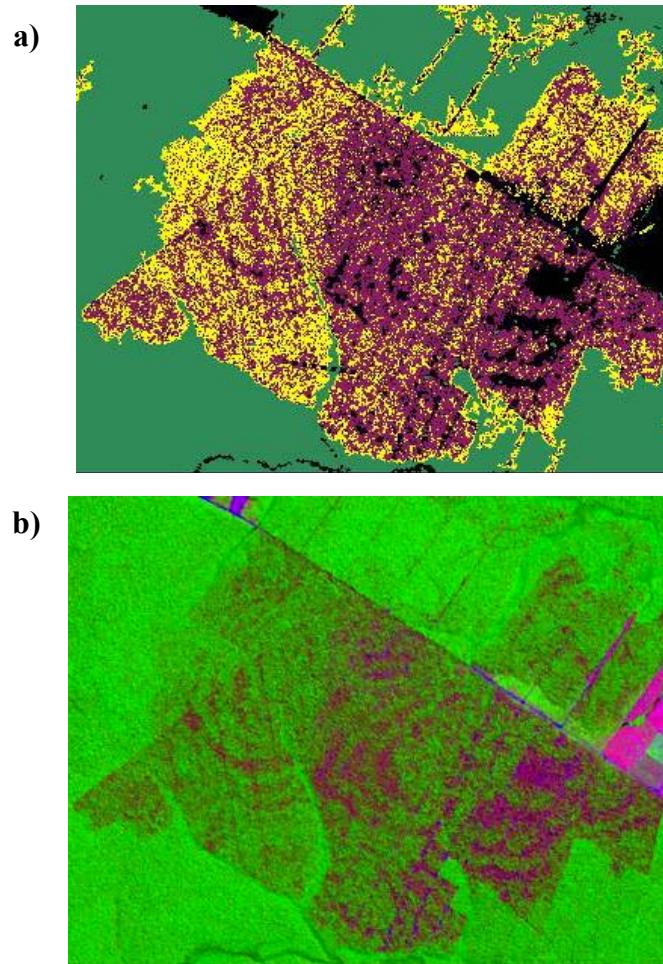


Figure 30. Example of forest canopy damage sub-classification for the transects 3, 4 and 5. In: a) forest degradation classes: burned (brown), logged (yellow) and clear cut (black). The corresponding fraction color composite (R=NPV, G=GV and B=Soil) of the classified area is shown in (b).

Conclusions

In this chapter, I demonstrated that generic image endmember can be obtained from well-reflectance calibrated Landsat images to generate fractions of GV, NPV, Soil and Shade. These fraction images are key to identify and detect canopy damaged forests as has been shown in Chapters II through IV. More accurate generic decision tree rules were also generated with a state-of-the art genetic algorithm perfected in this research. The GDTCA made it possible to overcome the limitations of the traditional partition algorithms used to generate decision tree rules, which include its human biased training sample selection and its top-to-bottom splitting optimization that creates suboptimal terminal nodes.

It is not the objective of this research to provide an estimate of the forest area affected by canopy damage due to selective logging and forest fires for the 40 Landsat scene areas used to test the generic endmembers. I have demonstrated in this dissertation that a time-series analysis would be required to accurately estimate the forest canopy damage areas. Mapping these types of degraded forests is an ongoing research effort that I will be leading in Brazil through Imazon, in collaboration with Dr. Roberts and Dr. Cochrane, from UCSB and University of South Dakota, respectively. More than 1,000 Landsat images covering the period of 2000 to 2004 are being assembled and will be processed using the algorithms developed in this research to provide an estimate of the forest area impacted.

CHAPTER VI: Summary and Conclusions

There has been a great need to develop agile remote sensing techniques and tools to monitor the Brazilian Amazon rain forests. Deforestation rates have been used to guide decision makers to formulate new policies to control the occupation and development of the Amazon region, which has generated environmental problems, particularly the loss of forest and biodiversity, at an unprecedented scale and rhythm. Selective logging and forest fires significantly degrade the Amazon forest, but they have not been monitored due to the lack of appropriate remote sensing techniques. I have developed new remote sensing techniques to detect and map forest degradation using Landsat images – the same type of images that have been used to monitor deforestation in the Amazon region. Landsat images were also chosen because the availability of extensive historical data for the Brazilian Amazon since the mid 70's. The main results, for each objective, and future research directions are presented in the sub-sections below.

6.1 Objective I

In this study, a statistical multi-temporal analysis was applied to evaluate the capability of reflectance, vegetation indices (NDVI and SAVI), normalized difference infrared indices (NDII5 and NDII7) and fraction images, derived from spectral mixture analysis (SMA), to distinguish Intact Forest from four classes of degraded forests: Non-mechanized Logging, Managed Logging, Logged and Logged and Burned. For this purpose, a robust time-series data set of Landsat TM/ETM+

images was used in conjunction with forest inventory transects and data on disturbance history. The study area is located near two important sawmill centers - Sinop and Cláudia, in Mato Grosso State - in the Southern Brazilian Amazon.

Most of the remote sensing measures used to distinguish Intact Forest from degraded forests showed statistically significant changes. Fraction images, particularly Green Vegetation (GV) and Non-photosynthetic Vegetation (NPV) were the most effective means tested for identifying Logged and Logged and Burned forest in the region. The GV change, detected from Intact Forest to Logged and Logged and Burned Forest classes, persists no more than one year, but the NPV change is still significantly different for up to two years. In the second and third years following a degradation event, a significant regeneration signal was observed in reflectance and fraction images, which can be useful for identifying these types of forest disturbances in areas where optical satellite images cannot be acquired every year.

Statistical multi-temporal analysis of reflectance, vegetation and infrared indices and fraction images, derived from SMA, showed that fraction images are more sensitive to changes in transitional forest environments due to selective logging and burning than the broad-band indices tested here. Low intensity logging, such as managed logging and non-mechanized logging are more difficult to distinguish from Intact Forest but a regeneration signal becomes significant in the second and third year. The time-series results showed that changes in GV and NPV fractions were higher when Intact Forest was changed to Logged and to Logged and Burned environments in the first year following the degradation event. In the Logged and Burned Forests, the NPV signal was more persistent, showing a burned signature

through the second year after forest burning. Therefore, both GV and NPV have the potential for use in change-detection classifiers for identifying and mapping Logged and Burned forests in the Brazilian Amazon, with images no more than one year apart.

6.2 Objective II

I proposed and validated a new spectral index, the Normalized Difference Fraction Index (NDFI), for enhanced detection of forest canopy damage caused by selective logging activities and associated forest fires. The NDFI synthesizes information from several component fraction images derived from spectral mixture models. Interpretation of the NDFI data is facilitated by a contextual classification algorithm (CCA) that enables accurate mapping of logging and fire-derived canopy damages. The CCA uses detected log landings from Soil fraction images as a starting location for a search through the NDFI image for canopy damage. This process allows us to separate canopy changes due to logging and associated forest fires from those caused by other natural disturbances. These methods were tested in the Sinop region, in the Southern Brazilian Amazon. Forest transect inventories, conducted along a gradient of degraded forests, were used to evaluate the performance of the NDFI. The NDFI was more sensitive to canopy damage than any individual component fraction and is shown to have the potential for further sub-classification of degradation levels in forest environments. Map accuracy of forest canopy damage

using the CCA classifier, assessed with aerial videography images, was 94%. The proposed NDFI–CCA classifier approach can be fully automated and, therefore, holds great promise as a forest monitoring tool in tropical forests.

The NDFI and the CCA classifier can contribute to ongoing efforts to map and monitor logging operations in the Brazilian Amazon. NDFI enhances the detection of canopy damage over existing techniques and can be used in conjunction with the CCA algorithm to unambiguously map forest canopy damage caused by selective logging and burning. Additionally, the proposed techniques can be integrated with existing image processing methods to classify the damaged forest canopy areas into sub-classes of degradation. Image processing improvements, including the development of fast and generic SMA techniques for generating consistent NDFI images across the Amazon region, will be necessary in order to fully automate such forest degradation analyses. This is important for practical monitoring applications by government environmental agencies and private institutions tasked with the monitoring of certified logging operations.

6.3 Objective III

A time-series analysis comprising twenty-one Landsat images acquired between 1984 and 2004 allowed quantification of the extent and annual rates of deforestation and degraded forests in Sinop region - Southern Brazilian Amazon. A novel spectral index, NDFI, and a CCA were used to first map forest canopy damaged areas due to selective logging and forest fires, the major anthropogenic forest degradation

processes in the study area. Next, a post-classification change detection algorithm was used to detect four types of forest changes: Forest to Clear-cut, Forest to Canopy Damage, Canopy Damage to Clear-cut and Canopy Damage to Forest. The forest change detection analysis revealed that the average annual rate of forest degradation (2.8%) is greater than the average annual rate of deforestation (1%) over the twenty-year time period. The time series analysis showed that 32% of the remaining forest area in 2004 had been degraded, and that 50% of this degraded forest had been damaged more than once. On average, 50% of the degraded forests are converted by deforestation within five years after the forest degradation event. Deforestation and forest degradation are independent events in the study area, and, therefore, must be accounted separately to capture the total forest area degraded by anthropogenic activities.

The long term remote sensing canopy damage detection and change analyses showed that forest degradation exceeded deforestation rates on average by three folds in the Sinop region. I also demonstrated that deforestation and forest degradation are independent events and, therefore, must be accounted separately to capture the total forest area under anthropogenic pressure; that single date canopy damage classification captures partially the amount of degraded forests; and finally that recurrent logging and forest fires events were detected in 50% of the degraded forests. The techniques to map canopy damages associated with anthropogenic forest degradation and the change detection techniques presented in the study have the

potential to be applied in other tropical forest contributing to the understanding of the real state of these forested areas.

6.3 Objective IV

Using the results of objectives I and II, I developed generic image classification algorithms for identifying, mapping and monitoring forest degradation caused by selective logging and forest fires in the Amazon forest. In Objective I, I demonstrated that fraction images derived from SMA can better detect degraded forests relative spectral bands and spectral indices. In Objective II, I developed a new spectral index (i.e., NDFI) based on fraction images that improved detection and mapping of forest degradation. The question addressed in Objective IV was: are the methods tested successfully in Sinop portable to other Amazon regions?

In order to port the remote sensing techniques tested in Sinop, standard fraction images were required. I applied the methodology proposed by Small (2004) to the Amazon region and found out that standard fractions could be generated using generic endmembers defined in the Landsat six-dimensional spectral space. Physically meaningful and spatially consistent fractions and NDFI images were obtained for forty Landsat images, covering several regions of the Brazilian Amazon. Next, an automated decision tree classification based on genetic algorithm (GDTCA) was proposed to generate land cover maps, in particular a forest/non-forest map, which is key to the implementation of the forest degradation mapping technique

tested in Sinop. The GDTCA also generated higher accurate trees to sub-classify canopy damaged forests.

6.4 Future Research

I intend to continue this research by answering the following question: how much forest in the Amazon region is degraded? This future research will be conducted at Imazon, with other collaborators, including Dr. Roberts from UCSB and Dr. Cochrane from SDSU (South Dakota State University). Currently, I am assembling a very large data set of about 1,000 Landsat images for the Brazilian Amazon from 2000 to 2004. This imagery data set will enable basin wide analyses with a robust time series to characterize the impacts of selective logging and forest fires. The remote sensing techniques developed in the scope of this dissertation have already being applied to this very large data set of Landsat images and the results are consistent with the ones obtained here. Therefore, these remote sensing techniques have the potential to be applied to characterize the degraded forests in the tropics.

Besides this research initiative, there are other research questions that I am interested in and could not be covered in this dissertation. The first one is the estimation of biophysical properties of degraded forests. I have demonstrated in one of the papers I wrote in the first year of my dissertation (Souza Jr., et al., 2003) that biomass of degraded forests could be estimated with NPV fractions. I have acquired forest biophysical data from seventy forest transects conducted in several regions of the Brazilian Amazon in collaboration with Dr. Roberts from UCSB. I intend to

extend the collaboration in this area with Dr. Cochrane, who has conducted about thirty forest transects in the Brazilian Amazon, to integrate remotely sensed data with forest biophysical properties to calibrate regression equations between these types of measurements. I envision that the NDFI – the new spectral index proposed and validated in the scope of this dissertation – has the potential to correlate better with forest biomass than NPV.

Basin wide analysis with time series will also help establish relationships between fractions and NDFI with forest biophysical properties, such as biomass, allowing us to quantify carbon fluxes due to forest degradation and deforestation in the Amazon region. The spatial distribution of carbon stocks is highly uncertain in the Amazon region (Houghton et al., 2001) and key information is needed to conduct research on carbon fluxes. Currently, I am collaborating with Marcio Sales and Dr. Kyriakidis to generate better estimates of carbon distribution over the Brazilian Amazon using geostatistical techniques. About 2,300 one-hectare plots of tree inventories from RADAMBRASIL Project were georeferenced and used in variogram analysis of biomass. The biomass variogram was used to provide the parameters for kriging interpolation to generate a map of biomass distribution for the state of Rondônia. The variogram and kriging analyses will be extended to the whole Brazilian Amazon to generate better maps of biomass distribution. Because the research results in this area are very promising, I envision using the remote sensing techniques presented in this dissertation to quantify carbon fluxes in the Amazon region due to forest degradation and deforestation.

Forest fragmentation is another type of forest degradation that has to be analyzed. Currently, Dr. Roberts is leading a research initiative at UCSB to assemble and process a robust data set of Landsat images encompassing 25 years and covering the whole state of Rondônia. Land cover maps have been produced using this very large data set and will allow us to characterize the forest fragmentation in this region. Fraction images and NDFI have been generated for Ji-Paraná and the preliminary results have shown that the degradation of forest fragments, in particular forest edges, can be enhanced with NDFI. The time series will also provide ways to estimate the rates of forest fragmentation and to characterize the temporal spectral signature of forest fragments. I am committed to help Dr. Roberts to continue this research activity after my Ph.D. graduation.

Given the fact that the Landsat ETM+ is not fully operational and that Landsat TM 5 is producing degraded data, the remote sensing techniques proposed in this dissertation have to be tested in other types of optical data. SPOT images have already been successfully used to generate fractions of GV, NPV, Soil and Shade in the Eastern Amazon (Souza Jr., et al., 2003). The fraction images obtained with SPOT images were useful to identifying and mapping degraded forests, and, therefore, can be used to generate NDFI which enhances the detection and mapping of these type of forests. ASTER images, which have better spectral resolution than SPOT and Landsat images, are other potential source of data to apply the techniques proposed in this dissertation. MODIS images may be useful to detect degraded forests using NDFI using time series because the spectral signature of degraded

forests change very fast and these spectral changes may be sensitive to MODIS.

Finally, mapping selective logging in flooded forests (*Varzea*) is a very challenge research issue that should be addressed with other type of remote sensing data (e.g., radar and lidar) and techniques.

References

- Adams, J. B., Smith, M. O., and Gillespie, A. R. (1993). Imaging spectroscopy: Interpretation based on spectral mixture analysis. In *Remote Geochemical Analysis: Elemental and Mineralogical Composition 7*, (V. M. Pieters and P. Englert, Eds.) Cambridge University Press, New York, pp. 145-166.
- Adams, J. B., Sabol, D. E., Kapos, V., Almeida, R., Roberts, D. A., Smith, M. O. and Gillespie, A. R. (1995). Classification of Multispectral Images Based on Fractions of Endmembers - Application to Land-Cover Change in the Brazilian Amazon. *Remote Sensing of Environment* **52**(2): 137-154.
- Alves, D. S. and D. L. Skole (1996). Characterizing land cover dynamics using multi-temporal imagery. *International Journal of Remote Sensing* 17(4): 835-839.
- Angenelli, D. Bollini, A. Lombardi, L. (2002). Image classification: an evolutionary approach. *Pattern Recognition Letters* (23) 303-309.
- Asner, G. P. (2001). Cloud cover in Landsat observation in the Brazilian Amazon. *International Journal of Remote Sensing*, 18, 3855-3862.
- Asner, G.P., Bustamante, M.M.C., Townsend, A. R. (2003). Scale dependence of biophysical structure in deforested areas bordering the Tapajós National Forest, Central Amazon., *Remote Sensing of Environment*, 87, 507-520.
- Asner, G.P., Keller, M., Pereira Jr, R. and Zweede, J.C. (2002). Remote sensing of selective logging in Amazonia: Assessing limitations based on detailed field observations, Landsat ETM+ and textural analysis. *Remote Sensing of Environment*. 80, 83-496.
- Asner, G.P., Keller, M. Pereira Jr., R., Zweede J.C. and Silva, J. (2004a). Canopy damage and recovery after selective logging in Amazonia: field and satellite studies. *Ecological Applications*, 14, s280-s298.
- Asner, G. P., Keller, M. and Silva, J. N. M. (2004b). Spatial and temporal dynamics of forest canopy gaps following selective logging in the eastern Amazon. *Global Change Biology* **10**(5): 765-783.
- Barros, A. C. and Uhl, C. (1995). Logging Along the Amazon River and Estuary - Patterns, Problems and Potential. *Forest Ecology and Management* 77(1-3): 87-105.

- Bateson, C. A., Asner, G. P and Wessman, C. A. (2000). Endmember bundles: a new approach to incorporating endmember variability into spectral mixture analysis. *IEEE Transactions on Geoscience and Remote Sensing*, 38(2):1083-1094.
- Bazzaz, F. A. (1998). Tropical forests in a future climate: Changes in biological diversity and impact on the global carbon cycle. *Climatic Change* 39(2-3): 317-336.
- Boardman, J. W., Kruse, F. A., Green, R. O. (1995), Mapping target signatures via partial unmixing of AVIRIS data: In Summaries of the 5th Airborne Earth Science Workshop, January 23-26. JPL Publication 95(1) 23-26.
- Breiman, Leo, Jerome Friedman, Richard Olshen, and Charles Stone. (1984). *Classification and Regression Trees*. Wadsworth Int. Group, 368p.
- Carlotto, M. J. (1999). Reducing the effects of space-varying, wavelength-dependent scattering in multispectral imagery. *International Journal of Remote Sensing*, 20(17):3333-3344.
- Casa Civil. (2004): Plano de Ação para a Prevenção e Controle do Desmatamento na Amazônia Legal, Brasília, DF. Relatório da Presidência da República, Casa Civil, (<http://www.amazonia.org.br/arquivos/101504.pdf>), 156 pp.
- Cochrane, M.A. (2001). Synergistic Interactions Between Habitat Fragmentation and Fire in Evergreen Tropical Forests. *Conservation Biology* 15(6): 1515-1521.
- Cochrane, M.A. (2003). Fire Science for Rainforests. *Nature* 421: 913-919.
- Cochrane, M. A.; Alencar, A.; Schulze, M.; Souza Jr., C.; Nepstad, D.; Lefebvre, P.; Davidson, E. (1999), Positive feedbacks in the fire dynamic of closed canopy tropical forest. *Science* 284:1832-1835.
- Cochrane, M. A. and Laurance, W. F. (2002). Fire as a large-scale edge effect in Amazonian forests. *Journal of Tropical Ecology* 18: 311-325.
- Cochrane, M.A. and Schulze, M. D. (1999). Fire as a recurrent event in tropical forests of the eastern Amazon: effects on forest structure, biomass, and species composition. *Biotropica*, 31, 2-16.
- Cochrane, M.A. and Souza Jr., C. (1998). Linear mixture model classification of burned forest in the eastern Amazon. *International Journal of Remote Sensing* 19 (17): 3433-3440.
- Cochrane, M.A., D.L. Skole, E.A.T. Matricardi, C. Barber and W. Chomentowski. (2004). Selective Logging, Forest Fragmentation and Fire Disturbance: Implications of Interaction and Synergy. Pp. 310-324 in *Working Forests in the*

- Neotropics: Conservation through Sustainable Management. (D.J. Zarin, et al. eds). Columbia University Press.
- Coppin, P. R. and M. E. Bauer (1995). The Potential Contribution of Pixel-Based Canopy Change Information to Stand-Based Forest Management in the Northern Us. *Journal of Environmental Management* 44(1): 69-8
- Delisle, K. (2004) Decision Trees and Evolutionary Programming. AI Depot, <http://ai-depot.com/Tutorial/DecisionTrees.html>.
- De Wasseige, C. and Defourny, P. (2004). Remote sensing of selective logging impact for tropical forest management. *Forest Ecology and Management*, 188, 161-173.
- Fearnside, P. M. (1989). Deforestation in the Amazon. *Environment* 31(7): 4-5.
- Fearnside, P. M. (1996). Amazonian Deforestation and Global Warming - Carbon Stocks in Vegetation Replacing Brazils Amazon Forest. *Forest Ecology and Management* 80(1-3): 21-34.
- Fearnside, P.M. and Salati, E. (1985). Explosive deforestation in Rondonia, Brazil. *Environmental Conservation* 12(4):355-356.
- Friedl, M. A. and Brodley, C. E.(1997). Decision Tree Classification of Land Cover from Remotely Sensed Data. *Remote Sensing of Environment* 61(3): 399-409.
- Furby, S. L. and Campbell, N. A. (2001). Calibrating images from different dates to 'like-value' digital counts. *Remote Sensing of Environment*, 77, 186 -196.
- Gerwing, J. J. and Farias, D. L. (2000). Integrating liana abundance and forest stature into an estimate of total aboveground biomass for an eastern Amazonian forest. *Journal of Tropical Ecology* 16(3): 327-335.
- Gerwing, J. (2002). Degradation of forests through logging and fire in the eastern Brazilian Amazon. *Forest Ecology and Management*, 157,131-141.
- Giambelluca, T. W. (2002). Hydrology of altered tropical forest. *Hydrological Processes* 16 (8 Special Issue SI): 1665-1669.
- Guariguata, M. R. and Dupuy, J. M. (1997). Forest regeneration in abandoned logging roads in lowland Costa Rica. *Biotropica* 29(1): 15-28.
- Holdsworth, A. R. and Uhl, C. (1997). Fire in amazonian selectively logged rain forest and the potential for fire reduction. *Ecological Applications*, 7: 713-725.

- Holland, J. H. (1975). *Adaptation in Natural and Artificial Systems*. University of Michigan Press, Ann Arbor, Michigan.
- Houghton, R. A., Laurence, K. T., Hackler, J. L. and Brown, S. (2001). The spatial distribution of forest biomass in the Brazilian Amazon: a comparison of estimates. *Global Change Biology* (7): 731-746.
- Houghton, R. A., Skole, D. L., Nobre, C. A., Hackler, J. L., Lawrence, K. T. and Chomentowski, W. H. (2000). Annual fluxes of carbon from deforestation and regrowth in the Brazilian Amazon. *Nature* 403(6767): 301-304.
- Hogg, R. V and A. Craig. (1994): *Mathematical Statistics*, 5th ed., Prentice Hall, New Jersey, pp. 251-2.
- Holdsworth, A. R. and Uhl., C. (1997): Fire in amazonian selectively logged rain forest and the potential for fire reduction. *Ecological Applications*, 7, 713-725.
- Houghton, R. A., Lawrence, K. T., Hackler, J. L. and Brown, S. (2001). The spatial distribution of forest biomass in the Brazilian Amazon: a comparison of estimates. *Global Change Biology* 7(7): 731-746.
- Huete, A. R. (1988). A Soil-Adjusted Vegetation Index (SAVI). *Remote Sensing of Environment*, 25: 295-309.
- Hunt, E. R. and Rock, B. N. (1989). Detection of changes in leaf water content using near and middle-infrared reflectances. *Remote Sensing of Environment*, 30, 43–54.
- IBGE (2005). *Mapa de Vegetação do Brasil*. <http://mapas.ibge.gov.br/website/vegetacao/viewer.htm>. Instituto Brasileiro de Geografia e Estatística.
- INPE (2003). *Monitoramento da floresta Amazônica Brasileira por satélite 1999-2001*. <http://www.dpi.inpe.br/prodesdigital>, Instituto Nacional de Pesquisas Espaciais.
- Johns, J. S., Barreto, P. and Uhl, C. (1996). Logging damage during planned and unplanned logging operations in the eastern Amazon. *Forest Ecology and Management* 89(1-3): 59-77
- Lambin, E. F. (1999). Monitoring forest degradation in tropical regions by remote sensing: some methodological issues. *Global Ecology and Biogeography*, 8, 191-198.

- Laurance, W. F., Laurance, S. G. and Delamonica, P. (1998). Tropical forest fragmentation and greenhouse gas emissions. *Forest Ecology and Management* **110**(1-3): 173-180.
- Laurance, W. F., Vasconcelos, H. L. and Lovejoy, T. E. (2000). Forest loss and fragmentation in the Amazon: implications for wildlife conservation. *Oryx* **34**(1): 39-45.
- Lawrence, R., Bunn, A., Powell, S. and Zambon, M. (2004). Classification of remotely sensed imagery using stochastic gradient boosting as a refinement of classification tree analysis. *Remote Sensing of Environment* **90**(3): 331-336.
- Lentini, M., A. Veríssimo and Sobral, L. (2003). Fatos Florestais da Amazônia. Imazon, http://www.imazon.org.br/upload/forest_facts_2003_v4a.pdf, 108 p.
- Lu, D., Moran, E. and Batistella, M. (2003). Linear spectral mixture model applied to Amazonian vegetation classification. *Remote Sensing of Environment*, 87, 456-469.
- Magnusson, W. E., O. P. de Lima, Reis, F. Q, Higuchi, N. e Ramos, J. F. (1999). Logging activity and tree regeneration in an Amazonian forest. *Forest Ecology and Management* 113(1): 67-74.
- Martini, A. Rosa, N. and Uhl., C. (1994). An attempt to predict which Amazonian tree species may be threatened by logging activities. *Environmental Conservation*, 21,152-162.
- Matricardi, E. A. T., Skole, D. L., Chomentowski, M. A., Cochrane, M. A. (2001). Multi-temporal detection of selective logging in the Amazon using remote sensing. Special Report BRSI Research Advances –Tropical Forest Information Center, Michigan State University N°. RA03-01\w, 27p.
- Monteiro, A. L. (2005). Monitoramento de indicadores de manejo florestal na Amazônia Legal utilizando Sensoriamento Remoto. Curitiba. M.Sc. Thesis. Setor de Ciências Florestais e da Madeira, Universidade Federal do Paraná. 100p.
- Monteiro, A. L., Souza Jr., C and Barreto, P. (2003). Detection of logging in Amazonian transition forests using spectral mixture models. *International Journal of Remote Sensing*. 1(24):151-159.
- Monteiro, A., Souza Jr., C. Barreto, P., Pantoja, F. and Gerwing, J. (2004). Impactos da exploração madeireira e do fogo em florestas de transição da Amazônia Legal. *Scientia Forestalis*, 65, 11-21.

- Moran, E. F. (1993). Deforestation and Land Use in the Brazilian Amazon. *Human Ecology* 21(1): 1-21.
- Moran, E. F., Brondizio, E. S., Mausel, P and Wu, Y. (1994). Integrating Amazonia vegetation, land use and satellite data. *Bioscience*, 44, 329-338.
- Murthy, S. A. (1998). Automatic construction of decision trees from data: a multi-disciplinary survey. *Data Mining and Knowledge Discovery*, 2, 345-389.
- Nelson, B. W., Kapos, V., Adams, J. B., Oliveira, W. J. and Braun, O. P. G. (1994). Forest disturbance by large blowdowns in the Brazilian Amazon. *Ecology*, 75(3), 853-858.
- Nelson, R. F., Kimes, D. S., Salas, W. A. and Routhier, M. (2000). Secondary forest age and tropical forest biomass estimation using thematic mapper imagery. *Bioscience* 50(5): 419-431.
- Nepstad, D.; A. Veríssimo, A. Alencar, C. Nobre, E. Lima, P. Lefebvre, P. Schlesinger, C. Potter, M. A. Cochrane, and Brooks, V. (1999): Large-scale impoverishment of Amazonian forests by logging and fire. *Nature*, 398, 505-508.
- Numata, I., Soares, J.V., Roberts, D., Leonidas, F.C., Chadwick, O.A., and Batista, G.T. (2003). Relationships among soil fertility dynamics and remotely sensed measures across pasture chronosequences in Rondônia, Brazil. *Remote Sensing of Environment*, 87, 446-466.
- Ott, L. (1992). An introduction to statistical methods and data analysis – 4th Edition, Duxbury Press, Belmont, California, 1051 pp.
- Pereira, R., Zweede, J., Asner, G. P. and Keller, M. (2002). Forest canopy damage and recovery in reduced-impact and conventional selective logging in eastern Para, Brazil. *Forest Ecology and Management* 168(1-3): 77-89.
- Powell, R. L., Matzke, N., Souza, C. Jr., Clark, M., Numata, I., Hess, L. L., Roberts, D. A. (2004). Sources of error in accuracy assessment of thematic land-cover maps in the Brazilian Amazon. *Remote Sensing of Environment*, 90, 221-234.
- RADAMBRASIL (1981) Projeto Radam Brasil, Levantamento de Recursos Naturais. Departamento de Produção Mineral. Folha SC.21 Juruena, Rio de Janeiro, V20, 30-40.
- Richard, J. and Jia, X. (1999). *Remote sensing digital analysis*, 3rd Ed. Springer-Verlag, Berlin, 363p.

- Rignot, E., Salas, W. A. and Skole, D. L. (1997). Mapping deforestation and secondary growth in Rondonia, Brazil, using imaging radar and thematic mapper data. *Remote Sensing of Environment* **59**(2): 167-179.
- Roberts, D. A., Smith, M. O. and Adams, J. B. (1993). Green-vegetation, non-photosynthetic vegetation, and soils in AVIRIS data. *Remote Sensing of Environment*, 44, 255-269.
- Roberts, D. A., Batista, G. T., Pereira, J. L. G., Walker, E. K. and Nelson, B. W. (1998). Change identification using multitemporal spectral mixture analysis: applications in eastern Amazon. In: *Remote Sensing Change Detection: Environmental Monitoring Methods and Applications* (Eds. Luneetta, R. S. and Elvidge. C. D.). Ann Arbor Press (Chelsea, Michigan), (9)137-159p.
- Roberts, D. A.; Numata, I.; Homes, K.; Batista, G.; Krug, T.; Monteiro, A. L.; Powell, B. and Chadwick, O. A. (2002). Large area mapping of land-cover change in Rondônia using multitemporal spectral mixture analysis and decision tree classifiers. *Journal of Geophysical Research* 107 (20): 40-1.40-18
- Rouse, J.W., R.H. Haas, J.A. Schell, D.W. Deering and Harlan, J.C. (1974). Monitoring the vernal advancement and retrogradation (greenwave effect) of natural vegetation, NASA/GSFC Type III Final Report, Greenbelt, Md 371 pp.
- Russel, S. and Norvig, P. (2003). *Artificial Intelligence: a modern approach*. Prentice Hall, New Jersey, 1081p.
- Santos, J. R. ; Krug, Thelma and Araújo, L.S. (2002). Corte de árvores visto do espaço. *Ciência Hoje*, Rio de Janeiro, RJ., v. 30, n. 179, p. 67-69 (In Portuguese).
- Sgrenzaroli, M., A. Baraldi, H. Eva, G. De Grandi and Achard, F. (2002). Contextual Clustering for Image Labeling: An Application to Degraded Forest Assessment in Landsat TM Images of the Brazilian Amazon. *IEEE Transactions On Geoscience and Remote Sensing*, **40**, 1833-1848.
- Skole, D. and Tucker, C. (1993). Tropical Deforestation and Habitat Fragmentation in the Amazon - Satellite Data from 1978 to 1988 (Vol 260, Pg 1909, 1993). *Science* 261(5125): 1104-1104.
- Small, C. (2004). The Landsat ETM+ spectral mixing space. *Remote Sensing of Environment*, 93, 1-17.
- Sörensen, K. and Janssens, G. K. (2003) Data mining with genetic algorithms on binary trees. *European Journal of Operational Research*, 151, 253-264.

- Souza, C. and Barreto, P. (2000). An alternative approach for detecting and monitoring selectively logged forests in the Amazon. *International Journal of Remote Sensing*, 21, 173-179.
- Souza Jr., C., Firestone, L. Silva, M. L. and Roberts, D. A. (2003). Mapping forest degradation in the Eastern Amazon from SPOT 4 through spectral mixture models. *Remote Sensing of Environment*, 87, 494-506.
- Souza Jr, C., Roberts, D. A. and Monteiro, A. (In press a). Multi-temporal Analysis of Degraded Forests in the Southern Brazilian Amazon. *Earth Interactions*.
- Souza Jr., C. M., Roberts, D. and Cochrane, M. A. (in press b). Combining Spectral and Spatial Information to Map Canopy Damages from Selective Logging and Forest Fires. *Remote Sensing of Environment*.
- Souza Jr., C. & Roberts, D. A. (2005). Mapping forest degradation in the Amazon region with Ikonos images. *International Journal of Remote Sensing*, 26, 425-429.
- Stone, T. A. and Lefebvre, P. (1998). Using multi-temporal satellite data to evaluate selective logging in Para, Brazil. *International Journal of Remote Sensing*, 19, 2517-2526.
- Uhl, C. and Kauffman, J. B. (1990). Deforestation, Fire Susceptibility, and Potential Tree Responses to Fire in the Eastern Amazon. *Ecology* 71(2): 437-449.
- Uhl, C. and Vieira, I. C. G. (1989). Ecological Impacts of Selective Logging in the Brazilian Amazon - a Case Study from the Paragominas Region of the State of Para. *Biotropica* 21(2): 98-106.
- Uhl, C., Barreto, P., Verissimo, A., Vidal, E., Amaral, P., Barros, A. C., Souza, C., Johns, J. and Gerwing, J. (1997). Natural resource management in the Brazilian Amazon. *Bioscience* 47(3): 160-168.
- Whitley, D. (1989). The GENITOR Algorithm and Selection Pressure: Why Rank-Based Allocation of Reproductive Trials is Best. In Schaffer, J. D. (ed.): *Proceedings of the Third International Conference on Genetic Algorithms*, San Mateo, California, USA: Morgan Kaufmann Publishers, 116-121.
- Verbyla, D. L. and S. H. Boles. 2000: Bias in land cover change estimates due to misregistration. *International Journal of Remote Sensing*, 21, 3553-3560.
- Verissimo, A.; Barreto, P.; Mattos, M.; Tarifa, R. and Uhl, C. (1992). Logging impacts and prospects for sustainable forest management in an old Amazon frontier: the case of Paragominas. *Forest Ecology and Management* 55: 169-199

- Veríssimo, A.; Barreto, P.; Tarifa, R. and Uhl, C. (1995). Extraction of a high-value natural resource in Amazônia: the case of mahogany. *Forest Ecology and Management* 72: 39-60.
- Veríssimo, A.; Cochrane, M. A.; Souza Jr., C. and Salomão, R. (2002). Priority areas for establishing national forests in the Brazilian Amazon. *Conservation Ecology* 6 (1): 4
- Vidal, E., J. Johns, J. Gerwing, P. Barreto and Uhl, C. (1997) Vine management for reduced-impact logging in the eastern Amazon. *Forest Ecology and Management*, **98**, 105-114.
- Watrin, O. S., and Rocha, A. M. A. (1992). Levantamento da vegetação natural e do uso da terra no Município de Paragominas (PA) utilizando imagens TM/Landsat. *Boletim de Pesquisa*, 124, EMBRAPA/CPATU, Belém-PA, 40 pp.
- Woodcock, C. E., Macomber, S. A., Pax-Lenney, M. and Cohen, W. B. (2001). Monitoring large areas for forest change using Landsat: Generalization across space, time and Landsat sensors. *Remote Sensing of Environment* **78**(1-2): 194-203.